MASTERARBEIT | MASTER'S THESIS

Titel | Title

Exploring vulnerabilities and dependencies of two transmissible cancers in the Tasmanian devil

verfasst von | submitted by

Carmen Isabelle Kreindl BSc

angestrebter akademischer Grad | in partial fulfilment of the requirements for the degree of

Master of Science (MSc)

Wien | Vienna, 2024

Studienkennzahl lt. Studienblatt | Degree programme code as it appears on the student record sheet:	UA 066 834
Studienrichtung lt. Studienblatt | Degree programme as it appears on the student record sheet:	Masterstudium Molekulare Biologie
Betreut von | Supervisor:	Univ-Prof. Dipl.-Ing. Dr. rer. nat. Richard Moriggl

Acknowledgements

I would like to express my gratitude to several people for their assistance during the journey of my master's thesis. Firstly, I would like to thank Univ-Prof. Dipl.-Ing. Dr. rer. nat. Richard Moriggl, not only for providing me with the wonderful opportunity to join his lab and contribute to this exciting project but also for the support, feedback, and scientific guidance.

I am incredibly thankful for my amazing supervisor, Anna Schönbichler, who not only guided me through this research journey but also became a supportive friend. Thank you for your input, continuous support, encouragement, and patience. I could not have asked for a better supervisor, and I'll truly miss working with you!

I also want to acknowledge and thank all the other lab members for their expertise and support. I truly appreciate the knowledge I have gained, and the wonderful experiences shared within the lab.

Lastly, I also want to thank my wonderful family, partner and friends for their constant encouragement and support throughout this journey. Your belief in me has been a constant source of strength and I am grateful for your presence in my life.

Table of Contents

List of common abbreviations

ALCL	Anaplastic Large Cell Lymphoma
ATP	Adenosine Triphosphate
B2M	Beta-2 Microglobulin
BSA	Bovine Serum Albumin
BTN	Bivalves' Transmissible Neoplasms
CCD	Coiled-Coil Domain
CML	Chronic Myeloid Leukemia
CTVT	Canine Transmissible Venereal Tumor
DBD	DNA-Binding Domain
DFTD	Devil Facial Tumor Disease
DMEM	Dulbecco's Modified Eagle Medium
DNA	Desoxyribonucleic Acid
DPIPWE	Tasmanian Department of Primary Industries, Parks, Water and Environment
EDTA	Ethylenediaminetetraacetic Acid
EGF(R)	Epidermal Growth Factor (Receptor)
EMA	European Medicines Agency
ER	Endoplasmic Reticulum
ERK	Extracellular Signal-Regulated Kinase
FCS	Fetal Calf Serum
FDA	U.S. Food and Drug Administration
FGF(R)	Fibroblast Growth Factor (Receptor)
FLT	Fms-like Tyrosine Kinase
GIST	Gastrointestinal Stromal Tumor
HDAC	Histone Deacetylase

HER	Human Epidermal Growth Factor Receptor
HLA	Human Leukocyte Antigen
IC_{50}	Half-maximal Inhibitory Concentration
JAK	Janus Kinase
JV	Jarvis
KDR	Kinase Insert Domain Receptor (VEGFR-2)
KD	Kinase domain
LD	Linker-Domain
MAPK	Mitogen-Activated Protein Kinases
MHC	Major Histocompatibility Complex
MSA	Most Synergistic Area
ND	N-Terminal Domain
NRG	Neuregulin
NRTK	Non-Receptor Tyrosine Kinases
NSCLC	Non-Small Cell Lung Cancer
PBS	Phosphate Buffered Saline
PDGF(R)	Platelet-Derived Growth Factor (Receptor)
POC	Percentage of Control
PRX	Periaxin
RCC	Renal Cell Carcinoma
RNA	Ribonucleic Acid
RPMI	Roswell Park Memorial Institute Medium
RTK	Receptor Tyrosine Kinase
RT-qPCR	Reverse Transcription Quantitative Polymerase Chain Reaction
RV	Red Velvet

SCLC	Small Cell Lung Cancer
SDS-PAGE	Sodium dodecyl sulfate-polyacrylamide-gel electrophoresis
SH2	Src-Homology Domain
STAT	Signal Transducer and Activator
STDP	Save the Devil Program
SN	Snug
TAD	Transcriptional Activation Domain
TAP	Transporter associated with Antigen Processing
TGF-α	Transforming Growth Factor alpha
TKI	Tyrosine Kinase Inhibitor
TMD	Transmembrane Domain
VEGF(R)	Vascular Endothelial Growth Factor (Receptor)
WCE	Whole-Cell Extract Buffer
ZIP	Zero Interaction Potency

Abstract

Devil facial tumor 1 and 2 (DFT1/2) are transmissible cancers that threaten the Tasmanian devil with extinction. There is no available cure for these rapidly spreading malignancies and vaccination attempts have so far remained unsuccessful, highlighting the need for a better understanding of disease mechanisms to develop effective treatments. Therefore, the aim of this project was to characterize core cancer pathways that drive DFT1/2 by analyzing the expression and function of selected proteins including Receptor Tyrosine Kinases (RTK) and STAT transcription factors. Cytotoxicity assays revealed that Sapitinib, an ERBB inhibitor, is selectively effective towards DFT1 cells while Imatinib, a PDGFR inhibitor, selectively affects DFT2 cells. Based on these revealed distinct vulnerabilities of DFT1/2, gene and protein expression analysis was performed. The results confirm increased levels of total and phosphorylated STAT3 in DFT1 cells compared to DFT2 cells and healthy fibroblasts. In DFT2, on the other hand, higher levels of STAT5 and PDGFRα were detected, suggesting an interplay between these molecules as a previously unexplored signaling axis only active in the second transmissible cancer. Due to a surprisingly high expression of ERBB3 in DFT2, despite the lack of response towards ERBB inhibition, combination treatments with Sapitinib and Imatinib were performed but only weak synergistic interactions between these two drugs were revealed. Analysis of DFT2 cell lines made resistant towards PDGFR inhibition, however, showed a change in RTK signaling and STAT3 activation as previously described in DFT1. Strikingly, this activation was accompanied by immune evasion mechanisms such as MHC-I downregulation. These findings do not only show that DFT2 demonstrates signaling plasticity upon treatment but connects RTK driven core cancer pathways with immune evasion.

In conclusion, the provided results demonstrate that both tumor cell lines are different in their signaling mechanisms but due to signaling plasticity alternative pathways might be used and contribute to immune evasion of the tumors. This knowledge can contribute to the development of more effective treatments and the conservation of the Tasmanian devil. Simultaneously, the insights about these transmissible cancers can be translated into human cancer research and advance our understanding of cancer signaling and immune evasion.

1. Introduction

1.1. The Tasmanian devil

The Tasmanian devil (*Sarcophilus harrisii*) is the largest living marsupial carnivore, endemic to the Australian island Tasmania. On mainland Australia the species disappeared between 3.200 and 3.500 years ago due to the arrival of dingoes (*Canis dingo*), increasing human population density and climate change. Tragically, a current and rapid decline of the Tasmanian devil population, mainly caused by the emerge of two transmissible cancers, might lead to global extinction of this iconic species (Johnson & Wroe, 2003; Kosack et al., 2019).

The Tasmanian devil is extremely important for the local ecosystem by serving as a scavenger and clearing dead animals from the landscape. The significant and widespread decline of the devil population consequently benefits invasive species such as feral cats and rodents. In turn, these invasive animals are endangering smaller native animals, immensely disrupting the ecosystem. The scavenging behavior is not only important for suppressing invasive species, but also for preventing diseases to both humans and livestock. Furthermore, by consuming dead animals, the Tasmanian devil redistributes nutrients back into the environment, which has a positive impact on plant growth and soil health (Andersen et al., 2020).

Wildlife is threatened by the emerge of infectious diseases worldwide. However, the emergence of contagious cancers, leading to critical population decline, is until now a unique phenomenon. The Tasmanian devil is affected by two independently arisen transmissible cancers that spread via biting and manifest on the animals' facial areas. The first devil facial tumor, DFT1, was observed in 1996 in the north-east of Tasmania and rapidly spread over the whole island. In 2014, the second devil facial tumor, DFT2, was discovered. By now, the disease affects nearly the whole Tasmanian devil population, with only a small number of animals remaining unaffected. Notably, DFT1 and DFT2 are the only known cancers, that threaten an entire species with extinction (Kosack et al., 2019). Transmissible cancer affecting the Tasmanian devil has led to a significant reduction of the devil population over the past 30 years with numbers decreasing by almost 70% from 53.000 in 1996 to 16.900 in 2020. In regions heavily affected by DFT1 and DFT2, a population decline up to 90% has been observed (Cunningham et al., 2021). This massive reduction of devils leads to cascading effects, described above, highlighting the importance of conservation efforts to protect the devil (Andersen et al., 2020).

In 2003 the Australian and Tasmanian government started the Save the Tasmanian Devil Program (STDP). Protections efforts that are going on include the development of vaccines, transportation to the mainland and safety populations. The Tasmanian State Government also established an Insurance Population within Tasmania to protect the Tasmanian devil. Captive breeding programs provide a safeguard against extinction and aim to breed individuals for reintroducing them back into the wild. Protecting devils directly in their natural habitat seems to be more challenging since there are no pre-diagnostic tests available yet. These tests are important to identify DFT1 and DFT2 before visible symptoms occur. A disease suppression program was performed in the south-east of Tasmania between 2004 and 2010, where they euthanized animals that were showing signs of DFT. But analysis revealed that this approach did not lead to a significant improvement. Another approach to protect the devil is to develop vaccines against DFTD to induce immune response (Woods et al., 2018). A vaccine against DFTD would serve as a crucial conservation tool in securing the future of wild Tasmanian devils. While there are indications of natural immune responses against DFTD in the wild, occurring in minority of devils, this factor has not led to a reduction of the population decline (Pye et al., 2018).

All described efforts above have not stopped the decline of this species. This lack of success is partly caused by the lack of knowledge concerning the molecular mechanisms of the transmissible cancers and cancer transmission in general. Naturally transmissible cancer is extremely rare but also found in dog and bivalves, besides endangering the Tasmanian devil. In all three animals, cancer cells need to find a route of transmission, maintain the ability to proliferate and escape the immune system of host animals.

1.2. Transmissible Cancer

Transmissible cancers are malignant cell lineages that stem from a single somatic cell that mutated into cancer. By acquiring the skill to transmit from individual to individual, they contradict our previous understanding that cancer cells are restrained to a single individual with whom they succumb. Therefore, transmissibility is not a hallmark of cancer. Strikingly, even though transmissible cancers cells are genetically different from their new host, they can escape the immune system. Transmissible cancers seem to be constrained by two primary factors: the recognition by the immune system and physical barriers that hinder the dissemination of cancer cells (Hanahan & Weinberg, 2011; Stammnitz et al., 2018). Natural cancer transmission is observed in three animal species: bivalve mollusks, dogs, and the Tasmanian devil. In rare cases, however, cancer transmission is also possible between humans (Metzger & Goff, 2016).

1.2.1. BTN/ Transmission trough water

Besides the Tasmanian devil, bivalves are known to be affected by transmissible cancer. Whereas transmissible cancer in the Tasmanian devil is transmitted through physical contact, bivalves' transmissible neoplasms (BTN) are transmitted via sea water. Hemic neoplasia, also known as disseminated cancers, manifests as a leukemia-like condition in various marine bivalves such as clams, cockles, mussels, and oysters. This disease is marked by the uncontrolled proliferation of cancer cells in their circulatory fluid leading to disruption of vital functions necessary for survival. The first documentation of this disease affecting soft-shell clams was in the 1970s. Mollusks lack a self/non-self-recognition system comparable to the MHC found in vertebrates. The absence of MHC (Major Histocompatibility Complex) in mollusks could potentially increase their vulnerability to infectious malignancies. The emergence of transmissible cancers in marine invertebrates, contributing to elevated mortality rates in soft-shell clams, may also extend the risk of heightened mortalities to other species. Bivalve mollusks play a crucial role in the marine ecosystem. Consequently, the occurrence of contagious cancer may lead to ecological consequences, ultimately affecting the availability of food for humans as well (Metzger et al., 2015; Metzger & Goff, 2016).

1.2.2. CTVT/ Sexual Transmission

Canine transmissible venereal tumor (CTVT) is the oldest characterized transmissible cancer and affects dogs. Unraveling the precise period of origin of CTVT presents a major challenge. However, the analysis of Murgia et al. indicates a likely occurrence between 200 and 2500 years ago. Determining whether this timeframe signifies the initial emergence of the tumor, or it shows a later stage characterized by increased spread of the tumor as a parasite. CTVT is also known as Sticker's sarcoma and is transmitted through direct contact including biting, licking, and sniffing tumor-affected body parts. Unlike the case of the Tasmanian devil, dogs do not face extinction due to this transmissible cancer. It is suggested that the dog's immune system plays a crucial role in spontaneous regression of CTVT. The hosts immune response may recognize and target foreign cancer cells. The mechanisms of this self-limiting characteristic of CTVT in dogs remains unclear (Metzger et al., 2015; Metzger & Goff, 2016; Murgia et al., 2006).

1.2.3. DFT1 and DFT2

The Tasmanian devil is affected by two transmissible cancers referred to as DFT1 and DFT2, which have a very similar phenotype. Both cancer cell lines are transmitted via biting, which is a social interaction between Tasmanian devils and promotes tumors on the face or inside the mouth, which metastasize to other organs. A comparison between healthy and tumor tissues showed that DFT1 and DFT2 developed from peripheral nerve tissue and more specifically Schwann cells. The myelin protein Periaxin (PRX) is used as a diagnostic marker for DFT1 while DFT2 tumors are, interestingly, negative for Periaxin, which indicates that they stem from varying differentiation stages (Patchett et al., 2020). Genetic profiling showed that DFT1 originated from a female devil, while DFT2 has fragments of Y-chromosomes in its genetic material and arose in a male Tasmanian devil. Whereas DFT2 already spread over the whole island, DFT2 is geographically restricted, but it is not clear, whether DFT2 is more aggressive or less competitive than DFT1. To evade the host immune system, both DFT1 and DFT2 employ distinct strategies due to differences in their MHC class I expression. DFT1 shows downregulated MHC expression, while in DFT2 the expression predominantly remains intact. How DFT1 and DFT2 signal and how the expression of MHC molecules influences immune escape is described below (Pye et al., 2016; Stammnitz et al., 2018).

Differences	DFT1	DFT2
First observation	1996 in north-east Tasmania	2014 in south-east Tasmania
Origin	female	male
Schwann cell origin	yes	yes
Periaxin (diagnostic marker)	positive	negative
Immune response	MHC class I is downregulated	MHC class I is mostly intact

Table 1: Differences between DFT1 and DFT2 (Kosack et al., 2019; Stammnitz et al., 2018)

1.2.4. Cancer transmission in humans

The transmission of cancer between humans is exceptionally rare due to the immune system's ability to recognize and reject foreign cells, thereby preventing the spread of cancer between individuals. However, specific circumstances allow such transmission of cancer, including organ transplantation and pregnancy. After organ transplantations, recipients experience a suppressed immune system, which facilitates the transmission of cancer from the donor. The compromised immune system fails to recognize and eliminate the cancer cells. The likelihood of receiving an organ from a donor with an undetected malignancy is extremely low (Desai et al., 2012; Greaves & Hughes, 2018; Metzger et al., 2015).

Over a span of nine years in the United Kingdom, cases of recipients acquiring cancer from their donors were identified. Among 30.765 transplants, 18 recipients were diagnosed with cancer, representing a rate of 0,05%. Additionally, during pregnancy 50% of the genetic material are shared between the mother and the fetus. The placenta is permeable for cells, which allows the transmission of cancer cells from the mother to the fetus and vice versa. The transmission of cancer between the fetus and mother is exceedingly rare, affecting 1 in 50.000 pregnancies, whereas only 90 cases are known of maternal-fetal transmission. Furthermore, cancer transmission can also occur between twins, which was documented in about 100 cases (Desai et al., 2012; Greaves & Hughes, 2018; Metzger et al., 2015).

1.2.5. Research on transmissible cancer

In all cases mentioned above, transmissible cancer shows the remarkable skill to survive the transfer between individuals, keep proliferating and to escape the hosts immune system. Studying transmissible cancer does not only provide insights into the complex interplay between cancer cells and their microenvironment but enhances our understanding of fundamental principles of cancer such as cancer proliferation and cancer immune evasion. By uncovering common proliferation pathways, potential therapeutic targets can be identified. Therefore, this research is not only important for developing treatment options for saving affected species, but also for understanding fundamental principles of cancer such as cancer proliferation and cancer immune evasion better.

1.3. Cancer Proliferation

1.3.1. Core Cancer Signaling – what is a cancer driver?

Core cancer signaling describes a complex network of molecular pathways and cellular processes which are dysregulated in cancer cells leading to abnormal cell growth. Understanding core cancer signaling is crucial for advancing targeted therapies and personalized treatments. Extensive sequencing efforts have revealed the genomic landscapes of prevalent human cancers. Typically, these landscapes exhibit a low number of frequently altered “mountain” genes and a larger array of less commonly altered “hill” genes. These studies have identified many driver genes, each contributing to the dysregulation of core cancer signaling pathways. Identifying cancer drives is essential for understanding cancer development since they are key components of core cancer signaling pathways and can be characterized by genetic alterations or mutations (Tokheim et al., 2016; Vogelstein et al., 2013).

Oncogenic mutations can lead to a variety of effects including the overexpression of genes, activation of signaling pathways, inactivation of tumor suppressors, resistance to cell death, induction of angiogenesis, metastasis or to dysregulation of protein activity. Additionally, cancer drivers can be categorized into 12 signaling pathways governing three fundamental cellular processes: cell fate, cell survival, and genome maintenance. Normal cells undergo cell death in response to genetic modifications as a safeguard mechanism against cancer. Whereas tumor cells have developed mechanisms to withstand genomic complexity, often by the acquisition of mutation in genes like *TP53*. Therefore, genomic complexity partly arises as a consequence of cancer rather than being the primary cause (Vogelstein et al., 2013).

1.3.2. Tyrosine Kinases and Receptor Tyrosine Kinases

Among the most important and well-characterized oncogenes are several proteins belonging to the group of tyrosine kinases. Tyrosine kinases are enzymes that play a crucial role in regulating signaling pathways including cell growth, proliferation, differentiation, and programmed cell death. They are responsible for catalyzing the phosphorylation of tyrosine residues on proteins using adenosine triphosphate (ATP). This post-translational modification leads to the activation or deactivation of proteins. Tyrosine kinases consist of two types, which include receptor tyrosine kinases (RTK) and non-receptor tyrosine kinases (NRTK). Receptor tyrosine kinases like Epidermal Growth Factor Receptor (EGFR) or Platelet-Derived Growth Factor Receptor (PDGFR) are transmembrane proteins that are located on the surface of the cell. RTKs are activated after a ligand like growth factors, hormones, or cytokines, binds to the extracellular domain (Figure 1). This binding event leads to conformational changes in the structure of the receptor, leading to dimerization or oligomerization. This then facilitates the autophosphorylation of tyrosine residues within their intracellular kinase domain. Autophosphorylation serves as an activation event that activates a downstream signaling cascade regulating various cellular processes (Paul & Mukhopadhyay, 2004).

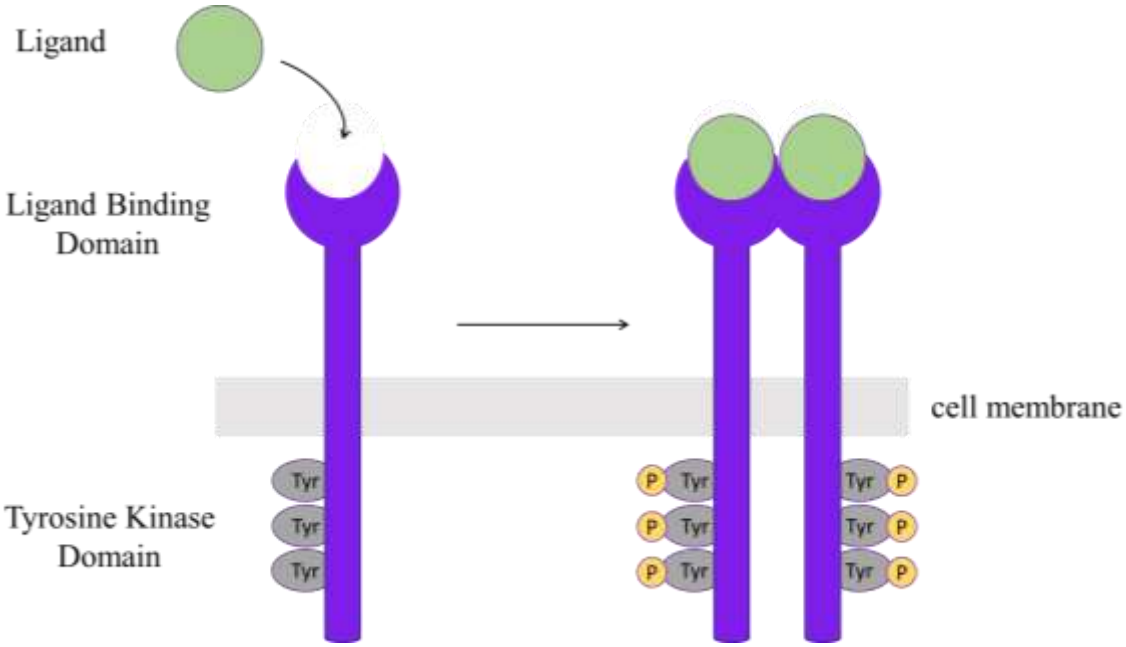

Figure 1: Structure of a Receptor Tyrosine Kinase and its ligand. RTKs are transmembrane proteins that are characterized by binding sites on their extracellular domain that specifically interact with ligands. Ligand binding leads to the activation of the RTK, which undergoes dimerization or oligomerization. These structural changes then lead to autophosphorylation of their tyrosine residues in the intracellular kinase domain, which activates downstream signaling. Classic RTKs, such as members of the ERBB family, contain two tyrosine kinase domains, whereas receptors like AXL and MERU only contain one. The image was created using PowerPoint (Saraon et al., 2021).

1.3.3. ERBB Signaling

Genes of the ERBB family are commonly targets for clinical therapies due to their frequent occurrences of overexpression, mutation, or amplification in human solid cancer. The ERBB family consists of ERBB1 (EGFR), ERBB2 (Human Epidermal Growth Factor Receptor 2, HER2), ERBB3 (HER3) and ERBB4 (HER4). Each member is responding to different ligands. ERBB1 binds to ligands like Transforming Growth Factor α (TGF-α), Amphiregulin, Epiregulin, Betacellulin and Epidermal Growth Factor (EGF). While ERBB2 does not have a known ligand, it has the ability to form heterodimers with other ERBB receptors to activate downstream signaling pathways. ERBB3 is the only RTK that is characterized by an inactive kinase domain (KD), therefore being reliant on other receptors for activation. Upon ligand binding such as Neuregulin-1 (NRG1), ERBB3 heterodimerizes with other receptors, like ERBB2, to modulate various biological processes. ERBB4 predominantly binds to TGF-α, NRGs, Betacellulin and Epiregulin (Majumder, 2023).

Therefore, ERBB signaling is triggered by ligand-induced activation, imitating downstream processes including the activation of transcription factors like STAT3/5 by tyrosine phosphorylation. In Schwann cells, ERBB2 and ERBB3 signaling plays an important role in regulating the expansion and migration of progenitor cells. It also contributes to various functions in myelination and repair of axons (Kosack et al., 2019).

1.3.4. PDGFR Signaling

PDGFR signaling is known for its crucial role in various cellular processes such as cell growth, differentiation, survival, and is often associated with the progression of cancer. The PDGFR/PDGF system consists of two receptors, PDGFRα and PDGFRβ, and four ligands, PDGF-A, PDGF-B, PDGF-C and PDGF-D. Ligand binding leads to the activation of these receptors, initiating downstream signaling. The aberrant activation of PDGFR signaling has been observed in several cancer types, highlighting its significance as a potential therapeutic target. The discovery that STAT5 serves as a novel downstream target of PDGFRβ in ALCL, which was more recently reported (Garces De Los Fayos Alonso et al., 2022).

1.3.5. VEGFR Signaling

Vascular endothelial growth factor (VEGF) and its receptors (VEGFRs) are important components for the control of angiogenesis and the development of the vascular system. Kinase Insert domain receptor (KDR, VEGFR-2), Fms-related tyrosine kinase 1 (FLT-1, VEGFR-1) and Fms-related tyrosine kinase 4 (FLT-4, VEGFR-3) are members of the vascular endothelial growth factor receptor (VEGFR) family and are therefore crucial for mediating the effects of VEGFs. KDR and FLT-1 are expressed by endothelial cells but can also be found in certain cancer cells. FLT-4 is known for its significant role in promoting angiogenesis, which is a process in the metastatic spread of cancer. Elevated levels of FLT-4 in certain cancer types can be associated with an unfavorable prognosis (Su et al., 2006).

1.3.6. Targeting RTKs in cancer

The abnormal activation of tyrosine kinases is often associated with cancers and other diseases. RTKs are important players in the development of cancer, making them promising targets for therapy. Different therapeutic strategies are available for targeting RTKs like monoclonal antibodies, small molecule inhibitors, and combination therapies. Despite promises some challenges remain when targeting RTKs in cancer, such as off-target effects, acquired resistance and tumor heterogeneity (Paul & Mukhopadhyay, 2004). Targeting RTKs in cancer therapy involves using small molecule inhibitors like tyrosine kinase inhibitors (TKIs), which are a class of pharmacological agents that interfere with the activity of tyrosine kinases. Tyrosine kinase inhibitors usually prevent phosphorylation of the tyrosine residues by binding to the ATP-binding site. Most of them are covalent inhibitors promoting ubiquitinoylation and degradation of the kinases as well. Therefore, downstream signaling, which is crucial for cancer cell growth and survival, is being disrupted (Attwood et al., 2021).

1.3.6.1. Imatinib

Imatinib (Gleevec) is an approved TKI that selectively inhibits BCR-ABL, c-Kit, and PDGFR. Imatinib was approved by the U.S. Food and Drug Administration (FDA) and European Medicines Agency (EMA) in 2001 for the treatment of chronic myelogenous leukemia (CML). Subsequently, it gained approval for the treatment of gastrointestinal stromal tumors (GIST) and other malignancies associated with BCR-ABL or c-Kit mutations (Attwood et al., 2021).

1.3.6.2. Sapitinib

Sapitinib (AZD-8931) is an inhibitor of EGFR family members that shows inhibitory effects on EGFR, ERBB2 and ERBB3. This experimental drug has undergone investigation in clinical trials for treating various cancer types, including non-small cell lung cancer (NSCLC) and breast cancer (Kurata et al., 2014). Sapitinib is currently undergoing phase 2 clinical trials for the treatment of NSCLC (National Library of Medicine).

1.3.6.3. Masitinib

Masitinib (Masipro) is a TKI, which inhibits c-Kit, PDGFR and fibroblasts growth factor receptor 3 (FGFR3). Masitinib has been studied for its potential use in the treatment of cancers including gastrointestinal stromal tumors (GIST), pancreatic cancer in men and mast cell tumors in dogs (National Library of Medicine).

1.3.6.4. Lapatinib

Lapatinib is a dual tyrosine kinase inhibitor, which inhibits EGFR and HER2. This TKI has been approved for treating metastatic HER2 positive breast cancer in combination with capecitabine (Abdelgalil & Alkahtani, 2023).

1.3.6.5. Sunitinib

Sunitinib is an approved multi-targeted TKI, targeting multiple receptors such as PDGFR, FGFR and VEGFR. It is primarily used for the treatment of GIST that are resistant to Imatinib or for treating metastatic renal cell carcinoma (RCC). Furthermore, Sunitinib has shown high efficacy in the treatment of other cancers as well (Le Tourneau et al., 2007).

1.3.6.6. Dasatinib

Dasatinib is a multi-targeted TKI, that targets BCR-ABL, Src family kinases, c-Kit, and other kinases. It is used for treating BCR-ABL driven CML and Philadelphia chromosome-positive acute lymphoblastic leukemia. Besides the high efficacy in treating leukemias, Dasatinib has also been studied in other cancers including GIST, prostate, lung or breast cancer (Fauziya et al., 2023).

1.3.7. Downstream RTK/STAT Signaling

The activation of RTKs lead to signaling cascades and the activation of downstream transcription factors. Among the transcription factors connected to cancer are STATs (Signal transducer and activator of transcription). The mammalian STAT family consists of STAT1, STAT2, STAT3, STAT4, STAT5A, STAT5B and STAT6 (Hu et al., 2021). Members of the STAT family play significant roles in various aspects of human cancer, including development, cancer initiation and progression, metastasis survival and drug treatment resistance. STAT3 and STAT5 are of high interest because their high activation status promotes tumor progression in various human cancers especially in leukemia and lymphomas (Moriggl et al., 2005; Wingelhofer et al., 2018).

STAT proteins are regulated by six functionally and structurally conserved domains: N-terminal domain (ND), coiled-coil domain (CCD), DNA-binding domain (DBD), linker domain (LD), Src-homology 2 (SH2) domain, tyrosine phosphorylation site (pY) and a transcriptional activation domain (TAD) at the C-terminus (Figure 2). Apart from STAT2 and STAT6, all STATs contain a conserved phospho-serine (pS) residue at the transcriptional activation domain. STAT proteins exist as isoforms due to alternative mRNA splicing or post-translational proteolytic processing. STAT proteins remain latent in the cytoplasm and undergo activation through phosphorylation, typically catalyzed by cytokine receptor-associated kinases (Janus kinase, JAKs) or growth factor receptor tyrosine kinases like the ones described above. Upon phosphorylation, STATs form homo-or hetero-dimers and translocate into the nucleus. The activation of STAT proteins involves the mediation of homo-and heterodimerization by the SH2 and the N-terminal domain. The highly conserved SH2 domain serves as a primary target for most STAT inhibitors. The coiled-coil domain acts as a nuclear localization signal through protein-protein interactions, whereas the C-terminal transcriptional activation domain undergoes serine-phosphorylation. This phosphorylation event facilitates the recruitment of additional transcriptional activators, leading to increased transcriptional activity of the STATs (Hu et al., 2021; Wingelhofer et al., 2018).

The DNA-binding domain is connected to the SH2 domain by the linking domain. The DBD is crucial for the recognition and binding to the DNA sequence in the regulatory region of the target genes. It also plays a crucial role in the regulation of nuclear export and import (Hu et al., 2021; Wingelhofer et al., 2018).

Figure 2: Structure of STAT proteins. The STAT proteins consist of six conserved domains: N-terminal domain (ND), coiled-coil domain (CCD), DNA-binding domain (DBD), linker domain (LD), Src-homology 2 (SH2) domain, tyrosine phosphorylation site (pY) and a transcriptional activation domain (TAD) at the C-terminus. The image was created using PowerPoint (Hu et al., 2021).

1.3.7.1. Signal transducer and activator of transcription 3 (STAT3)

STAT3 is a protein that plays a crucial role in cell signaling and transcriptional regulation. It is a key regulator of inflammatory signaling since its activation correlates with the induction of pro-inflammatory cytokines. The STAT3 gene is located on chromosome 17 in humans, while in the Tasmanian devil it is situated on chromosome 4 (NCBI Gene). Alternative splicing within exon 23 results in isoforms with different functions and properties. STAT3 undergoes activation through phosphorylation of tyrosine 705 in response to various ligands including Interferons, Interleukin 5 and 6 and Epidermal Growth Factor (EGF). Furthermore, the phosphorylation of serine 727 can contribute to the activation of STAT3, either through Mitogen-activated protein kinases (MAPK) or non-receptor tyrosine kinases like c-Src and ABL. The most important STAT3 activators are the members of the IL-6 family. The hyperactivation of STAT3 has been documented in various cancer types including acute myeloid leukemia (AML), multiple myeloma, and solid tumors affecting different organs such as the bladder, bone, breast, kidney and lung. Moreover, elevated levels of phosphorylated STAT3 expression can be associated with a poor clinal prognosis. As such, targeting STAT3 signaling has emerged a promising approach in cancer therapy. STAT1 is acknowledged as a tumor suppressor, while STAT3 is identified as a promotor of tumorigenesis, therefore it is believed that the balance between STAT1 and STAT3 expression is crucial (Verhoeven et al., 2020; Zammarchi et al., 2011).

1.3.7.2. Signal transducer and activator of transcription 5 (STAT5)

In humans, the STAT5 gene is located on chromosome 17, whereas in the Tasmanian devil STAT5B can be found on chromosome 4. STAT5A and STAT5B share approximately 92% identity at the amino acid level. Despite their high similarity, these proteins are transcribed by two different genes (NCBI Gene). In mammary glands, STAT5A is activated by Prolactin to regulate the milk production during lactation, highlighting the important role of STAT5 in physiological processes, especially in the context of reproductive and mammary gland function (Kanai et al., 2014).

STAT5 is activated by phosphorylation in response to cytokines and growth factors. This phosphorylation is commonly mediated by JAK family members in response to ligand binding to cell surface receptors. Upon phosphorylation, STAT5 proteins form homo- or heterodimers and translocate to the nucleus. In the nucleus, they act as transcription factors, regulating the expression of specific target genes. STAT5 is involved in the regulation of various cellular processes including cell proliferation, survival, and differentiation. It plays a crucial role in the signaling pathways of several cytokines such as interleukins, growth hormones, and prolactin. Additionally, it is also activated by growth factor receptor (GFR) (Sumiyoshi et al., 2016; Wingelhofer et al., 2018).

1.3.8. Core Cancer Signaling in DFT1/DFT2

As transmissible cancer is a rare phenomenon, not many insights have been gained in how contagious cancer cells survive and keep proliferating on a new host. However, DFT1 and DFT2 are suggested to be driven by RTKs and downstream signaling, such as many human cancers. It is important to note that the level of conservation between human and Tasmanian devil proteins differs substantially. While RTK are generally less conserved, STAT proteins and especially STAT3 and STAT5B are remarkably conserved between the species (Table 2). The remarkable conservation suggests that insights gained from studying STAT3 and STAT5B signaling in the Tasmanian devil can be used to understand its function and regulation in humans. Understanding gene conservation is crucial for linking fundamental research conducted in model organisms to its clinical relevance application in human diseases.

	identities [%]	
Protein	**Human**	**Mouse**
STAT1	85,73	84,29
STAT3	99,09	99,58
STAT5B	95,38	94,92
PDGFRα	78,85	81,83
PDGFRβ	77,52	74,75
ERBB3	84,75	82,77
EGFR	82,6	78,64

Table 2: Sequence alignment between Tasmanian devil and human/mouse (NCBI Primer Blast).

Interestingly, Kosack et al. proposed that DFT1 is driven by an ERBB-STAT3 signaling axis and the inhibition of ERBB or STAT3 leads to an arrest in the cancer cells. They discovered that DFT1 cancer cells were sensitive to ERBB inhibitors like Erlotinib, Lapatinib and Sapitinib. Protein expression analysis revealed elevated levels of ERBB2 and ERBB3 in the cancer cells compared to the fibroblasts, whereas EGFR expression was almost undetectable (Kosack et al., 2019).

Furthermore, they detected elevated serine (S727) and tyrosine (Y705) phosphorylation levels of STAT3 in DFT1 cancer cells. This increased phosphorylation was associated with increased activation of Extracellular Signal-Regulated Kinase 1/2 (ERK1/2), suggesting the activation of the RAS-RAF-MAPK/ERK pathway. The inhibition of STAT3 led to a decrease in the expression of ERBB2 and ERBB3, whereas inhibiting ERBB suppressed the phosphorylation of STAT3. These findings imply that DFT1 demonstrates an ERBB-dependent constitutive activation of STAT3, forming positive feedforward loop (Kosack et al., 2019). However, copy number gains of *PDGFRB* in the cancer genome suggest that there might be other core cancer pathways as well that are active in the first transmissible cancer (Stammnitz et al., 2018).

In DFT2, on the other hand, copy number gains of *PDGFRA* in the cancer genome suggest PDGFRα as an important player in cancer signaling, but the driving signaling axis has not been identified yet (Stammnitz et al., 2018). Even though the Tasmanian devil is on the brink of extinction, there is a lack of information about the molecular mechanisms that drive the cancers. Furthermore, it is unknown how the core cancer pathways contribute to the ongoing immune evasion. To find effective treatments and to develop a successful vaccine, more insights are needed.

1.4. Cancer Immune Escape

Transmissible cancers have the remarkable ability to hide from the host immune system. Non-transmissible cancers often employ mechanisms such as the downregulation of MHC molecules to escape immune surveillance and clearance. This immune evasion strategy emphasizes the complex interplay between the immune system and cancer cells, highlighting the importance of understanding immune escape mechanisms in both transmissible and non-transmissible cancer (Hewitt, 2003).

1.4.1. MHC and self-recognition

The MHC describes a group of cell surface proteins which are important for the role of the immune system in vertebrates. In humans, MHC is known as the Human Leukocyte Antigen (HLA) system. The genes that encode the HLA molecules are located on chromosome 6. The MHC molecules are responsible for the presentation of antigens to T-cells. There are two main classes of MHC molecules with different roles, which are called MHC class I and MHC class II. MHC class I are heterodimers composed of a α-chain and a β2-microglobulin (B2M), which are non-covalently connected (Figure 3). The α-chain is a complex structure that consists of three domains: α1, α2 and α3. A peptide-binding groove is formed on the surface of the MHC class I molecule by the α1 and α2 domain. This binding site is crucial for capturing short proteins derived from intracellular proteins. Genetic variation in the MHC genes leading to a diversity of the immune response results in a polymorphic peptide-binding groove. The B2M chain is smaller, non-polymorphic and provides stability (Hewitt, 2003).

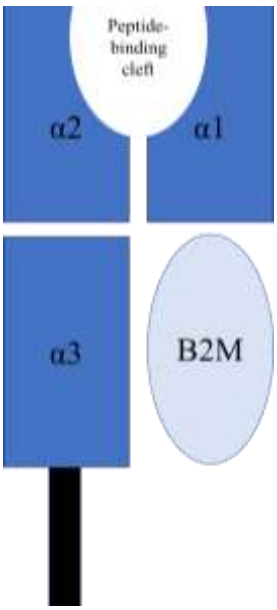

Figure 3: Structure of MHC class I, which is a heterodimer composed of an α-chain and a β2-microglobulin, which are non-covalently bound. The α-chain consists of three domains: α1, α2 and α3. The α1 and α2 domain form a peptide-binding groove on the surface of the MHC class I molecule. The image was created with PowerPoint (Hewitt, 2003).

The folding and assembly of MHC class I molecules is performed within the endoplasmic reticulum (ER) lumen. Therefore, peptides have to be transported from the cytosol into the ER lumen. The ER quality control apparatus examines the folding and assembly of newly synthesized proteins. In the case of misfolded proteins, they are transported back into the cytosol, where they undergo degradation by the proteasome. The transporter associated with antigen processing 1 and 2 (TAP1/2) form a heterodimeric complex, which is necessary for the translocation from the cytosol to the ER lumen. In the ER, chaperones support the proper folding of the MHC class I molecules. Then TAP associates with MHC class I molecules and the peptide binding process is supported by different molecules including Tapasin. Following the loading of peptides onto MHC class I molecules, dissociation of TAP occurs. The MHC class I-peptide complex is further transported to the surface of the cell, where it becomes accessible for the recognition by cytotoxic T-cells. This recognition triggers several events which lead to the activation of the immune system. Therefore, this process is crucial for the immune system being able to detect and eliminate foreign or abnormal cells, which could also be infected organs by viruses and intracellular bacteria (Hewitt, 2003).

1.4.2. MHC-I in cancer

Tumor immune surveillance includes the presentation of tumor-specific antigens by the MHC-I complex to T-cells. This mechanism allows the recognition and elimination of cancer cells. The alteration in the MHC class I expression, leading to a reduced ability of the immune system in recognizing and clearing cancer cells, is a crucial step for cancer immune evasion and can be found in various types of cancer. There are hints that the loss or downregulation of MHC-I not only plays an important role in the immune evasion, but also in the progression of cancer cells. Targeting MHC class I to restore the recognition and elimination process seems to be a promising therapy. To understand the interaction between MHC-I and the tumor cells is crucial for the development of efficient immunotherapies (Garrido et al., 2016; Wu et al., 2023).

1.4.3. MHC in transmissible cancers

Cell-surface MHC molecules are required for recognizing foreign antigens and for the differentiation between self and foreign cells. Since Tasmanian devils live on an isolated island, they show a low genetic diversity and a restricted variability on their MHC-I locus. This and the fact that MHC-I molecules are downregulated in DFT1, suggests that this is a major contributor to the ability to immune escape (Kreiss et al., 2011; Murchison et al., 2010).

However, it was shown that skin grafts that are transplanted from one Tasmanian devil to another are rejected and DFT2 cells generally show an intact MHC-I expression. This suggests that there are other factors, besides the low genetic diversity, leading to transmissibility of cancers (Kreiss et al., 2011; Murchison et al., 2010).

1.4.4. Connection between TK pathways and MHC expression

It was shown that core cancer pathways can influence the expression of MHC on cancer cells. In some human cancers, it has been observed that MAPK signaling is a negative regulator of MHC-I expression. The hyperactivated MAPK pathway can lead to downregulated MHC-I expression on cancer cells, contributing to immune evasion. Understanding the interplay between the negative regulatory role of the MAPK pathway and MHC-I expression is crucial for identifying therapeutic targets and improving outcomes for cancer patients (Wu et al., 2023).

Interestingly, in DFT1 core cancer signaling via ERBB leads to the downregulation of MHC-I (Figure 4). The hyperactive ERBB-STAT3 axis in DFT1 stimulates the expression of downstream genes linked to metastasis, such as MMP2, while simultaneously the expression of MHC class I genes, including B2M, is suppressed. The increased presence of phosphorylated STAT3 protein captures unphosphorylated STAT1 protein in heterodimers, hindering the transcriptional regulation of STAT1 downstream target genes like B2M. This proposed mechanism may play a role in immunity and the recognized absence of tumor rejection during horizontal transmission. The use of ERBB inhibitors or STAT3 inhibitors can be used to interfere with the hyperactivated ERBB-STAT3 axis, potentially resulting in the elimination of DFTD tumor cells and in restoring the expression of MHC- I (Kosack et al., 2019).

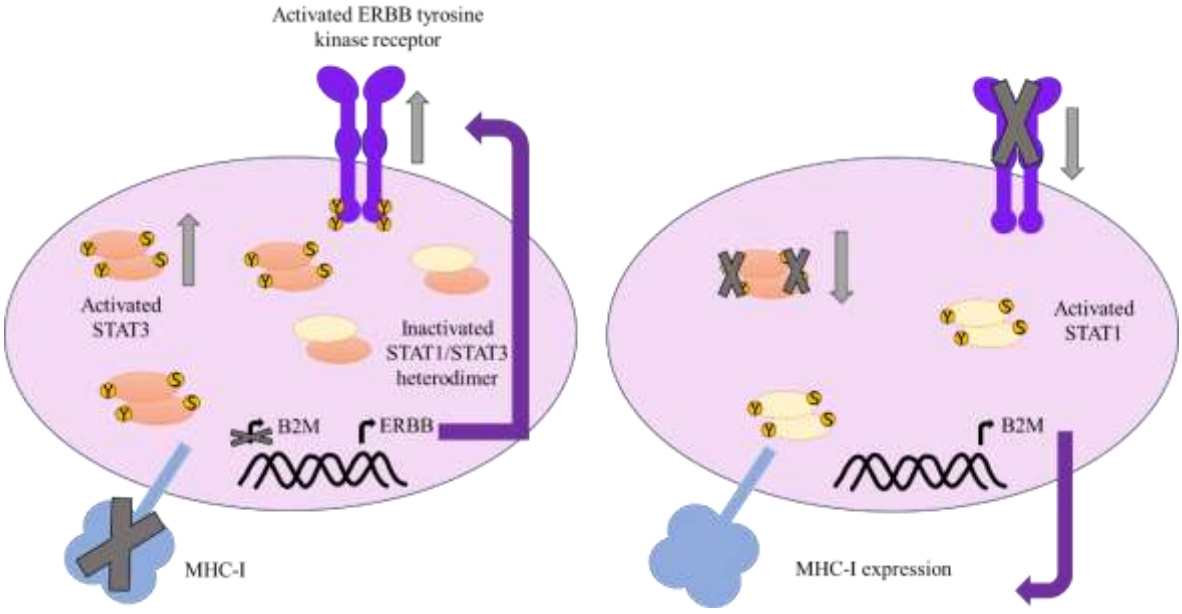

Figure 4: ERBB-STAT3 signaling axis in DFT1. The image was created using PowerPoint (Kosack et al., 2019).

2. Aim of the Master Thesis

DFT1 and DFT2 have caused a significant decline in the Tasmanian devil population in the last 30 years and without a better understanding and treatment options the Tasmanian devil will become extinct in the wild. Research on DFT1/2 is, however, not only important for species conservation but can help us to gain knowledge about human kinase driven cancers, cancer immune evasion and transmissible cancers in other species. The aim of this project is to further characterize DFT1/2 and to unravel key differences in cancer signaling between these two tumor cell lines. For this, drugs that specifically target DFT1 and DFT2 were validated, demonstrating their potential therapeutic effectiveness for further treatment. Considering these specific vulnerabilities, key players of the core cancer pathways were identified and analyzed for both cancers by *in vitro* methods such as RT-qPCR and Western blotting. Furthermore, combination treatments and resistance mechanisms were explored to investigate alternative pathways and signaling plasticity in one of the two transmissible cancers. Understanding plasticity within DFT is not only important for overcoming treatment resistance, but also provides perspectives into alternative pathways that may contribute to survival and immune evasion mechanisms. By advancing our knowledge of transmissible cancer, we can make progress towards conserving an endangered species and improving human health at the same time.

3. Material and Methods

3.1. Cell Culture

3.1.1. Cell line origins

All the cell lines were provided by Dr. Gregory Woods and Dr. Andy Flies from the University of Tasmania (Hobart, Australia). They were grown from primary cell cultures derived from fine needle aspirates collected from the wild (Table 3). DFT1 cell lines were established by A-M. Pearse and K. Swift of the Tasmanian Department of Primary Industries, Parks, Water and Environment (DPIPWE) under the approval of the Animal Ethics Committee of the Tasmanian Parks and Wildlife Service (permit numbers 33/2004-5 and 32/2005-6). DFT2 cell lines were established by A. Kreiss and R. Pye of Menzies Institute for Medical Research, University of Tasmania under the approval of the University of Tasmania Animal Ethics Committee (permit number A0012513) (Kreiss et al., 2011; Pearse & Swift, 2006; Pye et al., 2016).

Cell lines	Reference	Year of Collection
DFT1 Strain 1	(Deakin et al., 2012)	2006
DFT1 1426	(Siddle et al., 2013)	2005
DFT1 C5056	(Siddle et al., 2013)	2007
DFT2 Snug (SN)	(Pye et al., 2016)	2014
DFT2 Red Velvet (RV)	(Pye et al., 2016)	2014
DFT2 Jarvis (JV)	(Pye et al., 2016)	2015
Fibroblasts (FIBS)	(Murchison, et al., 2012)	-

Table 3: Cell lines used

3.1.2. Culture conditions

All cell lines were kept in T175 flasks (Sarstedt) at 37°C and 5% CO_2. DFT1 cell lines were kept in Roswell Park Memorial Institute Medium 1640 (RPMI 1640; Thermo Fisher Scientific) with 1% Penicillin-Streptomycin (Biowest), 1% L-Glutamine (Thermo Fisher Scientific) and 10% fetal calf serum (FCS; Thermo Fisher Scientific). DFT2 cell lines were grown in the same medium with the addition of AmnioMax (Thermo Fisher Scientific) and 50 µM beta-Mercaptoethanol. Fibroblasts were cultured in Dulbecco′s Modified Eagle′s Medium (DMEM; Thermo Fisher Scientific) with 10% FCS, 1% L-Glutamine and 1% Penicillin-Streptomycin.

3.1.3. Cell harvest

Cell harvesting for cell culture maintenance and experimentation for freezing was done under sterile conditions. After removing cell media, DFT1 cell lines were detached by rinsing them from the flask with Dulbecco's Phosphate Buffered Saline (PBS, Sigma Aldrich) or by using a cell scraper (Sarstedt). DFT2 cell lines were detached from the flask after incubation with 1 mM EDTA (PanReac AppliChem) in PBS for 5 minutes at 37°C and 5% CO_2. Fibroblasts were detached by chemical digestion using Trypsin EDTA (Thermo Fisher Scientific) for 5 minutes at 37°C and 5% CO_2. The detached cells were transferred into a Falcon tube and centrifuged for 5 min at 300 × g. The cells were washed in PBS once before further use.

3.1.4. Cell counting

The cells were counted using a 0,4% Trypan Blue solution and a Neubauer improved cell counting chamber. Briefly, 10 µl of the cell suspension were taken and mixed with 10 µl of Trypan Blue and pipetted between a counting chamber and the cover glass. Cells in 4 different grids were counted and the total cell number was calculated according to the formula below.

$$\frac{a1 + a2 + a3 + a4}{4} * 2\ (dilution\ factor) * 10^4 = \frac{cells}{ml}$$

3.2. Protein Analysis (Western Blot)

3.2.1. Preparation of Whole Extract (WCE) buffer

Whole cell extract buffer was prepared according to the Table 4) below and 1 ml aliquots were stored at -20°C.

Reagent	Volume [ml]
H_20	52,55
HEPES (pH 7,9/1 M)	2
Glycerol 87%	23
KCl (1 M)	5
EDTA (0,5 M)	0,2
NaCl (5 M)	8
Leupeptin (10 µg/ml)	0,05
Apoprotein (5 µg/ml)	0,1
PMSF (0,1 M)	1
Na_3VO_4	5
NaF	2
Beta-Glycerophosphate (0,5 M)	1
DTT	0,1

Table 4: Preparation of the Whole cell extract buffer

3.2.2. Cell lysis and protein isolation

After harvesting, cell pellets were resuspended in 30-50 µl whole cell extract buffer (WCE) depending on the size of the cell pellet (1× volume of the cell pellet). This suspension was vortexed, shock-frozen in liquid nitrogen and thawed 4 times. Afterwards, samples were centrifuged at 4°C at 16.000 × g for 15 minutes. The supernatant containing soluble proteins was transferred into fresh tubes, shock-frozen in liquid nitrogen and lysates were stored at -80°C.

3.2.3. Protein concentration measurement

The protein concentration was measured using Bradford reagent (Protein Assay Dye Concentrate, Bio-Rad), diluted 1:5 in ddH_2O water. The protein concentration was measured at a 595 nm absorbance with an Eppendorf Biophotometer plus. To create a standard curve, a Bovine Serum Albumin (BSA) dilution row of 16, 8, 4, 2 and 1 µg/ml in Bradford reagent was made. 1 µl of the lysates was then measured in 1 ml Bradford reagent and the protein concentration was determined by using linear equation of the standard curve.

3.2.4. Sample preparation

30 µg of protein in 20 µl lysis buffer were mixed with 4 µl loading dye (6× concentrated Laemmli-Buffer with 3% beta-Mercaptoethanol) (Table 5) and cooked 10 minutes at 95°C.

Reagent	Volume
DTT	2 g
SDS (20%)	4 ml
Tris-HCl (1M, pH 6,8)	1 ml
Glycerol	8 ml
Bromophenol-blue in H_2O	800 µl
dH_2O	20 ml

Table 5: Preparation of the loading dye (6x)

3.2.5. SDS-PAGE

Sodium dodecyl sulfate-polyacrylamide-gel electrophoresis (SDS-PAGE) was used to separate the proteins by their molecular weight. A 6% or 8% polyacrylamide running gel, depending on the size of the protein of interest, (Table 6) and the 5% stacking gel (Table 7) were made according to the table below.

Reagent	Volume 8% (ml)	Volume 6% (ml)
ddH_20	9,3	10,6
30% Acrylamide mix	5,3	4
Tris HCl (1,5 M, pH 8,8)	5	5
SDS (10%)	0,20	0,20
Ammonium persulfate (10%)	0,20	0,20
TEMED	0,012	0,016

Table 6: Preparation of the running gel (6% and 8%)

Reagent	Volume (ml)
ddH_20	3,4
30% Acrylamide mix	0,83
Tris HCl (1,5 M, pH 6,8)	0,63
SDS (10%)	0,05
Ammonium persulfate (10%)	0,02
TEMED	0,005

Table 7: Preparation of the stacking gel (5%)

For the gels water, acrylamide mix (Roth), Tris HCl, SDS (Roth) and APS (Sigma Aldrich) were mixed. After adding TEMED (Sigma Aldrich), the gel was pipetted into the apparatus. For smoothening of the surface of the running gel, 1 ml isopropanol (Roth) was added on top. Upon solidification the stacking gel was added, and a 1,5 mm 15-well comb was inserted. After polymerization, the gel was placed in a running module (Bio Rad) and running buffer (Table 8) was added.

Running buffer (1x), 2L	Volume (ml)
Tris-Glycine Buffer (10x)	200
dH_2O	1800
SDS (20%)	10

Table 8: Preparation of the running buffer for the Western Blot (1x)

The combs were removed and 20 µl of the prepared samples were loaded into the wells of the gel. 3 µl PageRuler Prestained Protein Ladder (Cat 26617, 10 to 180 kDa, Thermo Fisher Scientific) were used as protein marker. The gel ran for 20 minutes at 70 V and then at 120 V until the loading dye marking reached the bottom of the gel.

3.2.6. Protein transfer

The proteins were blotted on a nitrocellulose membrane (Thermo Fisher Scientific). For this, the membrane was activated in water before blotting. For the transfer, the membrane was placed on the gel, covered by two Whatman® papers and one foam pad on each side. The foam pads and the Whatman paper were soaked in transfer buffer (Table 9) before.

Then the cassette was put into a Criterion™ transfer system (Bio-Rad), which was filled with transfer buffer, in a way that proteins could migrate from the cathode (black) to the anode (red). Small proteins were transferred for 2 hours at 360 mA at 4°C, whereas bigger proteins (> 100 kDa) were transferred overnight at 120 mA at 4°C.

Transfer buffer (1×), 2L	Volume (ml)
Tris-Glycine Buffer (10×)	200
dH_2O	1400
Methanol	400

Table 9: Preparation of the Transfer buffer (1×)

3.2.7. Preparation of TBS and TBS-T

Reagent	TBS (10×), pH8
ddH_20	2000 ml
NaCl	175,32 g
Tris Base	121,14 g

Reagent	TBS [ml]	TBS-T [ml]
ddH_20	900	900
TBS (10×)	100	100
Tween	-	1

Table 10: Preparation of TBS and TBS-T

3.2.8. Immunodetection

The membrane was blocked for one hour at room temperature with a 5% BSA blocking solution. For the blocking solution 2,5 g of BSA (Roth) were diluted in 50 ml TBS-T. To increase the signal of ErbB3, a SuperSignal™ Western Blot Enhancer (Thermo Fisher Scientific) was used prior to the blocking following the recommended protocol provided by the manufacturer. After blocking, the membrane was incubated with primary antibodies diluted in TBS-T (Table 11) overnight at 4°C. Afterwards, the membranes were washed 3 times with TBS-T. Secondary antibodies (Table 12) were incubated in the dark for 2 hours at room temperature. The membrane was scanned using Odyssey Imaging Systems.

Primary Antibodies	Size [kDa]	Cat. No	Company	Species	Dilution
total STAT1	84/91	610115	BD Biosciences	mouse monoclonal	1:1.000
total STAT3	79,86	9139S	Cell Signaling	mouse monoclonal	1:1.000
pS-STAT3 (S727)	86	9134S	Cell Signaling	rabbit monoclonal	1:1.000
pY-STAT3 (Y705)	79,86	9131	Cell Signaling	rabbit polyclonal	1:1.000
total STAT5	92	610191	BD Biosciences	mouse monoclonal	1:1.000
HSC70	70	sc-7298	Santa Cruz	mouse monoclonal	1:5.000
anti-HER3/ERBB3	185	12708	Cell Signaling	rabbit monoclonal	1:1.000
anti-PDGFRα	195	ab124392	Abcam	rabbit polyclonal	1:1.000
anti-PDGFRβ	190	3169	Cell Signaling	rabbit monoclonal	1:1.000

Table 11: List of primary antibodies

Secondary antibodies	Cat. No	Company	Target	Species	Dilution
IRDye 680RD Goat anti-Mouse IgG	926-68070	LI-COR	anti-mouse	goat	1:10.000
IRDye 800CW Goat anti-Rabbit IgG	926-32211	LI-COR	anti-rabbit	goat	1:10.000

Table 12: List of secondary antibodies

3.2.9. Western Blot Quantification

Blotted proteins were quantified with ImageJ (1.53t) and visualized with GraphPad Prism (8.4.3). The quantification was based on the relative intensities of the protein bands normalized to the net intensities of their HSC70 loading control. The background signal was subtracted from the band signal to obtain the net intensity.

3.3. Gene Expression Analysis (RT-qPCR)

3.3.1. RNA isolation

To prevent RNA degradation, all equipment and gloves were cleaned with RNAse away spray (Molecular Bioproducts/ Thermo Fisher Scientific). Separated tips and tubes were used to avoid contamination. To isolate RNA from harvested cells, 750 µl TRIzol™ (Thermo Fisher Scientific) were added to a cell pellet of approximately 5-10 × 10^6 cells. After homogenization and 5 minutes incubation at room temperature, 150 µl of chloroform (Roth) were added. The samples were vortexed thoroughly and incubated at room temperature for 2-3 min. Next, the samples were centrifuged at 4°C and 12.000 × g for 15 min, which resulted in a 3-phase separation of the samples. The upper aqueous phase, containing the RNA, was pipetted off carefully and transferred into a fresh tube. 375 µl of 100% isopropanol (Roth) were added to the aqueous phase. The solution was mixed and incubated for 10 minutes at room temperature. Afterwards, the solution was centrifuged at 4°C and 12.000 × g for 15 min. The RNA pellet was washed in 500 µl 75% EtOH once (4°C and 12.000 × g for 5 min) and then dried at 55-60°C before resuspension in 30 µl RNase-free water. To clean the pellet from phenol contamination, 3 µl 3M Na-acetate (Thermo Fisher Scientific) and 90 µl 100% EtOH was added to the dissolved RNA and suspension was incubated over night at -80°C. On the next day, the samples were centrifuged at 4°C and full speed (16.000 × g) for 30 min. After centrifugation the supernatant was removed, and the visible RNA pellet was washed with cold 75% ethanol (4°C and 12.000 × g for 5 min). Ethanol was removed and the RNA pellet was dried 2-10 min on 55-60°C. The pellet was then resuspended in 30-50 µl RNAse free water and incubated 10-15 min at 55-56°C until completely dissolved.

3.3.2. RNA quantification

The RNA concentration of the samples was measured by using a Nanodrop (Thermo Fisher Scientific). The A260/280 ratio, indicating protein contamination, and the A260/230 ratio, indicating organic contamination, were between 1,9 and 2,1.

3.3.3. cDNA synthesis

For the cDNA synthesis, the RevertAid cDNA synthesis kit (Thermo Fisher Scientific) was used. The cDNA Master mix was prepared as shown in the following table (Table 13). 1 µg of RNA was resuspended in 11 µl nucleic acid free water. 9 µl of the master mix were then added to each sample. The RNA was converted to cDNA by using a thermocycler (Eppendorf), running 60 min on 42°C and 10 min on 70°C. The cDNA was diluted to 12,5 ng/µl (1:4) in nucleic acid free water and was stored at -20°C.

cDNA Master mix for 1 sample	Volume (µl)
5x Reaction buffer	4
RiboLock RNase inhibitor	1
10 mM dNTP Mix	2
RevertAid M-MuLV RT	1
Oligo dTs	1
Total	9

Table 13: Master mix preparation for one sample

3.3.4. RT-qPCR

For each sample 1 µl cDNA, containing 12,5 ng/µl cDNA, was mixed with 14 µl master mix (Table 14) in a transparent, low profile 96 well plate (Sarstedt). Primers used are shown in Table 16. Every sample was measured in triplicates and a no reverse transcription control (NRT; RNA not converted into cDNA) was included for every sample. For every target gene a no template control (NTC; nucleic acid free water) was included. On every plate, the expression of the housekeeping gene ribosomal protein L13a (RPL13A) was measured as reference gene. The plate was covered with a transparent plastic cover foil and shortly centrifuged before measuring the plate in a CFX96 Touch Real-Time PCR Detection System (Bio-Rad) with the protocol shown in Table 15.

Master Mix for 1 reaction	Volume (µl)
qPCR reagent	5
Forward primer (1:10 dilution)	2
Reverse primer (1:10 dilution)	2
Free DNAse Water	5
Total	14

Table 14: Master Mix preparation for one sample

	Temperature (°C)	Duration	Cycles
Polymerase Activation	95	2 minutes	1
Denaturation	95	15 seconds	40
Annealing and Extension	60	1 minute	
Melting Curve	65-95 in 0,5 steps	5 seconds / step	1

Table 15: RT-qPCR protocol

Primer		Sequence (5'->3')	Source
STAT1	Forward primer	CTAGCCTGCTCTGTGCCATC	NCBI Primer Blast
	Reverse primer	GCTTTTCCAACCAAGGTGCC	12.01.2023
STAT3	Forward primer	AGTTCAGGGGCTCAGATTGC	NCBI Primer Blast
	Reverse primer	TAGGGAAGTCAGCTGGTCCG	11.01.2023
STAT5B	Forward primer	TCAGCAGGTTGTGAACAATGGC	NCBI Primer Blast
	Reverse primer	CGATGGGGAAGTGCTGACC	11.01.2023
STAT6	Forward primer	CACCAGTATTCCCAGGACACC	NCBI Primer Blast
	Reverse primer	CCTGGGTGGAATCAGAACCTG	12.01.2023
PDGFRA	Forward primer	GAAACGAGAGGAGGAGACGGG	NCBI Primer Blast
	Reverse primer	CGGCCCTGTGAGGAGACATC	12.01.2023
PDGFRB	Forward primer	AGGCAATAAGAAAGGCAGGGAC	NCBI Primer Blast
	Reverse primer	GGGGGTTATCTTCAGTGCCTC	12.01.2023
ERBB3	Forward primer	ACCACAGGCCATCAGCAGTAAG	NCBI Primer Blast
	Reverse primer	TCTCACCCCGCTCCAAGTAG	12.01.2023
EGFR	Forward primer	GGACCTTCTTCGATCCGGTG	NCBI Primer Blast
	Reverse primer	AGGGAGAAATGTCCGGCAAG	12.01.2023
VEGFR-2	Forward primer	GCCAGTGCTCAACAGGATGG	NCBI Primer Blast
	Reverse primer	GAGGTCGGCAAAGAGAGTCC	12.01.2023
C-KIT	Forward primer	AAAGAACAAATCACCTCGCACAC	NCBI Primer Blast
	Reverse primer	CTGGACTTCATACATGGGTTTCTGG	16.01.2023
C-MYC	Forward primer	GGAAAAGCTGGCCTCCTACC	NCBI Primer Blast
	Reverse primer	CAAGTAGAGGCTGTGCGTCG	17.01.2023
SRC	Forward primer	CTTCCAGCTTATCTGTGTTTTGGC	NCBI Primer Blast
	Reverse primer	CGCCCCAATGCTACTTCCAG	11.01.2023
BTK	Forward primer	TTATGTCGTGTGCTCCACCC	NCBI Primer Blast
	Reverse primer	TCTCCCATGACCCATAGCCC	12.01.2023
MHC- I	Forward primer	CCGTGGGCTACGTGGACGATCAGC	(Siddle et al., 2013)
	Reverse primer	GTCGTAGGCGAACTGAAG	
TAP1	Forward primer	TGCCTCAGTATCAGCACCGGTATCTGC	(Siddle et al., 2013)
	Reverse primer	CTTCCATGACCTCCTCTAGCTCTGG	
TAP2	Forward primer	TGTGGGCTAAGGCAGATTCTGGCAGGG	(Siddle et al., 2013)
	Reverse primer	TCCCAGGAGGAGCTAAGCGTGG	
B2M	Forward primer	CTCCCAGAGTTCAGGTTTATTCCC	(Siddle et al., 2013)
	Reverse primer	AGGTTCTTTGAGGGTTGAATGGACC	
MDM2	Forward primer	TCATTCAGCCTCTTTGTGCCT	(Siddle et al., 2013)
	Reverse primer	ATGATGCACACAGTAAATGAGC	
MTOR	Forward primer	CAATGCAATGGAGGTGACCG	Anna Schönbichler
	Reverse primer	GTAGGAGTCTGTCCGCGTTC	
PI3K	Forward primer	GCCCGAGCGGAGCATTTTC	Anna Schönbichler
	Reverse primer	GCTGATCCTCTCCTTCTTGCT	
AKT1	Forward primer	CGGCTCTTCGCAGAATTGTT	Anna Schönbichler
	Reverse primer	TTCTCCTCGCTTATGCAGCC	

FLT-1	Forward primer Reverse primer	CACAGCACCATGCCTGAAAC AGTAACGGTGAAGTCTGGCG	Anna Schönbichler
FLT-4	Forward primer Reverse primer	AGAATGCAGGCACCTACACC ACCAGCTCCAGGCTGATTTC	Anna Schönbichler
RPL13A	Forward primer Reverse primer	CCCCACAAGACCAAGCGAGGC ACAGCCTGGTATTTCCAGCCAACC	(Siddle et al., 2013)

Table 16: Designed primers for RT-qPCR.

3.3.5. Data analysis

The obtained Ct values were analyzed using the Delta-Delta-Ct (ΔΔCt) method. The housekeeping gene RPL13a was used to normalize the Ct values of each sample. The data was visualized using GraphPad Prism (8.4.3).

3.4. Cell viability assays (Cytotoxicity assays)

To determine the half-maximal inhibitory concentrations (IC50) of clinically relevant drugs (Table 17) cytotoxicity assays were performed.

TKI	Target	Company	Cat No.
Imatinib	BCR/ABL, v-Abl, PDGFR, c-kit	MedChemExpress	HY-15463
Sapitinib	ErbB family	MedChemExpress	HY-13050
Saracatinib	Abl, src	Selleckchem	S1006
Ibrutinib	Bruton's tyrosine kinase (BTK)	MedChemExpress	HY-10997
Masitinib	Kit and PDGFRα/β	MedChemExpress	HY-10209
Crenolanib	PDGFRα/β	MedChemExpress	HY-13223
Cabozantinib	VEGFR2	Selleckchem	S1119
Dasatinib	Abl, src, c-kit		
Lapatinib	ErbB family	Adooq Biosciences	A10514
Sunitinib malate	VEGFR2 (Flk-1), PDGFRβ		
Tivozanib	VEGFR1/2/3	MedChemExpress	HY-10209

Table 17: TKI used for the Cytotoxicity Assay

3.4.1. Plate preparation

For the cytotoxicity assays transparent, flat bottom 96-well plates (Sarstedt) were used. The upper and the lower row were filled with PBS to ensure that the plates stayed humidified. Each drug was tested in triplicates as 10-point dose response curve (Figure 5). For this, 62,5 µl of the drug, suspended in medium at a 200 µM concentration, were pipetted into column 1. All other rows were filled with 50 µl medium. The drugs were diluted in a 1:5 serial dilution, transferring 12,5 µl from well to well, with the exception of the medium only wells in column 6. Column 12 was filled with 50 Bortezomib (MedChem Express) suspended in medium at a 20 µM concentration.

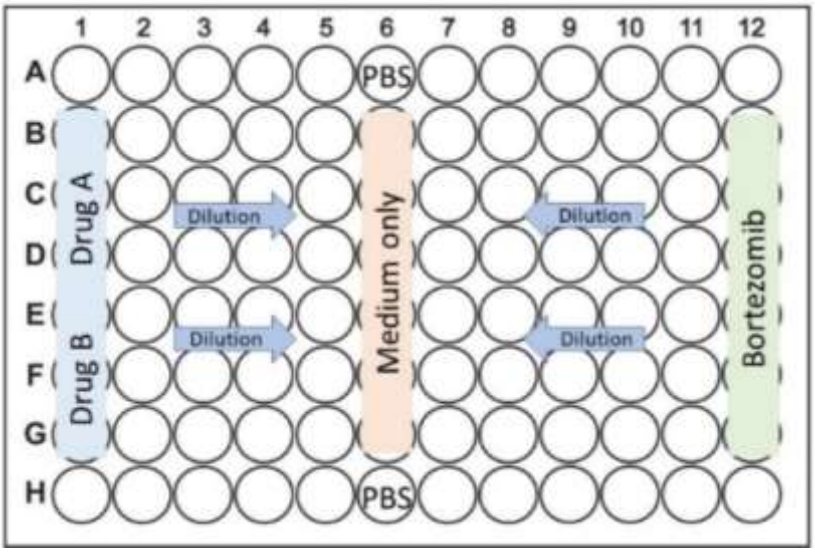

Figure 5: Template for Cytotoxicity Assay

3.4.2. Cell Seeding

Cells were harvested and resuspended in medium. To ensure confluence, the right cell seeding amount was determined in previous experiments and is shown in Table 18. 50 µl of cell suspension were added to each well, resulting in a 1:2 dilution of all drug concentrations.

Cell lines	Drugs	Wells (+extra)	µl per well	Number of cells
DFT1	2	80	50	$2{,}50*10^6$ in 5 ml
DFT2	2	80	50	$0{,}75*10^6$ in 5 ml
Fibroblasts	2	80	50	$1{,}50*10^6$ in 5 ml

Table 18: Number of cells for one Cytotoxicity plate

3.4.3. Measurement

After 72 hours, 20 µl of Celltiter Blue (diluted 1:5 in PBS; Promega) were added to every well. After 1-2 hours of incubation, the plates were measured using a GloMax Promega Plate reader. The measurement is based on the metabolism of resazurin to resorufin, which is a fluorescent end-product. IC50 values were determined using GraphPad Prism (Version 8.4.3) by determining the percentage of control (POC) with non-linear regression, setting the mean signal of the negative control wells (Bortezomib) to 0% and the mean signal of the medium only wells (column 6) to 100%.

3.5. Combination treatment experiments (Synergy)

To revealing potential synergistic interactions between clinically relevant drugs, we performed combination treatment experiments (Table 17). These assays aimed to uncover potential synergistic interactions between drugs providing valuable insights into combination therapies.

3.5.1. Plate preparation

For the synergistic assays transparent, two flat bottom 96-well plates (Sarstedt) were used. To maintain humidity, the right, and the left row of the first plate were filled with PBS. In the first plate, 31,25 µl of the first drug were pipetted into the starting column. The remaining wells were filled with 25 µl medium, except for the control column, which contained 50 µl RPMI. A 1:5 serial dilution of the drugs was performed by transferring 6,25 µl from well to well, following the provided Figure 6. The transfer and mixing process was progressed down the plate, with the 6,25 µl from the last column being discarded. For a 1:2 serial dilution row, the same procedure was followed, with 50 µl of the first drug being pipetted into the first column. The remaining wells were filled with 25 µl medium, and 25 µl of the drug were transferred.

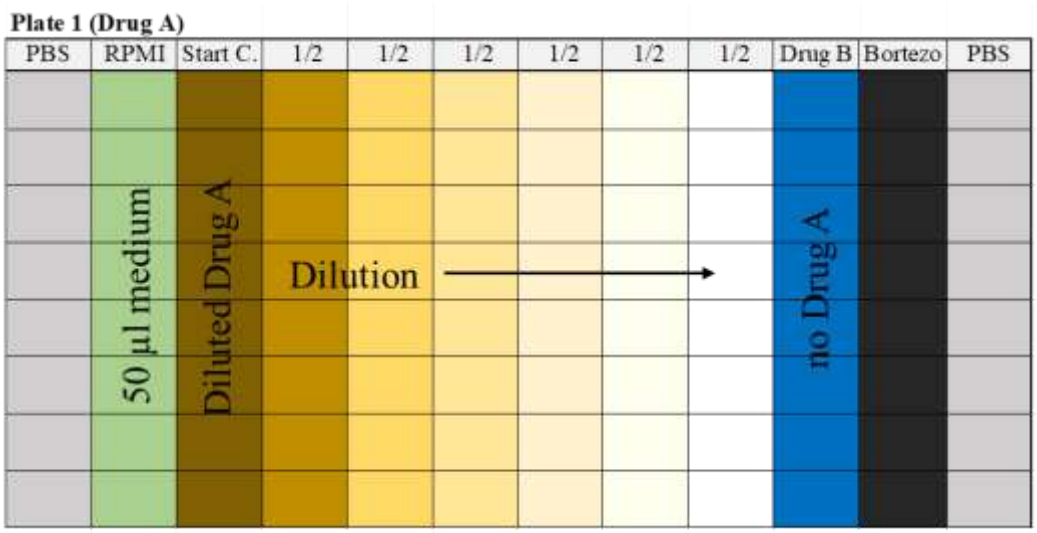

Figure 6: Layout of Plate A for Synergistic Assay

For the second plate the same procedure was repeated using the second drug and a different layout as shown in Figure 7. For a 1:5 dilution, 50 µl of the diluted drug were pipetted into the first row, with 10 µl being transferred into the other rows containing 40 µl of medium. The 10 µl for the last row were discarded. The volumes from the second plate were then transferred into the first plate, using 25 µl per well. For the last column of the first plate, media containing 50 µM Bortezomib was prepared and 50 µl were pipetted into the wells. Finally, 50 µl of the cell suspension were added to the rows after diluting the drugs.

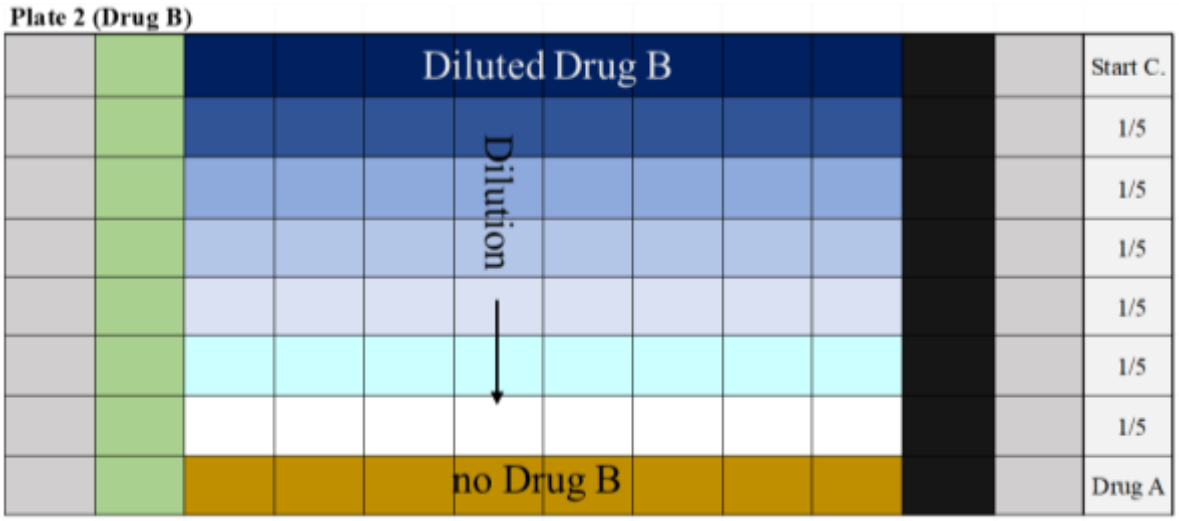

Figure 7: Layout of Plate B for Synergistic Assay

3.5.2. Measurement

After 72 hours, 20 µl of Celltiter Blue (diluted in 1:5 in PBS, Promega) were added to every well. After 12 hours of incubation, the plates were measured using a GloMax Promega Plate reader as described in chapter 3.4.3.

3.5.3. Data analysis

The data was analyzed by uploading the value matrix in SynergyFinder 3.0 application (Ianevski et al., 2022). The four-parameter logistic regression (LL4) was used as the curve-fitting algorithm. The degree of synergy was quantified using the Zero interaction potency (ZIP) model and the most synergistic area score (MSA) was used to compare different combination treatments with each other.

3.6. Generation of resistant DFT2 cell lines

To investigate whether DFT2 can be driven by alternative pathways, resistant cell lines were generated through gradual exposure of DFT2 cell lines Imatinib. To investigate whether DFT2 can be driven by alternative pathways, resistant cell lines were generated through gradual exposure of DFT2 cell lines to Imatinib. The experimental setup involved maintaining the cell lines DFT2 SN and DFT2 JV in small flasks and treating them with Imatinib. The control flask was treated with DMSO. To develop resistance, the drug concentrations were increased gradually over time. The treatment started with a concentration of 0,1 µM. As soon as the cells were confluent, the concentration was raised in steps of 0,05 µM for approximately 6 months until the cell lines showed a significance resistance towards Imatinib (see results). Resistant cell lines were analyzed with employing cytotoxicity assays, Western blotting, and RT-qPCR.

3.7. Statistics

For statistical analysis, a one-way ANOVA was performed comparing the mean of each column to the mean of every other column. For the statistical testing the Bonferroni test was used. The threshold for statistical significance was set to $P < 0,05$. P-value: < 0,05 (*), < 0,01 (**), < 0,001 (***), < 0,0001 (****). GraphPad Prism (8.4.3) was used for all statistics.

4. Results

To gain better understanding of transmissible cancer in the Tasmanian devil and explore treatment options, a drug screen including clinically relevant small molecule TKI was performed before the start of this study. This drug screen (Figure 8, Supplemental Table 1) revealed distinct vulnerabilities of DFT1 and DFT2. Specifically, it highlights the effectiveness of targeting PDGFRα/β, VEGFR1-3, Abl, c-Kit and the Src family in DFT2. In contrast, DFT1 was responsive to targeting the ERBB family and BTK. Bromodomain-containing proteins (BRD), Histone deacetylases (HDACs) and STAT3/5 are possible ways to target both DFT1 and DFT2 at the same time. The differences between both cancers that were revealed in this drug screen served as a base to this project. It should be noted that we mainly focused further on TKIs due to translational clinical aspects of best-tested drugs.

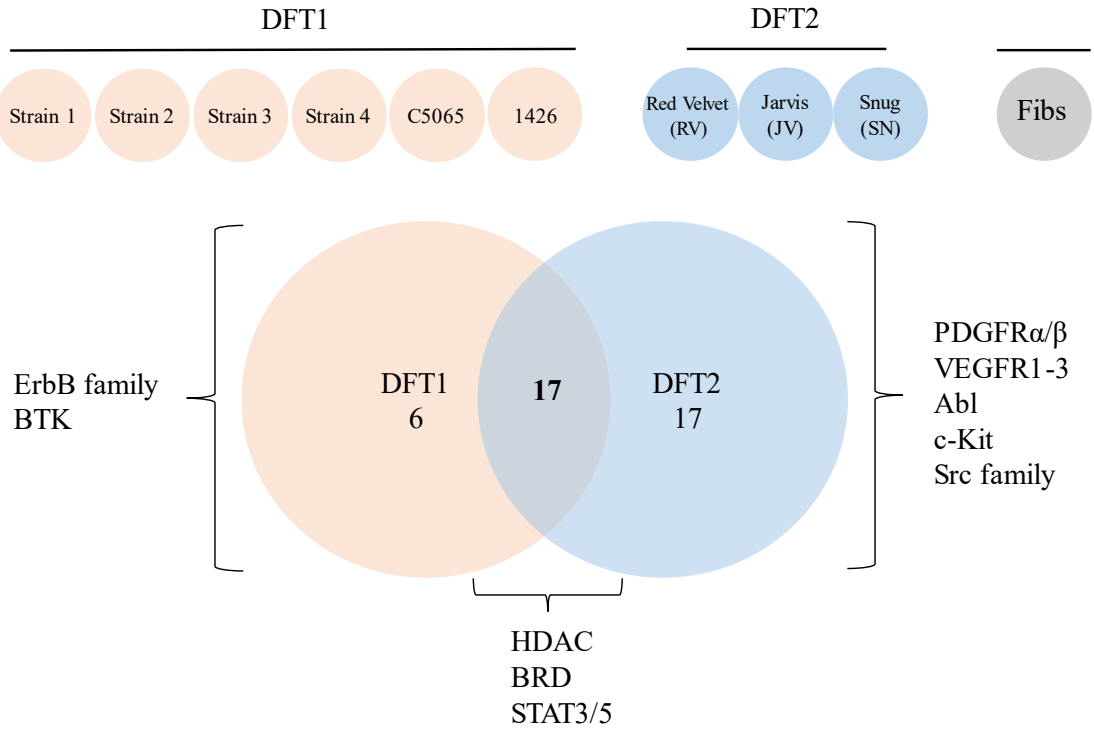

Figure 8: Recently performed TKI focused drug screen with DFT1, DFT2 and fibroblasts. The drug screen reveals the different vulnerabilities between DFT1 and DFT2. The blue circle indicates the vulnerabilities of DFT2, whereas the pink circle represents the vulnerabilities of DFT1. The intersection between both circles shows vulnerabilities that are shared by DFT1 and DFT2. The small circles underneath DFT1 and DFT2 indicate the specific cell lines that were used for this drug screen. For this drug screen, 6 DFT1 cell lines, 3 DFT2 cell lines and fibroblasts were used.

4.1. Pharmaceutical inhibition of DFT1 and DFT2 cells

To validate the findings from the drug screen, cytotoxicity assays using selected and clinically relevant drug hits were performed (Table 19). DFT1 cell lines, DFT2 cell lines and a healthy fibroblast control cell line were used for every assay. IC_{50} values, which serve as marker for the concentration of a substance required to inhibit the cells by 50%, were used to compare the sensitivity of the cell lines towards employed inhibitors (Aykul & Martinez-Hackert, 2016). The treatments duration amounted to 72 hours.

Inhibitor	Target	HITS
Imatinib	v-Abl, c-Kit, PDGFR	DFT2
Masitinib	c-Kit, PDGFRα/β	DFT2
Sunitinib malate	VEGFR-2, PDGFRβ	DFT2
Lapatinib	ERBB family inhibitor	DFT1
Sapitinib	ERBB family inhibitor	DFT1

Table 19: Selected clinically relevant drug hits for DFT1 and DFT2.

4.1.1. Sapitinib

First, the effect of Sapitinib, an ERBB receptor TKI, was validated. DFT1 cells showed high sensitivity to the ERBB inhibitor Sapitinib (Figure 9). Notably, DFT2 cells and the healthy fibroblasts were not as sensitive to ERBB inhibition and showed a >90-fold increase in their IC_{50} values compared to DFT1 cells. This finding confirms the significant involvement of ERBB receptors in DFT1 signaling pathways and suggests the RTK as a potential therapeutic target.

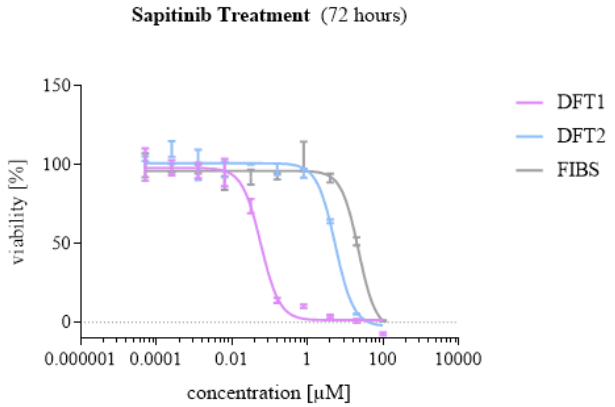

	DFT1	DFT2	FIBS
IC50 (µM)	0,06	5,46	22,47
fold change	1	91	>100

Figure 9: Cell viability and IC50 values/ fold change of DFT1 cells, DFT2 cells and healthy fibroblasts after 72h Sapitinib treatment. The graph shows one representative experiment with three technical replicates using DFT1 strain 1, DFT2 JV and fibroblasts. Error bars indicate the standard error of the mean. Dose response curves and IC_{50} values were calculated using nonlinear regression in GraphPad Prism. N=1.

4.1.2. Imatinib

For further characterization of the cell lines, they were additionally treated with Imatinib, a broad range TKI that also inhibits PDGFR. The treatment with Imatinib showed that DFT2 cells were significantly more sensitive to PDGFR inhibition compared to DFT1 cells and the fibroblasts (Figure 10). This is demonstrated by an IC_{50} fold change of 88 between DFT2 and DFT1. Since DFT2 is sensitive to Imatinib, the role of PDGFRs as key regulators in DFT2 signaling is highlighted. This and the importance of PDGFR signaling in cancer transmission will be further investigated in this thesis.

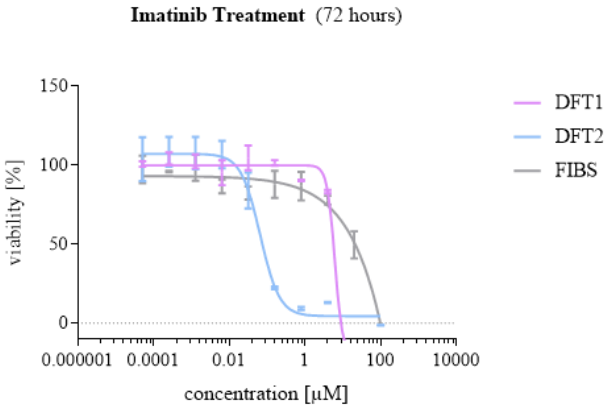

	DFT1	DFT2	FIBS
IC50 (µM)	6,17	0,07	>100
fold change	88	1	>100

Figure 10: Cell viability and IC50 values/ fold change of DFT1 cells, DFT2 cells and healthy fibroblasts after 72h Imatinib treatment. The graph shows one representative experiment with three technical replicates using DFT1 strain 1, DFT2 JV and fibroblasts. Error bars indicate the standard error of the mean. Dose response curves and IC50 values were calculated using nonlinear regression in GraphPad Prism. N=1.

4.1.3. Masitinib

Masitinib, just like Imatinib, is a PDGFR inhibitor, which additionally inhibits c-Kit and FGFR3. This assay revealed that DFT2 cells respond highly sensitive to the treatment with Masitinib, which is indicated by an IC_{50} of 0,01 (Figure 11). This heightened sensitivity to Masitinib further emphasizes the significance of PDGFR in DFT2 signaling mechanisms. The IC_{50} fold change greater than 100 indicates that DFT1 cells and fibroblasts exhibit lower sensitivity to this PDGFR inhibitor and PDGFR signaling in general.

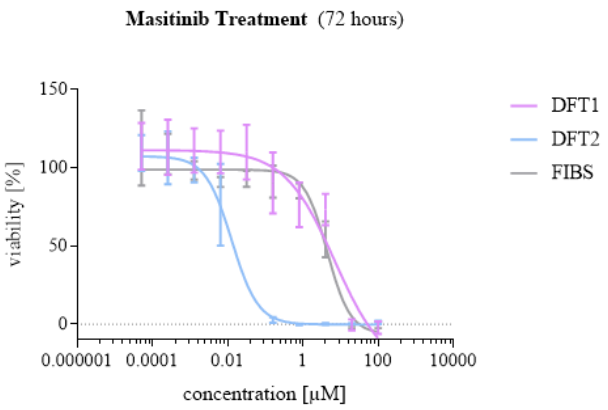

	DFT1	DFT2	FIBS
IC50 (µM)	7,03	0,01	4,44
fold change	>100	1	>100

Figure 11: Cell viability and IC50 values/ fold change of DFT1 cells, DFT2 cells and healthy fibroblasts after 72h Masitinib treatment. The graph shows one representative experiment with three technical replicates using DFT1 strain 1, DFT2 JV and fibroblasts. Error bars indicate the standard error of the mean. Dose response curves and IC50 values were calculated using nonlinear regression in GraphPad Prism. N=1.

4.1.4. Sunitinib malate

Sunitinib is a multi-targeted RTK inhibitor that targets VEGFR and PDGFR. DFT2 exhibited a significantly higher sensitivity to Sunitinib with an IC50 of 0,008 (Figure 12) than other cell lines in this assay. DFT1 cells and FIBS were less sensitive, which is indicated by a fold change greater than 100 compared to DFT2. Imatinib, Masitinib and Sunitinib are RTKIs that target PDGFR, and all selectively target DFT2 cells, highlighting the importance of PDGFR in the context of DFT2 signaling, which seems to be of lesser importance in DFT1 cells.

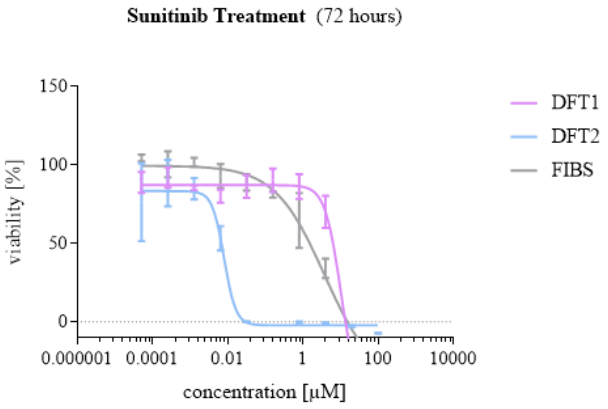

	DFT1	DFT2	FIBS
IC50 (µM)	9,96	0,008	3,74
fold change	>100	1	>100

Figure 12: Cell viability and IC50 values/ fold change of DFT1 cells, DFT2 cells and healthy fibroblasts after 72h Sunitinib treatment. The graph shows one representative experiment with three technical replicates using DFT1 strain 1, DFT2 JV and fibroblasts. Error bars indicate the standard error of the mean. Dose response curves and IC50 values were calculated using nonlinear regression in GraphPad Prism. N=1.

4.1.5. Lapatinib

Lapatinib is a dual RTK inhibitor which targets EGFR and ERBB2. As seen in Figure 13 DFT1 demonstrated sensitivity to treatment with Lapatinib evidenced by an IC_{50} of 0,03 in this assay. DFT2 exhibited reduced sensitivity with an IC_{50} of 1,18. This finding highlights the importance of ERBB family members in the core cancer signaling pathways of DFT1, which could not be observed in DFT2 cells in these assays.

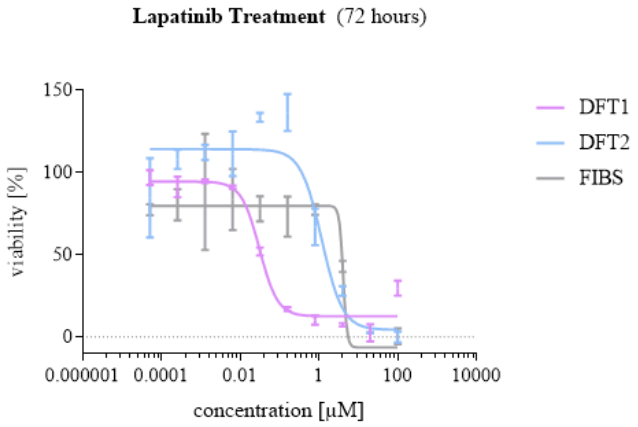

	DFT1	DFT2	FIBS
IC50 (µM)	0,03	1,18	4,1
fold change	1	39	>100

Figure 13: Cell viability and IC50 values/ fold change of DFT1 cells, DFT2 cells and healthy fibroblasts after 72h Lapatinib treatment. The graph shows one representative experiment with three technical replicates using DFT1 1426, DFT2 JV and fibroblasts. Error bars indicate the standard error of the mean. Dose response curves and IC50 values were calculated using nonlinear regression in GraphPad Prism. N=1.

4.2. Analysis of core cancer pathways in DFT1 and DFT2 cells

Because DFT1 and DFT2 responded to distinct tyrosine kinase inhibitors, we analyzed target proteins and possible downstream signaling partners to characterize core cancer signaling in both cancers. To investigate the involvement of these targets in DFT1 and DFT2, their gene expression levels were analyzed via RT-qPCR and protein expression levels were analyzed via Western blotting.

4.2.1. RTK expression

4.2.1.1. ERBB family

Following the findings from the cytotoxicity studies, which indicate that DFT1 cells are sensitive to the ERBB inhibitions, we decided to investigate the expression levels of ERBB family members in both cancers. Notably, it was shown by Kosack et al. that *ERBB3* expression is upregulated in DFT1 cells (Kosack et al., 2019). These results could be replicated in the presented RT-qPCR analysis. Surprisingly, the analysis showed even higher *ERBB3* gene expression levels in DFT2 cells compared to DFT1 cells and the fibroblasts (Figure 14C).

The Western blot analysis revealed that also protein expression levels of ERBB3 were higher in DFT1 cells compared to fibroblasts (Figure 14A/B) and confirmed even higher expression levels in DFT2 compared to DFT1. This finding suggests the importance of ERBB3 in the cancer signaling pathways of both DFT1 and DFT2 but raises the question why only DFT1 cells show vulnerability towards ERBB inhibition.

Further exploration of the molecular profiles of DFT1 and DFT2 to unravel key mechanisms underlying their respective pathogenic processes is needed. Another member of the ERBB family is the Epidermal Growth Factor Receptor (EGFR), which is an important transmembrane protein that is necessary for cell growth, proliferation, and survival. The overexpression or activation of EGFR can be found in various cancer types, making this receptor tyrosine kinase an important therapeutic target (Kurata et al., 2014). The RT-qPCR analysis revealed that *EGFR* is expressed much higher in the fibroblasts compared to DFT1 and DFT2 cells (Figure 14D). Both DFT1 and DFT2 showed minimal expression of *EGFR,* and this suggest a limited role of this RTK in the cancers.

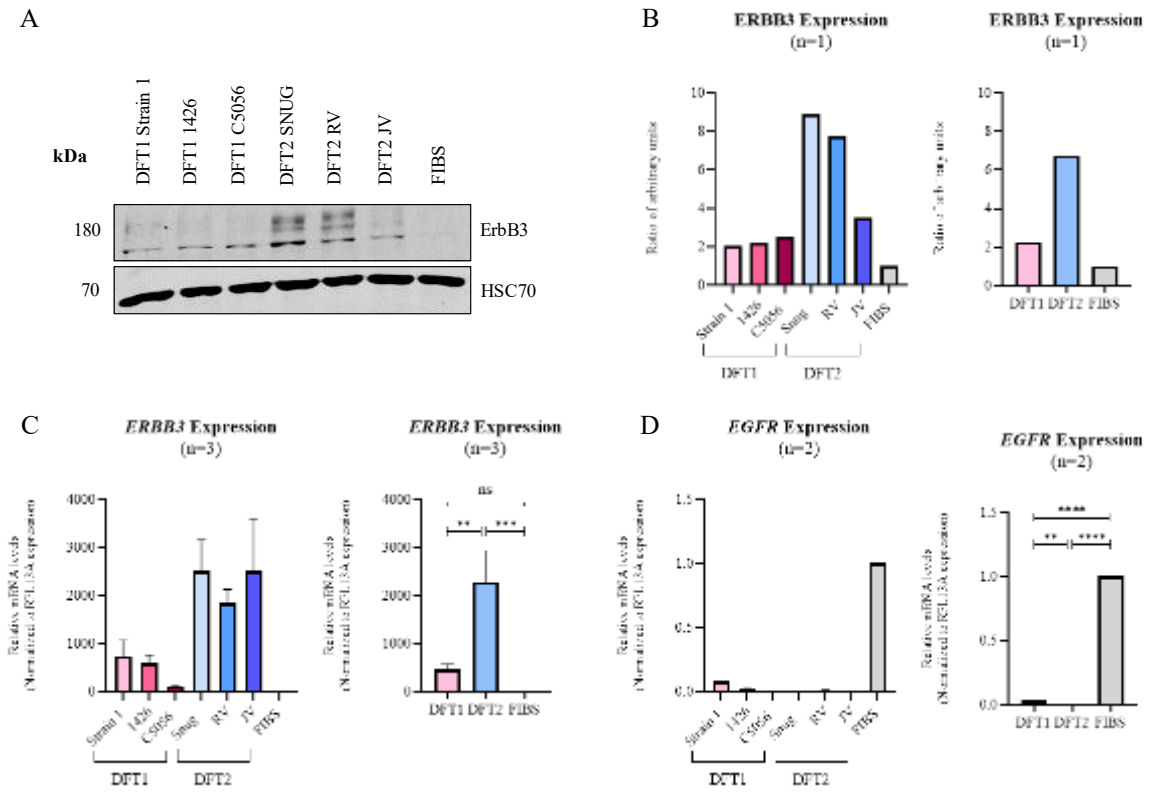

Figure 14: ERBB family Gene and Protein Expression Analysis. (A) Representative Western blot analysis showing basal ERBB3 protein expression levels in DFT1 strain 1, DFT1 1426, DFT1 C5056, DFT2 Snug, DFT2 RV, DFT2 JV and fibroblasts. HSC70 was used as loading control (n=1). (B) Quantification of representative Western blot showing ERBB3 protein expression levels (n=1). (C-D) Relative *ERBB3* (n=3) and *EGFR* (n=2) gene expression in DFT1 strain 1, DFT1 1426, DFT1 C5056, DFT2 Snug, DFT2 RV, DFT2 JV and fibroblasts was determined via RT-qPCR. *RPL13A* was used as a housekeeping gene for normalization. The ΔΔCt-Method was used to calculate the relative fold gene expression. The error bars indicate the standard error of the mean. To determine statistical significance a two-way ANOVA with Bonferroni comparison was performed. ns = non-significant, * = p-value < 0.05, *** = p-value < 0.001, **** = p-value < 0.0001. The statistical analysis for the graphs depicting all cell lines is available in the supplements (Supplemental Table 2).

4.2.1.2. PDGFR

Because cytotoxicity assays revealed that DFT2 is highly sensitive to PDGFR inhibitors like Imatinib, Masitinib and Sunitinib, the PDGFR expression levels were validated on mRNA and protein levels. PDGFR expression and activation was suggested to be of high significance in DFT cancer signaling, since it was previously shown that DFT2 possesses gene duplications of *PDGFRA* in its genome, whereas DFT1 demonstrates copy number gains of *PDGFRB* (Stammnitz et al., 2018). Overall, PDGFRs are important RTKs that plays a key role in mediating cell growth, proliferation, and differentiation. As seen in Figure 15**,** significant differences in PDGFR expression levels could be observed between DFT1 and DFT2. RT-qPCR analysis revealed higher gene expression of *PDFRB* in DFT1 (Figure 15E) and higher levels of *PDGFRA* in DFT2 (Figure 15D). Consistent with these findings, DFT1 showed an elevated protein expression of PDGFRβ, whereas DFT2 exhibited an increased PDGFRα expression (Figure 15A-C). These findings demonstrate the crucial role of PDGFR signaling in DFT, but the differential upregulation of the two PDGFR forms alpha, and beta imply that the molecular signatures between DFT1 and DFT2 are distinct. The fact that only DFT2 showed vulnerability towards PDGFR inhibition underscores this difference and highlights the need for further investigation of driver pathways in both cancers.

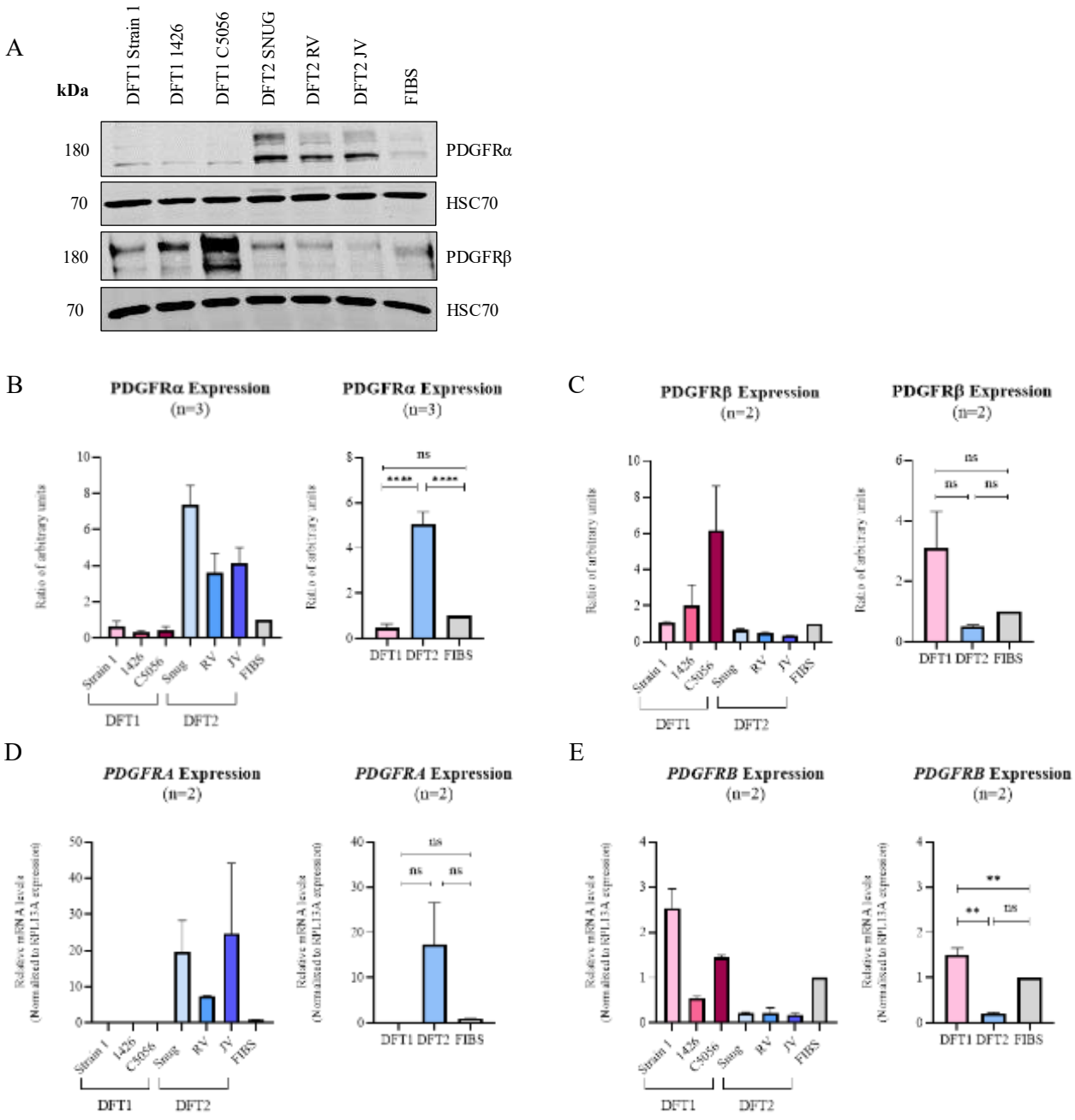

Figure 15: PDGFR Gene and Protein Expression Analysis. (A) Representative Western blot analysis showing basal PDGFRα and PDGFRβ protein expression levels in DFT1 strain 1, DFT1 1426, DFT1 C5056, DFT2 Snug, DFT2 RV, DFT2 JV and fibroblasts. HSC70 was used as loading control (n=1). (B-C) Quantification of representative Western blot showing PDGFRα (n=3) and PDGFRβ (n=2) protein expression levels. (C-D) Relative *PDGFRA* (n=2) and *PDGFRB* (n=2) gene expression in DFT1 strain 1, DFT1 1426, DFT1 C5056, DFT2 Snug, DFT2 RV, DFT2 JV and fibroblasts was determined via RT-qPCR. *RPL13A* was used as a housekeeping gene for normalization. The ΔΔCt-Method was used to calculate the relative fold gene expression. The error bars indicate the standard error of the mean. To determine statistical significance a two-way ANOVA with Bonferroni comparison was performed. ns = non-significant, * = p-value < 0.05, *** = p-value < 0.001, **** = p-value < 0.0001. The statistical analysis for the graphs depicting all cell lines is available in the supplements (Supplemental Table 3).

4.2.1.1. VEGFR

Due to the evolutionary and structural proximity of VEGFR and PDGFR, which are consequently also targeted by some of the employed TKI in this study, gene expression of these VEGFR was investigated (Shibuya, 2011). A low expression of *KDR* was observed in DFT1 and DFT2 compared to fibroblasts (Figure 16A). Additionally, the expression of *FLT-1* was observed to be lower in DFT1 and DFT2 in comparison to the fibroblasts (Figure 16B). *FLT-4,* on the other hand, exhibits significantly higher expression levels in DFT1 and DFT2 compared to the fibroblasts (Figure 16C). These results suggest that at least some VEGFR forms could be of importance in DFT, together with PDGFR signaling. Whether DFT1 and DFT2 employ these RTKs in a different level is still to be investigated.

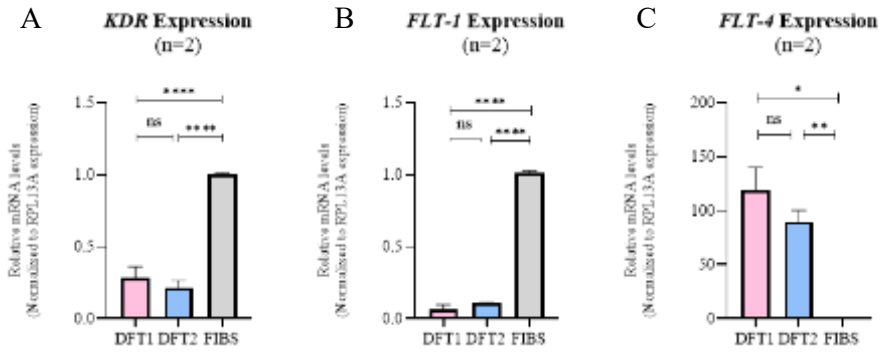

Figure 16: *VEGFR* Gene Expression Analysis. (A-C) Relative *KDR* (n=2), *FLT-1* (n=2) and *FLT-4* gene expression in DFT1 cells, DFT2 cells and fibroblasts was determined via RT-qPCR. *RPL13A* was used as a housekeeping gene for normalization. The ΔΔCt-Method was used to calculate the relative fold gene expression. The error bars indicate the standard error of the mean. To determine statistical significance a two-way ANOVA with Bonferroni comparison was performed. ns = non-significant, * = p-value < 0.05, *** = p-value < 0.001, **** = p-value < 0.0001.

4.2.2. STAT downstream signaling

ERBB and PDGFR receptor expression is significantly upregulated in DFT1 and DFT2. Since RTKs frequently signal via STAT transcription factors and STAT3 was shown to be a prominent driving force in DFT1, we decided to examine the expression levels of different STAT molecules. STAT1 is a key player in the JAK-STAT signaling pathway and is important in mediating immune response. In cancer, interactions between STAT1 and STAT3 have been observed, affecting both immune response and tumor progression. Specifically, in DFT1 it was demonstrated that elevated levels activated STAT3, which can capture STAT1, thereby facilitating immune evasion (Kosack et al., 2019). STAT5 is a transcription factor that can be activated by PDGFR. All three transcription factors play prominent roles in cell growth, differentiation, and survival in human cancers (Sumiyoshi et al., 2016).

To investigate the involvement of the above-mentioned STATs in DFT1 and DFT2, their gene expression levels were analyzed via RT-qPCR and protein expression and activation levels were analyzed via Western blotting.

4.2.2.1. STAT3

As seen in Figure 17, DFT1 cell lines exhibit elevated levels in total and phosphorylated STAT3 compared to DFT2 cell lines and fibroblasts. Both serine and tyrosine phosphorylation of STAT3 were investigated to assess the activation levels. The RT-qPCR results further validate the upregulation of *STAT3* gene expression in DFT1 compared to DFT2 and fibroblasts (Figure 17E). These findings underscore the significant role of STAT3 in the signaling of DFT1. This supports the finding that DFT1 is driven by an STAT3 axis, which was previously published by Kosack et al. in Cancer Cell (Kosack et al., 2019). More importantly, however, this analysis demonstrates that DFT2 is not as much driven by STAT3 expression and activation, but its activity status is clearly detectable. This suggests that it could become active since it autoregulates itself.

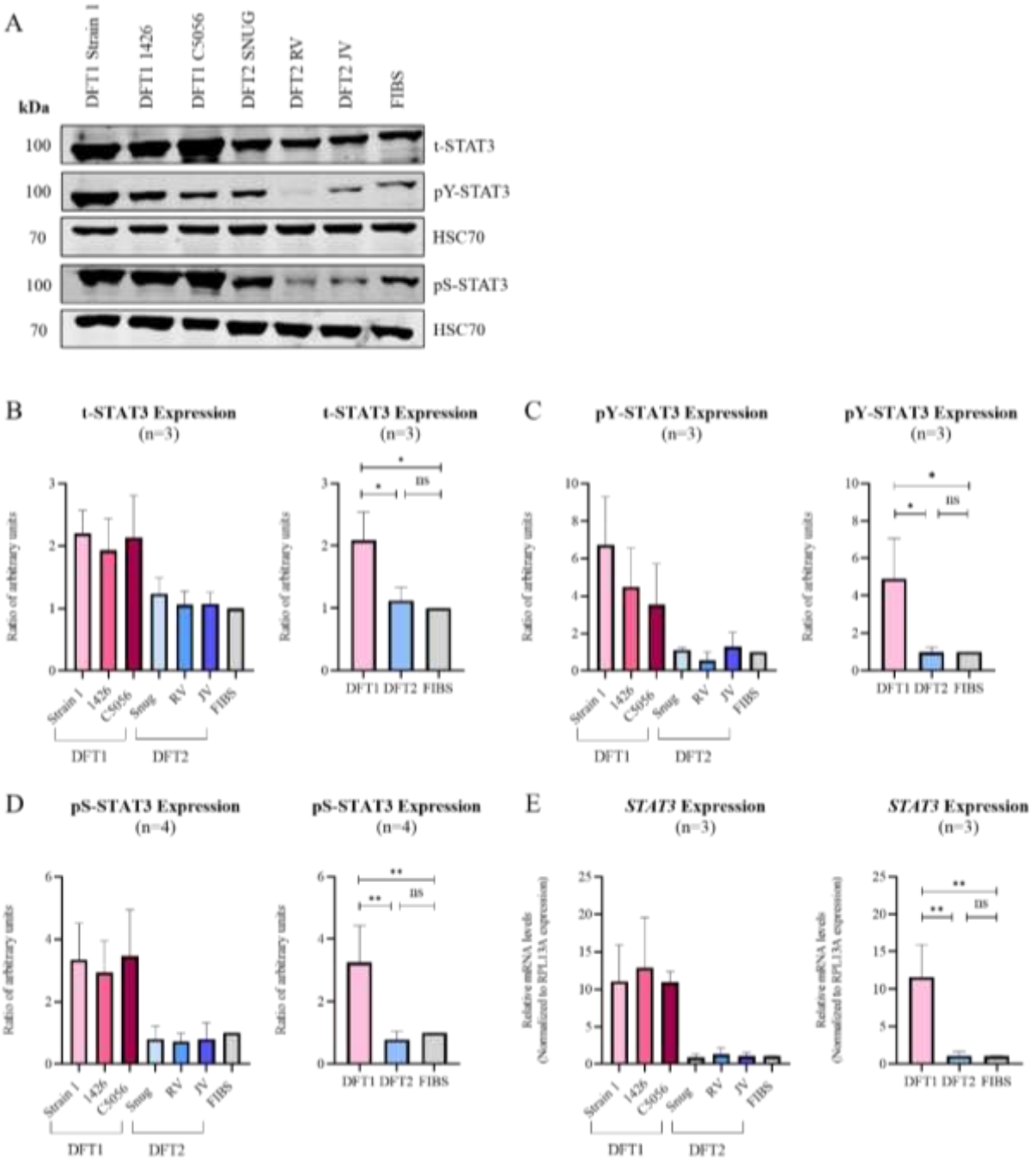

Figure 17: STAT3 Gene and Protein Expression Analysis. (A) Representative Western blot analysis showing basal t-STAT3, pS-STAT3 and pY-STAT3 protein expression levels in DFT1 strain 1, DFT1 1426, DFT1 C5056, DFT2 Snug, DFT2 RV, DFT2 JV and fibroblasts. HSC70 was used as loading control (n=1). (B-D) Quantification of representative Western blot showing t- STAT3 (n=3), pY-STAT3 (n=3) and pS-STAT3 (n=4) protein expression levels. (E) Relative *STAT3* (n=3) gene expression in DFT1 strain 1, DFT1 1426, DFT1 C5056, DFT2 Snug, DFT2 RV, DFT2 JV and fibroblasts was determined via RT-qPCR. *RPL13A* was used as a housekeeping gene for normalization. The ΔΔCt-Method was used to calculate the relative fold gene expression. The error bars indicate the standard error of the mean. To determine statistical significance a two-way ANOVA with Bonferroni comparison was performed. ns = non-significant, * = p-value < 0.05, *** = p-value < 0.001, **** = *p*-value < 0.0001. The statistical analysis for the graphs depicting all cell lines is available in the supplements (Supplemental Table 5).

4.2.2.2. STAT5

As seen in Figure 18, all cell lines express a form of STAT5. Due to the uncertainty of a STAT5A gene product, primers were designed for STAT5B only. Notably, STAT5A in the Tasmanian devil is marked as a low-quality protein (NCBI Pubmed). The RT-qPCR results showed that *STAT5B* gene expression is upregulated in DFT2 in comparison to DFT1 and fibroblasts (Figure 18C). Also, STAT5 protein levels were higher in DFT2 cell lines compared to DFT1 cell lines and fibroblasts. These results imply the involvement of STAT5 in the DFT2 cancer signaling network, which could be activated by hyperactive PDGFRα. Further, this supports the hypothesis that both tumors are driven by different core cancer pathways and highlights the importance of further investigation of STAT5 expression and activation in DFT2 pathogenesis.

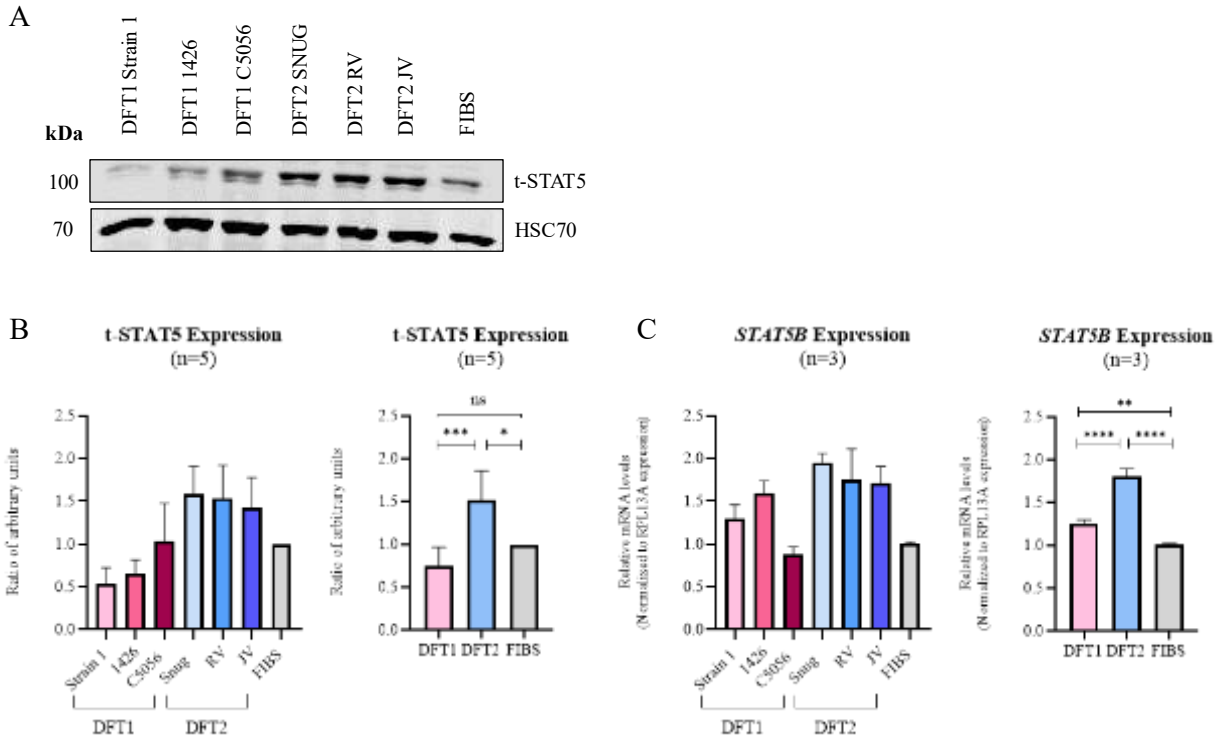

Figure 18: STAT5 Gene and Protein Expression Analysis. (A) Representative Western blot analysis showing basal t-STAT5 protein expression levels in DFT1 strain 1, DFT1 1426, DFT1 C5056, DFT2 Snug, DFT2 RV, DFT2 JV and fibroblasts. HSC70 was used as loading control (n=1). (B) Quantification of representative Western blot showing t- STAT5 (n=5) protein expression levels. (C) Relative STAT5B (n=3) gene expression in DFT1 strain 1, DFT1 1426, DFT1 C5056, DFT2 Snug, DFT2 RV, DFT2 JV and fibroblasts was determined via RT-qPCR. RPL13A was used as a housekeeping gene for normalization. The ΔΔCt-Method was used to calculate the relative fold gene expression. The error bars indicate the standard error of the mean. To determine statistical significance a two-way ANOVA with Bonferroni comparison was performed. ns = non-significant, * = p-value < 0.05, *** = p-value < 0.001, **** = p-value < 0.0001. The statistical analysis for the graphs depicting all cell lines is available in the supplements (Supplemental Table 4).

4.2.2.3. STAT1

STAT1 is a protein that plays an important role in the JAK-STAT pathway. As mentioned above, STAT1 is also known to have a crucial function in the immune evasion strategy of DFT1. It was shown that inactivated STAT1 can be captured by activated STAT3, resulting in the inhibition of transcriptional regulation of STAT1 downstream target genes like B2M (Kosack et al., 2019). Gene expression analysis showed that the expression of *STAT1* is also lower in DFT1 and DFT2 in comparison to the fibroblasts (Figure 19C). This indicates that similar immune evasion mechanisms as seen in DFT1 could evolve in DFT2 over time. The protein expression results, however, showed that STAT1 was present in a lower level in DFT1, compared to DFT2 and fibroblasts (Figure 19B). This goes hand in hand with the observation that MHC expression remains intact on most DFT2 cells.

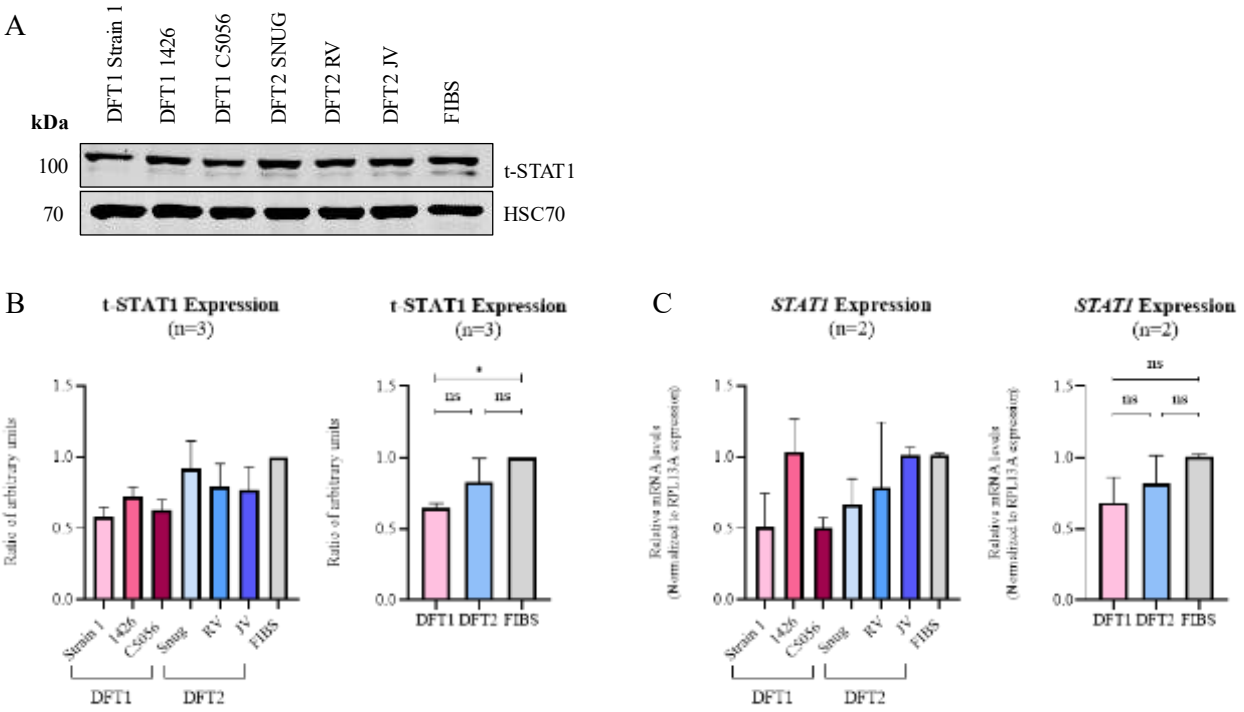

Figure 19: STAT1 Gene and Protein Expression Analysis. (A) Representative Western blot analysis showing basal t-STAT1 protein expression levels in DFT1 strain 1, DFT1 1426, DFT1 C5056, DFT2 Snug, DFT2 RV, DFT2 JV and fibroblasts. HSC70 was used as loading control (n=1). (B) Quantification of representative Western blot showing t- STAT1 (n=*3*) protein expression levels. (C) Relative *STAT1* (n=*2*) gene expression in DFT1 strain 1, DFT1 1426, DFT1 C5056, DFT2 Snug, DFT2 RV, DFT2 JV and fibroblasts was determined via RT-qPCR. *RPL13A* was used as a housekeeping gene for normalization. The ΔΔCt-Method was used to calculate the relative fold gene expression. The error bars indicate the standard error of the mean. To determine statistical significance a two-way ANOVA with Bonferroni comparison was performed. ns = non-significant, * = p-value < 0.05, *** = p-value < 0.001, **** = p-value < 0.0001. The statistical analysis for the graphs depicting all cell lines is available in the supplements (Supplemental Table 4).

4.2.3. MHC signaling

After exploring the differences in RTK and STAT gene and protein expression levels in DFT1 and DFT2 and establishing a possible connection between the observed differences and immune escape via MHC expression, genes connected to this pathway were analyzed. MHC signaling is important for understanding immune responses within these tumors. It has been demonstrated that the interplay between STAT3 and STAT1 in DFT1 leads to immune evasion by blocking the transcriptional regulation of STAT1 downstream target genes. DFT1 shows a hemizygous deletion of B2M, which is a stabilizing component of MHC class I, and this potentially leads to the observed downregulation of MHC in DFT1. In DFT2, both copies of B2M remain intact. These differences between DFT1 and DFT2 strengthen the theory that they imply different immune evasion strategies (Kosack et al., 2019; Stammnitz et al., 2018).

The RT-qPCR results showed a lower expression of *MHC-I* in DFT1 and DFT2 compared to the fibroblasts (Figure 20A). *B2M* levels are upregulated in DFT2 compared to DFT1. However, the expression of *B2M* in DFT2 is lower compared to the healthy fibroblasts (Figure 20B). This supports the notion that DFT2 will follow the trend of downregulating MHCI as a means of immune escape in the course of DFT2 evolution. TAP1 and TAP2 are proteins involved in the MHC class I antigen presentation pathway. These proteins play a crucial role in the immune system by facilitating the transport of antigenic peptides into the ER, where they can then bind to MHC class I molecules. Strikingly, TAP1 expression is significantly reduced in DFT1 and DFT2 compared to the levels observed in fibroblasts (Figure 20C). *TAP2* exhibits elevated expression levels in DFT2 compared to DFT1, where its expression is extremely low (Figure 20D).

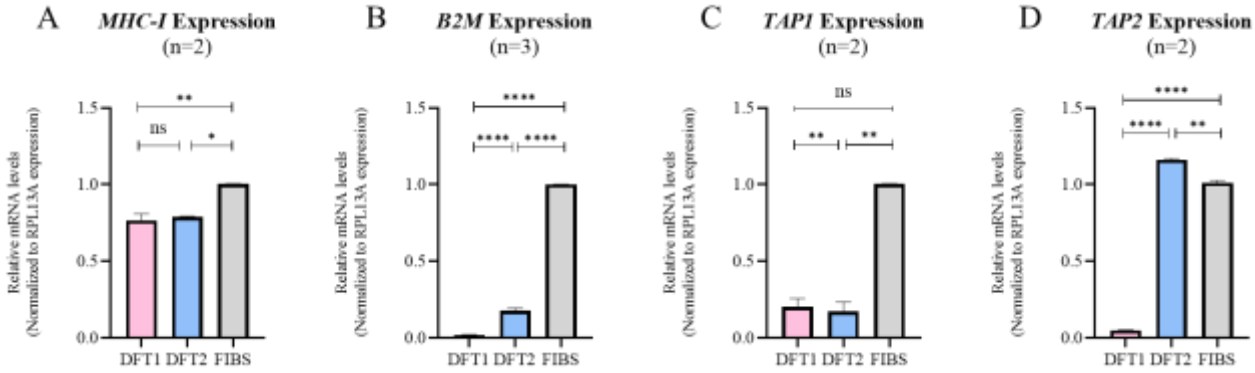

Figure 20: Immune Gene Expression Analysis. (A-D) Relative *MHC- I* (n=2), *B2M* (n=3), *TAP1* (n=2), *TAP2* (n=2) gene expression in DFT1 cells, DFT2 cells and fibroblasts was determined via RT-qPCR. *RPL13A* was used as a housekeeping gene for normalization. DFT1 consists of the mean value of DFT1 strain 1, DFT1 1426, DFT1 C5056 and DFT2 cells of the mean value of DFT2 Snug, DFT2 RV, DFT2 JV. The ΔΔCt-Method was used to calculate the relative fold gene expression. The error bars indicate the standard error of the mean. To determine statistical significance a two-way ANOVA with Bonferroni comparison was performed. ns = non-significant, * = p-value < 0.05, *** = p-value < 0.001, **** = p-value < 0.0001.

4.3. Combination treatment in DFT2 cells

The unexpected upregulation of ERBB3 in DFT2 cells, in addition to PDGFRα upregulation, which is their hypothesized main vulnerability, suggests potential signaling plasticity and resistance towards drug treatment. To explore this, combination treatments targeting different RTK at the same time were performed. Synergistic interactions between different drugs may suggest the existence of alternative pathways that can be targeted to improve therapeutic efficacy. These assays are therefore not only a powerful method for optimizing treatment approaches, but also for uncovering pathways that may act as alternative routes for cell survival and proliferation. One of the key advantages of synergies is to overcome resistance mechanisms that can arise due to mutations in the core cancer pathways (Tallarida, 2011).

4.3.1. Imatinib and Sapitinib Combination Treatment

Imatinib is a TKI that mainly targets PDGFR while the TKI Sapitinib targets ERBB proteins. Combining both drugs when treating DFT2 cells unveiled only weak synergistic interactions. Using SynergyFinder 3.0 as a read-out application, MSA scores around 10 were calculated (Table 20). Scores below 10 imply drug additivity, whereas scores greater than 10 indicate synergy (Ianevski et al., 2022). Here, the observed weak synergistic effect supports the suggested main reliance of DFT2 cells on a PDGFRα axis. PDGFR inhibition might be so effective in killing the cancer cells that simultaneous ERBB inhibition might not heighten the cytotoxicity. A maximum inhibition capacity might be reached with Imatinib treatment alone.

Cell Line	Most Synergistic Area Score
DFT2 Snug	13,90 (n=4)
DFT2 RV	12,04 (n=3)
DFT2 JV	12,50 (n=2)

Table 20: The representative Synergistic Assay assesses the interaction between Imatinib and Sapitinib across DFT2 cell lines Snug (n=4), RV (n=3) and JV (n=2).

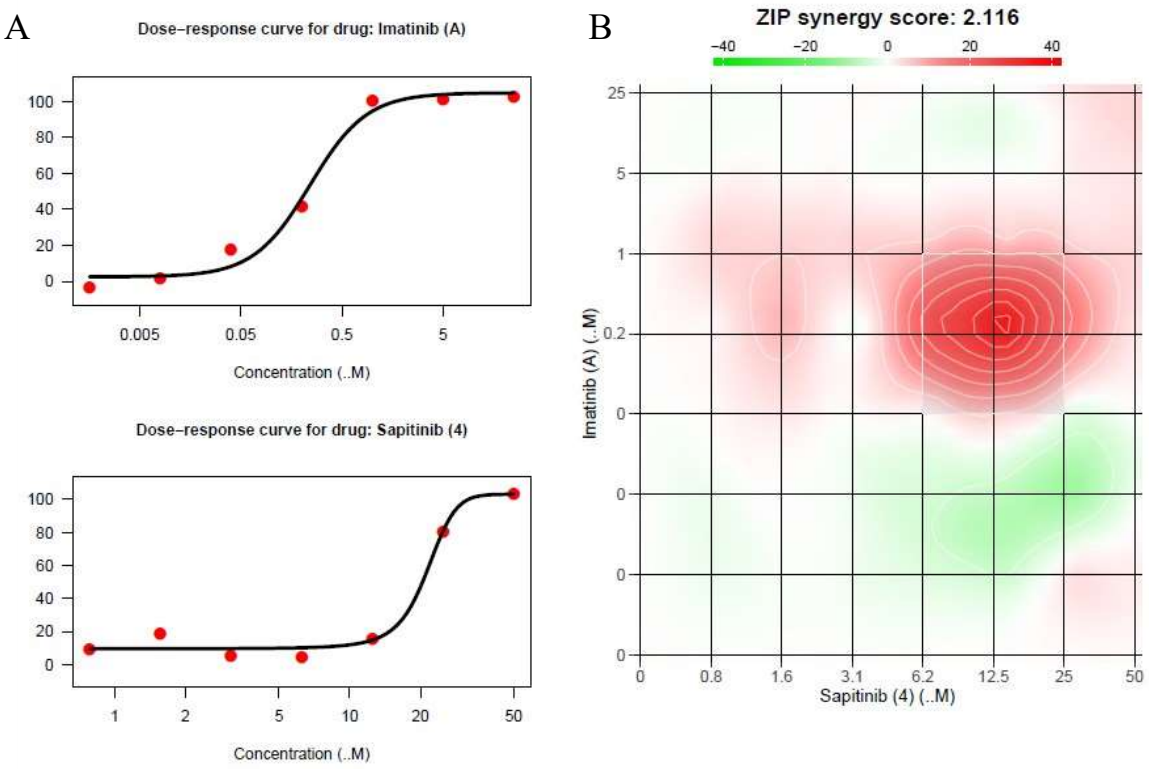

Figure 21: Representative Synergistic Assay combining Imatinib and Sapitinib in DFT2 Snug. (A-B) Dose response curve for Imatinib and Sapitinib and the synergy distribution. The four-parameter logistic regression (LL4) was used as the curve-fitting algorithm. The degree of synergy was quantified using the Zero interaction potency (ZIP) model and the most synergistic area score (MSA) was used to compare different combination treatments with each other.

4.3.2. Dasatinib and Sapitinib Combination Treatment

Considering weak synergies between ERBB and PDGFR inhibition, as seen above, targeting other RTK in combination with ERBB inhibition was explored. Dasatinib is a multi-targeted inhibitor that targets Abl, Src and c-Kit. Notably, combination treatments with Dasatinib and Sapitinib reveal synergistic interactions between these two TKI, indicated by MSA scores greater than 10 (Table 21). This implies that, besides PDGFR, also other RTKs including ERBB are active in DFT2.

Cell Line	Most Synergistic Area Score
DFT2 RV	23,11 (n=2)
DFT2 JV	16,96 (n=2)

Table 21: The representative Synergistic Assay assesses the interaction between Dasatinib and Sapitinib across DFT2 cell lines RV (n=2) and JV (n=2).

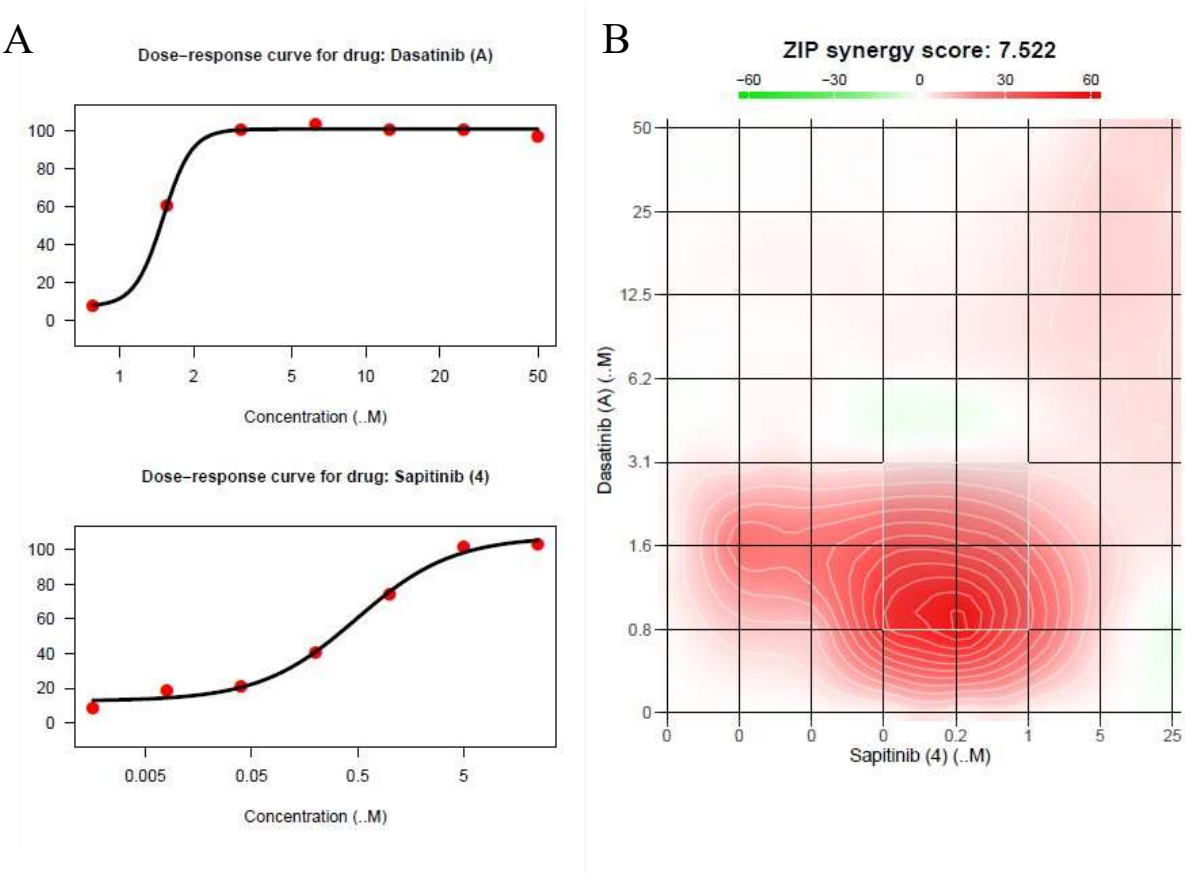

Figure 22: Representative Synergistic Assay combining Dasatinib and Sapitinib in DFT2 JV. (A-B) Dose response curve for Imatinib and Sapitinib and the synergy distribution. The four-parameter logistic regression (LL4) was used as the curve-fitting algorithm. The degree of synergy was quantified using the Zero interaction potency (ZIP) model and the most synergistic area score (MSA) was used to compare different combination treatments with each other.

4.4. Exploring resistance mechanisms of DFT2

PDGFR signaling seems to be the main driver of DFT2 cells. However, the observed cytotoxicity upon treating alternative RTK, including ERBB3, in a combined manner in DFT2 cells suggest possible signaling plasticity and escape mechanisms. To investigate this hypothesis, we generated DFT2 cell lines resistant to Imatinib. Western blot and RT-qPCR analysis allowed the investigation of gene expression alterations of the resistant cells. To understand drug resistant mechanisms within cancer cells is not only important for overcoming treatment challenges, but also offers insights into alternative pathways that may contribute to survival and adaption.

4.4.1. Altered vulnerabilities of resistant cell lines (Cytotox)

4.4.1.1. Imatinib

To demonstrate the acquired resistance in the DFT2 cell lines, cytotoxicity assays were performed, comparing the response of resistant cell lines with non-resistant control towards PDGFR inhibition by Imatinib. The results show that the resistant DFT2 cell lines Snug and JV were less responsive to Imatinib compared to the control group. IC_{50} values of resistant DFT2 cell lines were significantly higher than those of the control group upon Imatinib treatment (Figure 23).

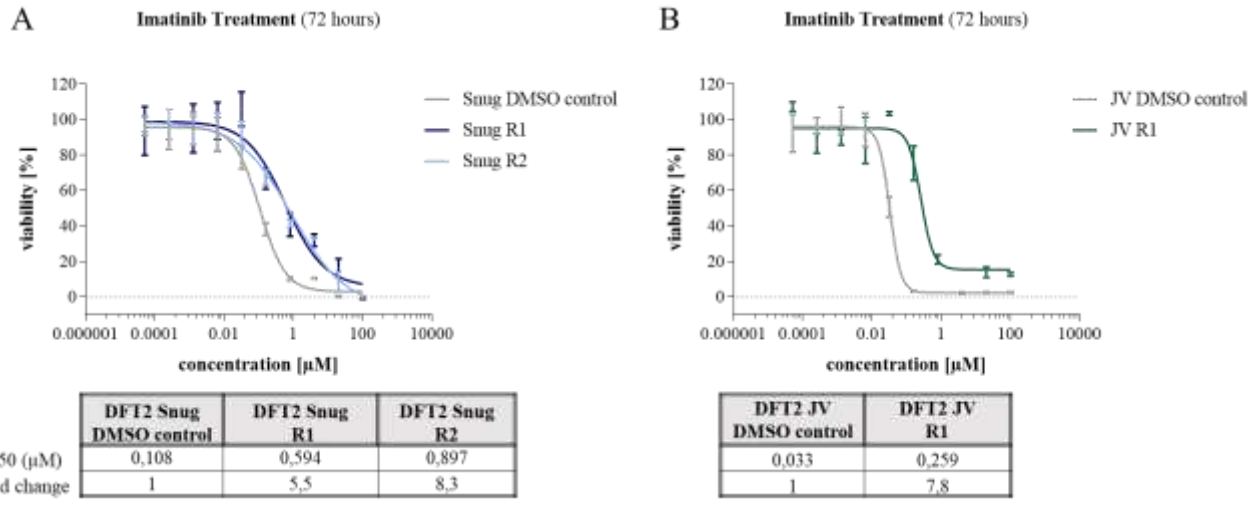

	DFT2 Snug DMSO control	DFT2 Snug R1	DFT2 Snug R2
IC50 (µM)	0,108	0,594	0,897
fold change	1	5,5	8,3

DFT2 JV DMSO control	DFT2 JV R1
0,033	0,259
1	7,8

Figure 23: Cell viability and IC50 values/ fold change of DFT2 resistant cells and non-resistant control after 72h Imatinib treatment. (A) The graph shows one representative experiment with three technical replicates using DFT2 Snug non-treated control, DFT2 Snug R1 and DFT2 Snug R2 (n=1). (B) The graph shows one representative experiment with three technical replicates using DFT2 JV non-treated control and DFT2 JV R1 (n=1). Error bars indicate the standard error of the mean. Dose response curves and IC50 values were calculated using nonlinear regression in GraphPad Prism.

4.4.1.1. Sapitinib

To investigate whether the acquired resistance towards PDGFR inhibition led to an increased vulnerability towards ERBB inhibition, the resistant cells were treated with Sapitinib. However, the results show that the resistant DFT2 cells were also less sensitive to ERBB inhibition by Sapitinib compared to non-resistant controls, indicated by a IC_{50} fold change greater than 3 (Figure 24). This implies that DFT2 cells resistant to PDGFR inhibition might use other RTK as alternative signaling pathways.

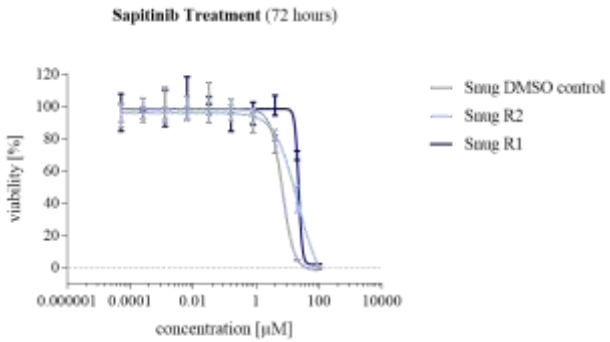

	DFT2 Snug DMSO control	DFT2 Snug R1	DFT2 Snug R2
IC50 (µM)	6,83	23,4	20,78
fold change	1	3,4	3,3

Figure 24: Cell viability and IC50 values/ fold change of DFT2 resistant cells and non-resistant control after 72h *Sapitinib* treatment. The graph shows one representative experiment with three technical replicates using DFT2 Snug non-treated control, DFT2 Snug R1 and DFT2 Snug R2 (n=1). Error bars indicate the standard error of the mean. Dose response curves and IC50 values were calculated using nonlinear regression in GraphPad Prism.

4.4.2. Altered gene expression in resistant cell lines

To explore signaling alterations of resistant cell lines, we performed Western blot and gene expression analysis to elucidate changes to gain better insight into resistance mechanisms.

4.4.2.1. PDGFR

Firstly, PDGFRα and PDGFRβ expression levels of DFT2 cell lines resistant towards PDGFR inhibition were investigated. Gene expression of *PDGFRA* and *PDGFRB* was significantly lower in the resistant cell lines. Our findings also revealed a decrease in the protein expression levels of PDGFRα (Figure 25B).

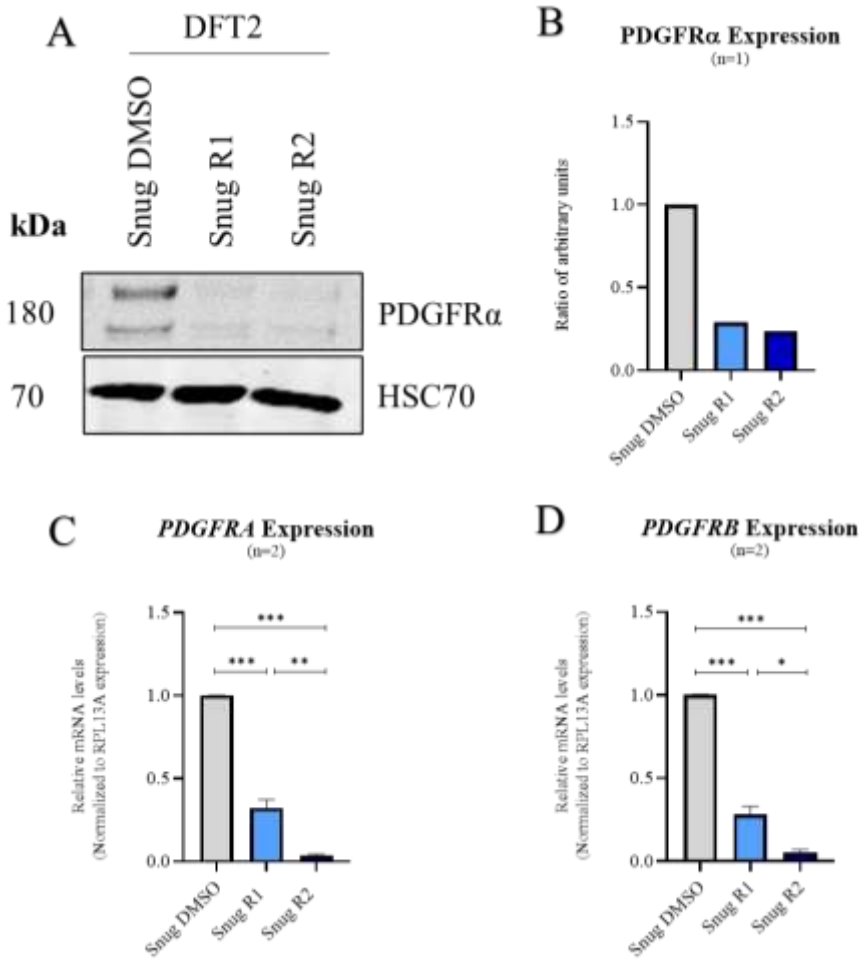

Figure 25: PDGFR Gene and Protein Expression Analysis. (A) Representative Western blot analysis showing basal PDGFRα protein expression levels in DFT2 non-resistant Snug, DFT2 Snug R1 and DFT2 Snug R2. HSC70 was used as loading control (n=1). (B) Quantification of representative Western blot showing PDGFRα (n=1) protein expression levels. (C-D) Relative *PDGFRA* (n=2) and *PDGFRB* (n=2) gene expression in DFT2 non-resistant Snug, DFT2 Snug R1 and DFT2 Snug R2 was determined via RT-qPCR. *RPL13A* was used as a housekeeping gene for normalization. The ΔΔCt-Method was used to calculate the relative fold gene expression. The error bars indicate the standard error of the mean. To determine statistical significance a two-way ANOVA with Bonferroni comparison was performed. ns = non-significant, * = p-value < 0.05, *** = p-value < 0.001, **** = p-value < 0.0001.

4.4.2.2. Changes in ERBB gene expression

Even though vulnerability towards ERBB inhibition did not increase in the resistant cell lines, ERBB gene expression was further analyzed. Results reveal a decreased expression of *ERBB3*, supporting the results above (Figure 26A). Interestingly, however, resistant cell lines showed an increased expression of *EGFR* (Figure 26B). This protein was previously shown to be not significantly expressed in DFT cells compared to healthy fibroblasts and the developed expression implies a drastic change in signaling and a possible resistance mechanism via EGFR signaling in resistant DFT2 cells.

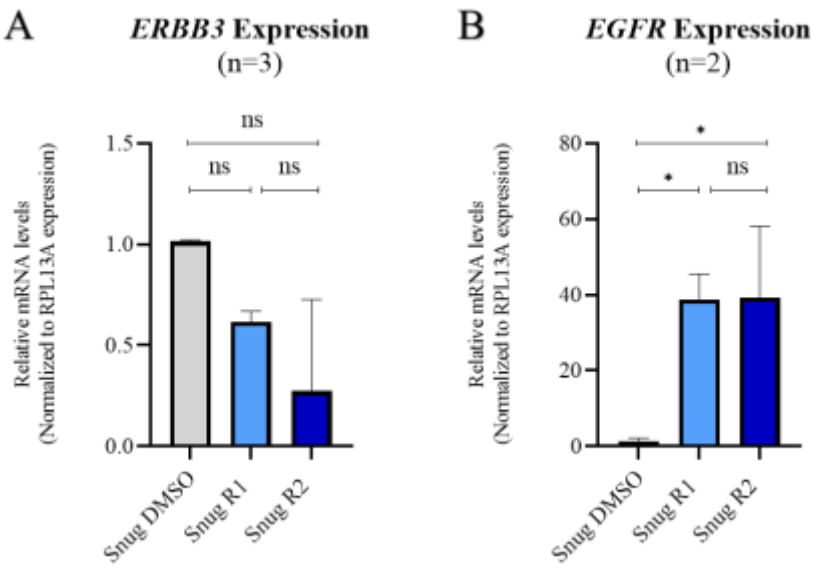

Figure 26: ERBB family Gene Expression Analysis (A-B) Relative *ERBB3* (n=3) and *EGFR* (n=2) gene expression in DFT2 non-resistant Snug, DFT2 Snug R1 and DFT2 Snug R2 was determined via RT-qPCR. *RPL13A* was used as a housekeeping gene for normalization. The ΔΔCt-Method was used to calculate the relative fold gene expression. The error bars indicate the standard error of the mean. To determine statistical significance a two-way ANOVA with Bonferroni comparison was performed. ns = non-significant, * = p-value < 0.05, *** = p-value < 0.001, **** = p-value < 0.0001.

4.4.2.3. Changes in STAT expression and activation

STAT3 signaling drives proliferation and immune escape in DFT1 cells, whereas the results above imply the importance of STAT5B signaling in DFT2 cells. To investigate changes in STAT signaling in DFT2 cells upon resistance towards PDFGR inhibition, the basal protein levels of total and activated STAT3 and total STAT5 were analyzed in the resistant cell lines via Western blotting and compared to the wildtype cells (Figure 27A-E). Strikingly, STAT3 activation in resistant DFT2 cells was observed (Figure 27D), whereas the total STAT3 levels remain unchanged (Figure 27B). This suggests that STAT3 becomes a main driver in the resistant cells in response to decreased PDGFR signaling, resembling the core cancer pathway that drives DFT1 cells. Whether STAT3 is activated downstream of the observed upregulated EGFR expression remains to be explored further. *STAT5B* gene expression significantly decreased in one of two resistant cell lines. However, protein expression levels remained stable in one cell line resistant to PDGFR inhibition, whereas in the other resistant cell line STAT5B protein expression levels are increasing (Figure 27E). Interestingly, a decrease in *STAT3* gene expression can be observed in both resistant cell lines (Figure 27F).

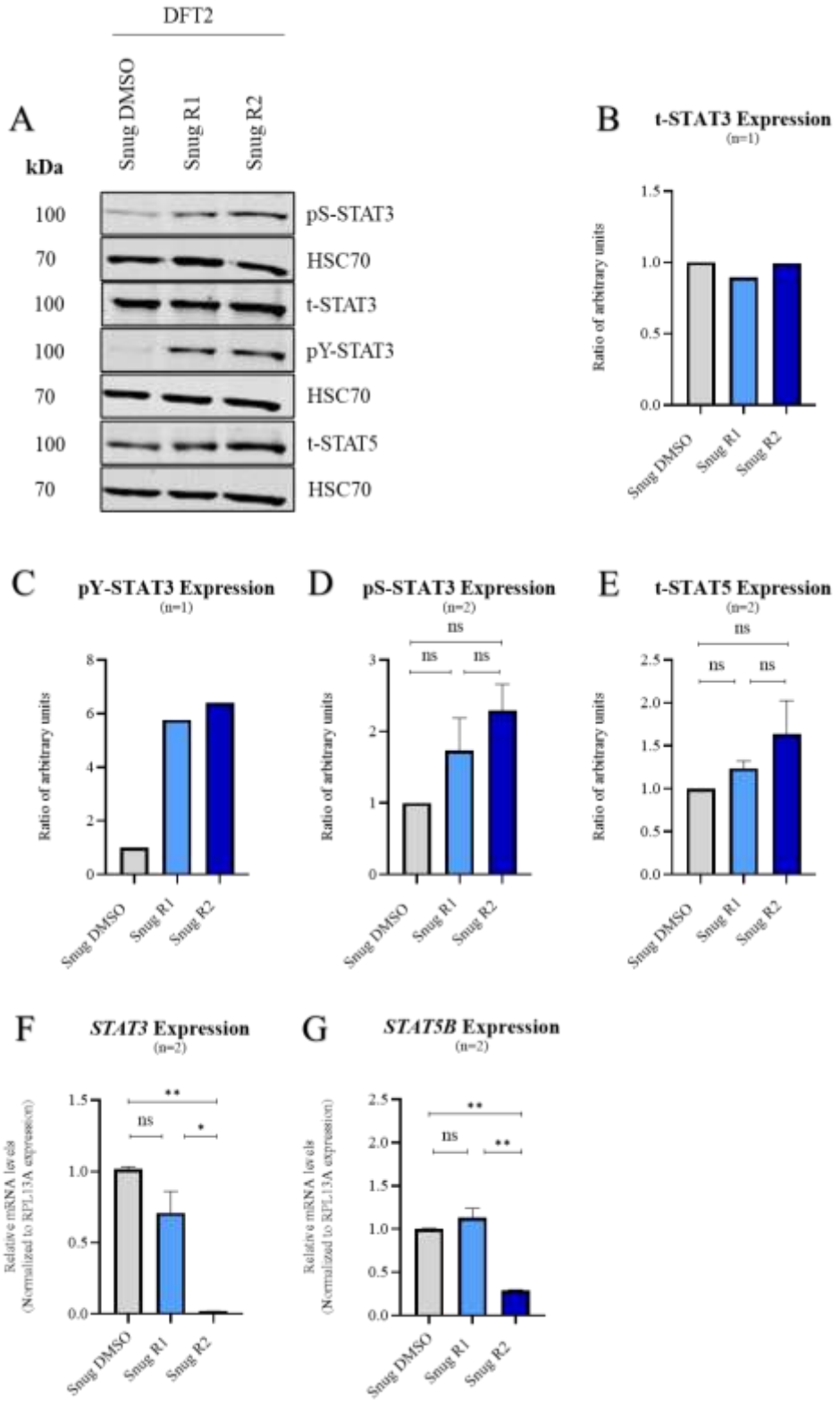

Figure 27: STAT3 and STAT5 Gene and Protein Expression Analysis. (A) Representative Western blot analysis showing basal t-STAT3, pY-STAT3, pS-STAT3 and STAT5 protein expression levels in DFT2 non-resistant Snug, DFT2 Snug R1 and DFT2 Snug R2. HSC70 was used as loading control (n=1). (B-E) Quantification of representative Western blot showing t-STAT3 (n=1), pY-STAT3 (n=1), pS-STAT3 (n=2) and t-STAT5 (n=2) protein expression levels. (F-G) Relative *STAT3* (n=2) and *STAT5B* (n=2) gene expression in DFT2 non-resistant Snug, DFT2 Snug R1 and DFT2 Snug R2 was determined via RT-qPCR. *RPL13A* was used as a housekeeping gene for normalization. The ΔΔCt-Method was used to calculate the relative fold gene expression. The error bars indicate the standard error of the mean. To determine statistical significance a two-way ANOVA with Bonferroni comparison was performed. ns = non-significant, * = p-value < 0.05, *** = p-value < 0.001, **** = p- value < 0.0001.

4.4.2.4. Development of possible immune escape mechanisms

DFT2 cells resistant to PDGFR inhibition show changes in RTK expression and an established STAT3 activation. The previously described ERBB-STAT3 signaling axis drives both proliferation and immune escape in DFT1 cells (Kosack et al., 2019). Therefore, RT-qPCR was performed to look at the gene expression levels of genes connected with immune mechanisms in the resistant DFT2 cells. Gene expression of *STAT1* decreased in the resistant cell lines compared to non-resistant control cells (Figure 28A), whereas *MHC-I* levels remained consistent (Figure 28B). Interestingly, *B2M*, *TAP1* and *TAP2* gene expression levels decreased in the resistant cell lines (Figure 28C-E). This indicates that DFT2 cells with inhibited PDGFR signaling and increased STAT3 activation downregulate genes important for immune recognition. This happens in a similar fashion as in DFT1 cells.

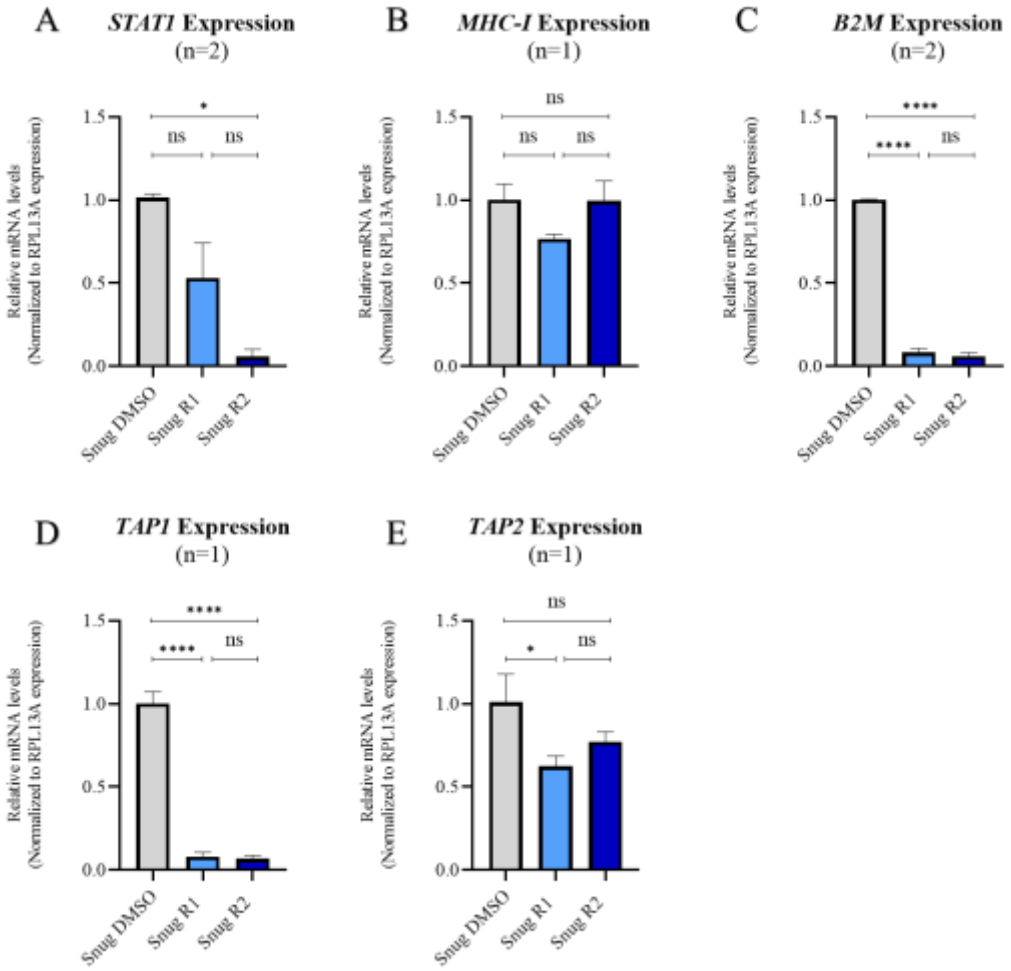

Figure 28: Immune Gene Expression Analysis. (A-E) Relative *STAT1* (n=2), *MHC- I* (n=1), *B2M* (n=2), *TAP1* (n=1), *TAP2* (n=1) gene expression in DFT2 non-resistant Snug, DFT2 Snug R1 and DFT2 Snug R2 was determined via RT-qPCR. *RPL13A* was used as a housekeeping gene for normalization. The ΔΔCt-Method was used to calculate the relative fold gene expression. The error bars indicate the standard error of the mean. To determine statistical significance a two-way ANOVA with Bonferroni comparison was performed. ns = non-significant, * = p-value < 0.05, *** = p- value < 0.001, **** = p-value < 0.0001.

5. Discussion

Transmissible cancers are extremely rare since foreign cells are usually detected and cleared by the immune system. Only three animal groups are naturally affected by transmissible cancer, and it seems that certain species have a higher vulnerability to develop these kind of cancers (Metzger et al., 2015; Murgia et al., 2006). The Tasmanian devil faces extinction due to two transmissible cancers, named DFT1 and DFT2, which arose independently. It is not yet known how these cancers can be transmitted between Tasmanian devil individuals. Even with limited MHC diversity, the Tasmanian devil has a developed immune system and rejects foreign skin grafts. It is therefore crucial to investigate the signaling pathways that drive both tumors and are possibly connected with immune evasion in order to understand these cancers better, find a possibility to target vulnerabilities pharmaceutically and save the species from extinction. DFT1 and DFT2 have a very similar phenotype and analyses show that both DFT1 and DFT2 are kinase-driven tumors from Schwann cell origin. However, it was revealed and further demonstrated in this project, that both tumor cell lines are strikingly different in their signaling mechanisms (Kosack et al., 2019; Kreiss et al., 2011; Patchett et al., 2020).

EGFR and PDGFR are both members of the RTK family, and therefore share similarities in their signaling pathways (Figure 29). Upon ligand-specific binding, both receptors undergo dimerization, leading to autophosphorylation of their tyrosine residues. These conformational changes lead to the activation of downstream signaling pathways, including the Phosphoinositide 3-kinase (PI3K)/AKT pathway, Mitogen-Activated Protein Kinase (MAPK)/ Extracellular Signal-Regulated Kinase (ERK) pathway, JAK/STAT pathway, Phospholipase C-gamma (PLCγ)/Protein Kinase C (PKC) pathway, Ras/Raf/MAPK pathway, and the activation of Src kinases. These signaling pathways are responsible for the regulation of many cellular processes, such as cell proliferation, differentiation, survival, angiogenesis and migration (Perrone et al., 2009).

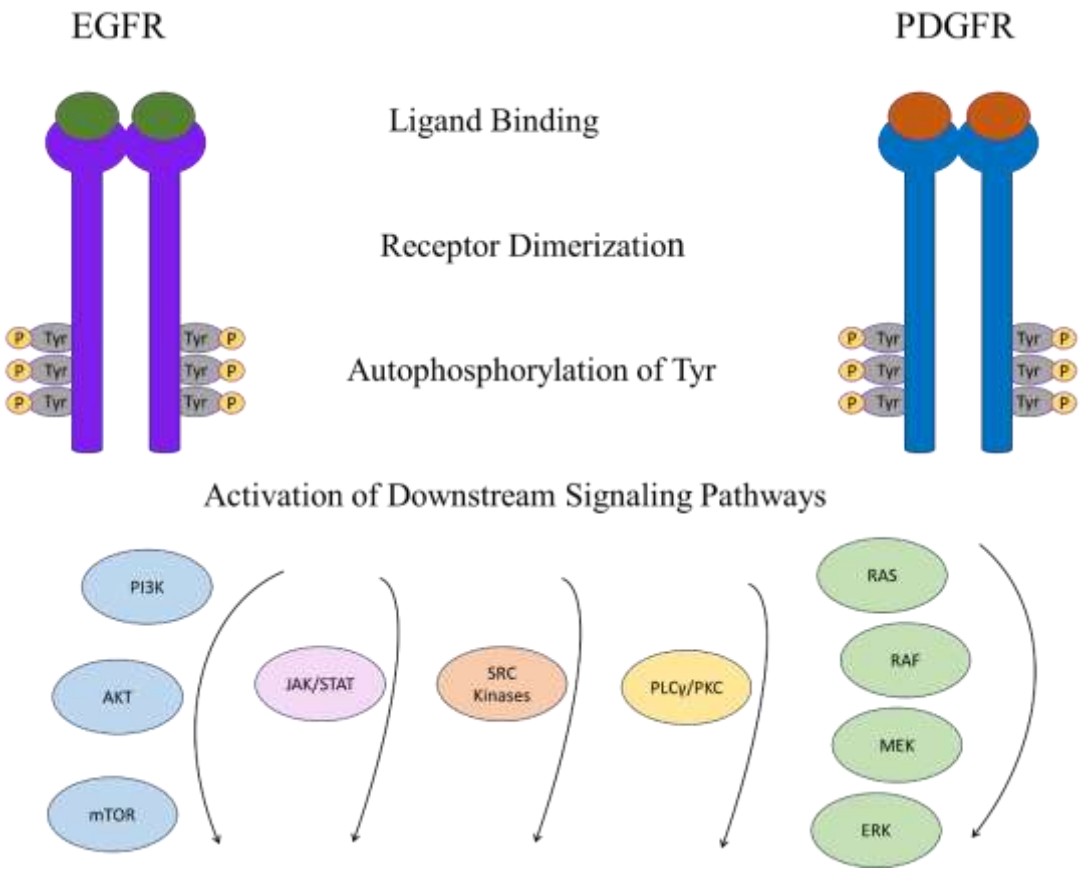

Figure 29: Simplified EGFR and PDGFR signaling. EGFR and PDGFR are both members of the RTK family and therefore share some similarities in their signaling pathways. They both activate several common downstream signaling pathways including JAK/STAT, PI3K/AKT, RAS/RAF/ERK, PLCγ//PKC and the activation of Src kinases. This image was created using PowerPoint (Perrone et al., 2009).

A previously performed drug screen revealed distinct vulnerabilities of DFT1 and DFT2. Notably, PDGFRα/β, VEGFR1-3, Abl, c-Kit and the Src family exhibited high efficacy in DFT2, whereas DFT1 showed responsiveness to ERBB family and BTK inhibition. Additionally, HDACs, BRD and STAT3/5 emerged as potential targets for both DFT1 and DFT2.

Sapitinib is an inhibitor of ERBB family members, that shows inhibitory effects on ERBB2 and ERBB3 (Kosack et al., 2019). It is an experimental drug that has been studied in clinical trials for the treatment of different types of cancer such as NSCLC and breast cancer (Kurata et al., 2014). Sapitinib shows remarkably inhibitory effects on DFT1 cells, compared to DFT2 cells and fibroblasts, highlighting the significant role of ERBB receptors in DFT1 signaling pathways and therefore suggesting this RTK as a potential therapeutic target. In addition to Sapitinib, Lapatinib, which targets EGFR and ERBB2, demonstrates effectiveness against DFT1 and therefore underscoring the statement above. In DFT1, ERBB receptors and the downstream transcription factor STAT3 are among the key drivers of tumor growth and survival (Kosack et al., 2019).

ERBB2/3 signaling is essential for the migration of progenitor cells in Schwann cells and myelination. The mutation or overexpression of ERBB receptors is very common in cancer and leads to uncontrolled cell growth, proliferation and promotes tumor progression and survival. Therapies that target ERBB signaling have shown promising effects in various types of cancer (Kosack et al., 2019).

Imatinib, an approved TKI, shows selective inhibition of PDGFR, BCR/ABL and c-Kit. Imatinib was approved by the FDA and EMA in 2001 for the treatment of CML. Later it was also approved for the treatment of GIST and other malignancies (Attwood et al., 2021). The treatment with Imatinib revealed that DFT2 cells were significantly more sensitive to PDGFR inhibition in comparison to DFT1 cells and fibroblasts. Therefore, underscoring the important role of PDGFR in DFT2 signaling. Masitinib, which is also a PDGFR inhibitor that also inhibits c-Kit and FGFR3, additionally supports our hypothesis that PDGFR is crucial for DFT2 signaling. DFT2 exhibit much higher sensitivity to Masitinib treatment compared to DFT1 and fibroblasts.

Following the findings from the cytotoxicity assays, which indicate that DFT1 cells are sensitive to ERBB inhibition and DFT2 to PDGFR inhibition, expression levels of these RTK were investigated in both cancers. It was shown by Kosack et al. that DFT1 is driven by an ERBB-STAT3 axis, characterized by upregulated ERBB and STAT3 expression levels. These findings could be confirmed by RT-qPCR and Western blot analysis. DFT1 showed elevated *ERBB3* gene expression levels compared to the fibroblasts. Surprisingly, our analysis revealed that DFT2 exhibits even higher levels of *ERBB3*. Western blot analysis showed that ERBB3 protein expression levels are elevated in DFT2 as well. This finding suggests that ERBB3 plays an important role in the cancer signaling of both cancers. But simultaneously raises the question why only DFT1 cells are sensitive towards ERBB inhibition. Another ERBB family member is EGFR, which is much higher expressed in fibroblasts suggesting a limited role in DFT1 and DFT2.

Given the sensitivity of DFT2 towards PDGFR inhibition, the PDGFR expression levels were validated at mRNA and protein levels. DFT2 shows copy number gains of *PDGFRA* and signaling via PDGFR pathways is therefore likely to be important in DFT2 cells. Whereas DFT1 possesses gene duplication of *PDGFRB* in its genome. PDGFR signaling promotes cell proliferation and survival and is known to play an important role in several human cancers (Garces De Los Fayos Alonso et al., 2022; Stammnitz et al., 2018).

Here, RT-qPCR experiments proof that the expression of *PDGFRA* is upregulated in DFT2 and targeting PDGFRα could therefore be a potential therapeutic strategy for the treatment of DFT2. The dysregulation and overexpression of PDGFRA can be linked to certain types of cancer. However, *PDGFRB* is higher expressed in DFT1. These findings highlight the important role of PDGFR signaling in DFT1. The differences in the upregulation of PDGFRA and PDGFRB coupled with the sensitivity exclusively observed in DFT2 upon PDGFR inhibition, suggests that both DFT1 and DFT2 use distinct pathway strength or threshold of TKR signal transduction.

STATs frequently serve as signaling partners for RTKs, and since DFT1 has been demonstrated to be driven by a STAT3 axis, the expression levels of STATs were investigated at gene and protein expression levels. STAT1, STAT3 and STAT5 play important roles in cell growth, differentiation and survival in human cancers (Sumiyoshi et al., 2016). DFT1 exhibits increased *STAT3* expression levels in comparison to DFT2 and fibroblasts. Protein analysis revealed elevated total and phosphorylated STAT3 levels in DFT1. The upregulation of STAT3 is also often associated with cancer progression including metastasis, which was reported in several types of cancer. This supports the finding that DFT1 is driven by STAT3, as previously published. However, it simultaneously highlights that DFT2 is not driven by an STAT3 signaling axis (Kosack et al., 2019).

Since STAT5 shows a similar structure to STAT3 and plays a major role in human PDGFR driven cancers, it could be an important protein in DFT2 (Sumiyoshi et al., 2016). Indeed, elevated *STAT5B* expression levels could be observed in DFT2 cells lines. Additionally, increased STAT5 protein expression was observed in DFT2 cell lines compared to DFT1 and healthy control fibroblasts. The STAT5 upregulation is often associated with cell proliferation and differentiation. In DFT2 tumors STAT5 may lead to the promotion of tumor growth by increasing cell division and preventing cell death. Further research needs to investigate the underlying mechanisms of the STAT5 and PDGFRα upregulation in DFT2 (Stammnitz et al., 2018).

In addition to STAT3 and STAT5, STAT1 also seems to be significant in the signaling pathways of DFT cells, given its key role in mechanisms of immune evasion. Previously, it was shown that DFT1 downregulates downstream transcription genes of STAT1 due to STAT3 capturing STAT1 in heterodimers (Kosack et al., 2019). Gene expression analysis reveals decreased *STAT1* expression in DFT1 and DFT2 in comparison to the fibroblasts, which suggests that DFT2 may develop similar immune evasion mechanisms as observed in DFT1.

Whereas protein expression analysis revealed that STAT1 is lower expressed in DFT1 compared to DFT2 and fibroblasts. This observation aligns with the downregulation of MHC-I in DFT1, while its expression remains mostly intact in DFT2.

To explore potential connections between the observed differences and immune evasion through MHC expression, genes associated with this pathway were analyzed in both DFT1 and DFT2. Understanding MHC signaling is important for understanding immune response mechanisms within DFT. Gene expression analysis reveals a downregulation of *MHC-I* levels in both DFT1 and DFT2 compared to fibroblasts, while the expression levels are lower in DFT1 than DFT2. Interestingly, DFT1 cells exhibit a hemizygous deletion of B2M, which is important for stabilizing MHC class I and could therefore potentially lead to the observed downregulation of MHC-I. In DFT2, however, B2M remains intact. *B2M* levels are higher in DFT2 compared to DFT1, but still lower than the levels observed in the fibroblasts. TAP1/2 are important for the antigen presentation pathway. *TAP1* is downregulated in both DFT1 and DFT2, whereas *TAP2* is much higher expressed in DFT2 compared to healthy fibroblasts. Whereas DFT1 exhibits lower levels of *TAP2* compared to DFT2 and fibroblasts. These finding reinforces the hypothesis that DFT2 cells employ downregulation of MHC-I as an immune evasion mechanism similar to DFT1.

The unexpected elevated *ERBB3* gene and protein expression observed in DFT2 cells, combined with the upregulation of PDGFRα, suggests potential signaling plasticity and resistance towards drug treatments. This led us to further investigate combinational treatments. Synergistic assays revealed weak synergistic interactions between Imatinib and Sapitinib in DFT2 cells, which supports the hypothesis that DFT2 cells are reliant on PDGFRα. It might be that the inhibition of PDGFR is extremely potent in killing DFT2 cells, such that simultaneous inhibition of ERBB may not further enhance cytotoxicity. This could indicate that Imatinib treatment alone is the most effective approach for killing DFT2. Interestingly, combining Dasatinib, an ERBB inhibitor, and Sapitinib also revealed weak synergistic effects, indicating that besides PDGFR other RTK might be active in DFT2.

DFT2 cells seem to be driven by PDGFR signaling. The observed sensitivity towards targeting alternative RTK, including ERBB3 in combinational treatments, indicates that there could be alternative pathways or escape mechanisms possibly leading to drug resistance. Understanding drug resistance mechanisms within cancer is not only important for overcoming therapeutic challenges, but also to gain knowledge about alternative signaling pathways that may lead to survival and adaptation.

Therefore, resistant DFT2 cell lines towards DFT2 were generated and analyzed. Cytotoxicity assays revealed that the resistant cell lines are less sensitive towards Imatinib, but interestingly they are also less sensitive to ERBB inhibition by Sapitinib, suggesting that DFT2 uses other RTK as alternative signaling pathways.

Gene expression of *PDGFRA* and *PDGFRB* was significantly lower in the resistant cell lines. Furthermore, we revealed a decrease in the protein expression levels of PDGFRα. Despite the vulnerability towards ERBB inhibition did not increase in the resistant cell lines, ERBB expression was further analyzed. Gene expression analysis revealed a decrease in the *ERBB3* levels. Interestingly, the resistant cell lines show increased *EGFR* expression levels, which was shown to be elevated in the fibroblasts, but not in DFT cells. This indicates that there are changes going on in the signaling and possible resistance mechanisms via EGFR occur.

In DFT1 proliferation and immune escape is driven by STAT3, whereas the results above highlight the importance of STAT5B in DFT2 signaling. To investigate changes in the STAT expression in resistant DFT2 cells, the gene expression levels of *STAT3* and *STAT5B* and the basal protein levels of total and activated STAT3 and total STAT5 were analyzed. Strikingly, an increased serine- and tyrosine phosphorylation of STAT3 could be observed in the resistant cell lines, whereas the total STAT3 levels remained unchanged. This suggests that STAT3 could become an important signaling partner in DFT2 cell lines in response to resistance towards PDGFR. If the STAT3 activation occurs downstream of the elevated EGFR expression, needs to be further explored. But interestingly, the gene expression of *STAT3* is decreasing in both resistant cells. This could suggest that post-translational or post-transcriptional modifications occur upon PDGFR resistance. The expression of *STAT5B* is significantly decreasing in one of the two cell lines resistant to PDGFR inhibition. The total STAT5 protein expression levels are increasing in one of the two resistant cell lines. The observed changes in the activation of STAT3 indicate that there are alternative mechanisms that are driving DFT2.

The ERBB-STAT3 signaling axis drives both proliferation and immune escape in DFT1. Therefore, RT-qPCR analysis was performed to examine the gene expression levels of immune-related genes in DFT2 cells. The resistant cell lines exhibited decreased levels of *STAT1*, whereas the *MHC-I* levels remained consistent. Furthermore, *B2M* and *TAP1/2* significantly decreased in the resistant cell lines compared to the non-resistant control. This observation indicates that resistant DFT2 cells downregulate genes that are important for immune recognition, which can be observed in DFT1 cells as well.

Resistant DFT2	**protein expression compared to wildtype**
tSTAT3	-
pS-STAT3	↑
pY-STAT3	↑
tSTAT5	↑
PDGFRα	↓
Resistant DFT2	**gene expression compared to wildtype**
STAT1	↓
STAT3	↓
STAT5B	-
PDGFRA	↓
PDGFRB	↓
EGFR	↑
ERBB3	↓
MHC-I	-
TAP1/2	↓
B2M	↓

Table 22: Summary of the protein and gene expression changes in the resistant cell lines compared to the wildtype. The arrow indicates if there was an increase or decrease in the protein/gene expression in the resistant cell line. The "-" indicates that the levels remained unchanged.

Alterations in the antigen presentation of the resistant cell lines may have led to a decrease in recognition and elimination of foreign cells by the immune system. This compromised antigen presentation represents an important immune evasion mechanism that allows the resistant cell lines to evade immune surveillance. There are several factors that may contribute to this compromised antigen presentation, including the downregulation of several genes that are involved in the antigen/MHC-I presentation. Besides the above shown genes such as B2M, TAP1/2, also other genes can be involved in this process. Interferon gamma and its receptor are both important for MHC class I expression and antigen presentation. Mutations in one of those genes can lead to decreased immune recognition, thereby supporting immune evasion by cancer cells (Jhunjhunwala et al., 2021).

Confirming the major signaling differences between DFT1 and DFT2 highlights that it will be difficult to find tyrosine kinase inhibitors that target DFT1 and DFT2 simultaneously. Blocking these driving pathways may nevertheless be a promising option for pharmaceutical treatment and it is thus crucial to explore connected players in these pathways.

Generally, pharmaceutical treatment of a wild species such as the Tasmanian devil brings along its complications. However, together with ongoing vaccine trials, Tasmanian devils could be treated in sanctuaries with clinically relevant inhibitors.

Synergistic effects from tyrosine kinase inhibition and the provoked immune response could be a way to clear the Tasmanian devils from their tumor burden. On another note, the conducted research does not only profit the Tasmanian devil, but the obtained results are translatable into human cancer research. In humans, transmissible cancers are extremely rare since foreign cells can be recognized and rejected before they can spread. There are, however, special settings that allow the transmission of cancer. For example, donor transmitted cancers can occur after organ transplantation when a tumor is transferred via the transplanted organ. This can happen because the organ recipient's immune system is suppressed medically. Additionally, cases of transmitted tumors during pregnancy exist. Cancer can be transmitted from mother to the fetus, from the fetus to the mother or between twins. The placenta usually prevents cancer cells from crossing the barrier between mother and child but there is small chance that cancers like leukemia or lymphomas can be transmitted and not recognized because 50% of genetic material is shared between mother and offspring. This demonstrates that cancer transmission is not impossible, and, in the future, more species could be affected by this type of disease (Metzger & Goff, 2016). What is more relevant for the present day is the possibility to translate the employed mechanisms to human cancer immune evasion, human metastasis and even organ transplantation. By exploring the fascinating skill of the transmissible cancers to hide from a developed immune system, many lives could be saved by an improved organ acceptance rate during organ transplantation.

All in all, DFT1 and DFT2 can help us to gain a better understanding of cancer immune evasion, MHC-I related immune escape mechanisms, tumor metastasis and tyrosine kinase signaling. By advancing our knowledge of transmissible cancer, we can make progress towards conserving an endangered species and improving human health.

Bibliography

Abdelgalil, A. A., & Alkahtani, H. M. (2023). Lapatinib: A comprehensive profile. In *Profiles of Drug Substances, Excipients and Related Methodology* (Vol. 48, pp. 135–166). Elsevier. https://doi.org/10.1016/bs.podrm.2022.11.005

Andersen, G. E., McGregor, H. W., Johnson, C. N., & Jones, M. E. (2020). Activity and social interactions in a wide-ranging specialist scavenger, the Tasmanian devil (Sarcophilus harrisii), revealed by animal-borne video collars. *PLOS ONE*, *15*(3), e0230216. https://doi.org/10.1371/journal.pone.0230216

Attwood, M. M., Fabbro, D., Sokolov, A. V., Knapp, S., & Schiöth, H. B. (2021). Trends in kinase drug discovery: Targets, indications and inhibitor design. *Nature Reviews Drug Discovery*, *20*(11), 839–861. https://doi.org/10.1038/s41573-021-00252-y

Aykul, S., & Martinez-Hackert, E. (2016). Determination of half-maximal inhibitory concentration using biosensor-based protein interaction analysis. *Analytical Biochemistry*, *508*, 97–103. https://doi.org/10.1016/j.ab.2016.06.025

Cunningham, C. X., Comte, S., McCallum, H., Hamilton, D. G., Hamede, R., Storfer, A., Hollings, T., Ruiz-Aravena, M., Kerlin, D. H., Brook, B. W., Hocking, G., & Jones, M. E. (2021). Quantifying 25 years of disease-caused declines in Tasmanian devil populations: Host density drives spatial pathogen spread. *Ecology Letters*, *24*(5), 958–969. https://doi.org/10.1111/ele.13703

Deakin, J. E., Bender, H. S., Pearse, A.-M., Rens, W., O'Brien, P. C. M., Ferguson-Smith, M. A., Cheng, Y., Morris, K., Taylor, R., Stuart, A., Belov, K., Amemiya, C. T., Murchison, E. P., Papenfuss, A. T., & Marshall Graves, J. A. (2012). Genomic Restructuring in the Tasmanian Devil Facial Tumour: Chromosome Painting and Gene Mapping Provide Clues to Evolution of a Transmissible Tumour. *PLoS Genetics*, *8*(2), e1002483. https://doi.org/10.1371/journal.pgen.1002483

Desai, R., Collett, D., Watson, C. J., Johnson, P., Evans, T., & Neuberger, J. (2012). Cancer Transmission From Organ Donors—Unavoidable But Low Risk. *Transplantation*, *94*(12), 1200–1207. https://doi.org/10.1097/TP.0b013e318272df41

Fauziya, Gupta, A., Nadaf, A., Ahmad, S., Hasan, N., Imran, M., Sahebkar, A., Jain, G. K., Kesharwani, P., & Ahmad, F. J. (2023). Dasatinib: A potential tyrosine kinase inhibitor to fight against multiple cancer malignancies. *Medical Oncology*, *40*(6), 173. https://doi.org/10.1007/s12032-023-02018-5

Gaczynska, M., Rock, K. L., & Goldberg, A. L. (1993). γ-Interferon and expression of MHC genes regulate peptide hydrolysis by proteasomes. *Nature*, *365*(6443), 264–267. https://doi.org/10.1038/365264a0

Garces De Los Fayos Alonso, I., Zujo, L., Wiest, I., Kodajova, P., Timelthaler, G., Edtmayer, S., Zrimšek, M., Kollmann, S., Giordano, C., Kothmayer, M., Neubauer, H. A., Dey, S., Schlederer, M., Schmalzbauer, B. S., Limberger, T., Probst, C., Pusch, O., Högler, S., Tangermann, S., … Kenner, L. (2022). PDGFRβ promotes oncogenic progression via STAT3/STAT5 hyperactivation in anaplastic large cell lymphoma. *Molecular Cancer*, *21*(1), 172. https://doi.org/10.1186/s12943-022-01640-7

Garrido, F., Aptsiauri, N., Doorduijn, E. M., Garcia Lora, A. M., & Van Hall, T. (2016). The urgent need to recover MHC class I in cancers for effective immunotherapy. *Current Opinion in Immunology*, *39*, 44–51. https://doi.org/10.1016/j.coi.2015.12.007

Greaves, M., & Hughes, W. (2018). Cancer cell transmission via the placenta. *Evolution, Medicine, and Public Health*, *2018*(1), 106–115. https://doi.org/10.1093/emph/eoy011

Hanahan, D., & Weinberg, R. A. (2011). Hallmarks of Cancer: The Next Generation. *Cell*, *144*(5), 646–674. https://doi.org/10.1016/j.cell.2011.02.013

Hewitt, E. W. (2003). The MHC class I antigen presentation pathway: Strategies for viral immune evasion. *Immunology*, *110*(2), 163–169. https://doi.org/10.1046/j.1365-2567.2003.01738.x

Hu, X., Li, J., Fu, M., Zhao, X., & Wang, W. (2021). The JAK/STAT signaling pathway: From bench to clinic. *Signal Transduction and Targeted Therapy*, *6*(1), 402. https://doi.org/10.1038/s41392-021-00791-1

Ianevski, A., Giri, A. K., & Aittokallio, T. (2022). SynergyFinder 3.0: An interactive analysis and consensus interpretation of multi-drug synergies across multiple samples. *Nucleic Acids Research*, *50*(W1), W739–W743. https://doi.org/10.1093/nar/gkac382

Jhunjhunwala, S., Hammer, C., & Delamarre, L. (2021). Antigen presentation in cancer: Insights into tumour immunogenicity and immune evasion. *Nature Reviews Cancer*, *21*(5), 298–312. https://doi.org/10.1038/s41568-021-00339-z

Johnson, C. N., & Wroe, S. (2003). Causes of extinction of vertebrates during the Holocene of mainland Australia: Arrival of the dingo, or human impact? *The Holocene*, *13*(6), 941–948. https://doi.org/10.1191/0959683603hl682fa

Kanai, T., Seki, S., Jenks, J. A., Kohli, A., Kawli, T., Martin, D. P., Snyder, M., Bacchetta, R., & Nadeau, K. C. (2014). Identification of STAT5A and STAT5B Target Genes in Human T Cells. *PLoS ONE*, *9*(1), e86790. https://doi.org/10.1371/journal.pone.0086790

Kosack, L., Wingelhofer, B., Popa, A., Orlova, A., Agerer, B., Vilagos, B., Majek, P., Parapatics, K., Lercher, A., Ringler, A., Klughammer, J., Smyth, M., Khamina, K., Baazim, H., De Araujo, E. D., Rosa, D. A., Park, J., Tin, G., Ahmar, S., … Bergthaler, A. (2019). The ERBB-STAT3 Axis Drives Tasmanian Devil Facial Tumor Disease. *Cancer Cell*, *35*(1), 125-139.e9. https://doi.org/10.1016/j.ccell.2018.11.018

Kreiss, A., Cheng, Y., Kimble, F., Wells, B., Donovan, S., Belov, K., & Woods, G. M. (2011). Allorecognition in the Tasmanian Devil (Sarcophilus harrisii), an Endangered Marsupial Species with Limited Genetic Diversity. *PLoS ONE*, *6*(7), e22402. https://doi.org/10.1371/journal.pone.0022402

Kurata, T., Tsurutani, J., Fujisaka, Y., Okamoto, W., Hayashi, H., Kawakami, H., Shin, E., Hayashi, N., & Nakagawa, K. (2014). Inhibition of EGFR, HER2 and HER3 signaling with AZD8931 alone and in combination with paclitaxel: Phase I study in Japanese patients with advanced solid malignancies and advanced breast cancer. *Investigational New Drugs*, *32*(5), 946–954. https://doi.org/10.1007/s10637-014-0112-7

Le Tourneau, C., Raymond, E., & Faivre, S. (2007). Sunitinib: A novel tyrosine kinase inhibitor. A brief review of its therapeutic potential in the treatment of renal carcinoma and gastrointestinal stromal tumors (GIST). *Therapeutics and Clinical Risk Management*, *3*(2), 341–348. https://doi.org/10.2147/tcrm.2007.3.2.341

Majumder, A. (2023). HER3: Toward the Prognostic Significance, Therapeutic Potential, Current Challenges, and Future Therapeutics in Different Types of Cancer. *Cells*, *12*(21), 2517. https://doi.org/10.3390/cells12212517

Metzger, M. J., & Goff, S. P. (2016). A Sixth Modality of Infectious Disease: Contagious Cancer from Devils to Clams and Beyond. *PLOS Pathogens*, *12*(10), e1005904. https://doi.org/10.1371/journal.ppat.1005904

Metzger, M. J., Reinisch, C., Sherry, J., & Goff, S. P. (2015). Horizontal Transmission of Clonal Cancer Cells Causes Leukemia in Soft-Shell Clams. *Cell*, *161*(2), 255–263. https://doi.org/10.1016/j.cell.2015.02.042

Moriggl, R., Sexl, V., Kenner, L., Duntsch, C., Stangl, K., Gingras, S., Hoffmeyer, A., Bauer, A., Piekorz, R., Wang, D., Bunting, K. D., Wagner, E. F., Sonneck, K., Valent, P., Ihle, J. N., & Beug, H. (2005). Stat5 tetramer formation is associated with leukemogenesis. *Cancer Cell*, *7*(1), 87–99. https://doi.org/10.1016/j.ccr.2004.12.010

Murchison, E. P., Tovar, C., Hsu, A., Bender, H. S., Kheradpour, P., Rebbeck, C. A., Obendorf, D., Conlan, C., Bahlo, M., Blizzard, C. A., Pyecroft, S., Kreiss, A., Kellis, M., Stark, A., Harkins, T. T., Graves, J. A. M., Woods, G. M., Hannon, G. J., & Papenfuss, A. T. (2010). The Tasmanian Devil Transcriptome Reveals Schwann Cell Origins of a Clonally Transmissible Cancer. *Science*, *327*(5961), 84–87. https://doi.org/10.1126/science.1180616

Murgia, C., Pritchard, J. K., Kim, S. Y., Fassati, A., & Weiss, R. A. (2006). Clonal Origin and Evolution of a Transmissible Cancer. *Cell*, *126*(3), 477–487. https://doi.org/10.1016/j.cell.2006.05.051

Patchett, A. L., Coorens, T. H. H., Darby, J., Wilson, R., McKay, M. J., Kamath, K. S., Rubin, A., Wakefield, M., Mcintosh, L., Mangiola, S., Pye, R. J., Flies, A. S., Corcoran, L. M., Lyons, A. B., Woods, G. M., Murchison, E. P., Papenfuss, A. T., & Tovar, C. (2020). Two of a kind: Transmissible Schwann cell cancers in the endangered Tasmanian devil (Sarcophilus harrisii). *Cellular and Molecular Life Sciences*, *77*(9), 1847–1858. https://doi.org/10.1007/s00018-019-03259-2

Paul, M. K., & Mukhopadhyay, A. K. (2004). Tyrosine kinase – Role and significance in Cancer. *International Journal of Medical Sciences*, 101–115. https://doi.org/10.7150/ijms.1.101

Pearse, A.-M., & Swift, K. (2006). Transmission of devil facial-tumour disease. *Nature*, *439*(7076), 549–549. https://doi.org/10.1038/439549a

Perrone, F., Da Riva, L., Orsenigo, M., Losa, M., Jocollè, G., Millefanti, C., Pastore, E., Gronchi, A., Pierotti, M. A., & Pilotti, S. (2009). PDGFRA, PDGFRB, EGFR, and downstream signaling activation in malignant peripheral nerve sheath tumor. *Neuro-Oncology*, *11*(6), 725–736. https://doi.org/10.1215/15228517-2009-003

Pye, R. J., Patchett, A., McLennan, E., Thomson, R., Carver, S., Fox, S., Pemberton, D., Kreiss, A., Baz Morelli, A., Silva, A., Pearse, M. J., Corcoran, L. M., Belov, K., Hogg, C. J., Woods, G. M., & Lyons, A. B. (2018). Immunization Strategies Producing a Humoral IgG Immune Response against Devil Facial Tumor Disease in the Majority of Tasmanian Devils Destined for Wild Release. *Frontiers in Immunology*, *9*, 259. https://doi.org/10.3389/fimmu.2018.00259

Pye, R. J., Pemberton, D., Tovar, C., Tubio, J. M. C., Dun, K. A., Fox, S., Darby, J., Hayes, D., Knowles, G. W., Kreiss, A., Siddle, H. V. T., Swift, K., Lyons, A. B., Murchison, E. P., & Woods, G. M. (2016). A second transmissible cancer in Tasmanian devils. *Proceedings of the National Academy of Sciences*, *113*(2), 374–379. https://doi.org/10.1073/pnas.1519691113

Saraon, P., Pathmanathan, S., Snider, J., Lyakisheva, A., Wong, V., & Stagljar, I. (2021). Receptor tyrosine kinases and cancer: Oncogenic mechanisms and therapeutic approaches. *Oncogene*, *40*(24), 4079–4093. https://doi.org/10.1038/s41388-021-01841-2

Shibuya, M. (2011). Vascular Endothelial Growth Factor (VEGF) and Its Receptor (VEGFR) Signaling in Angiogenesis: A Crucial Target for Anti- and Pro-Angiogenic Therapies. *Genes & Cancer*, *2*(12), 1097–1105. https://doi.org/10.1177/1947601911423031

Siddle, H. V., Kreiss, A., Tovar, C., Yuen, C. K., Cheng, Y., Belov, K., Swift, K., Pearse, A.-M., Hamede, R., Jones, M. E., Skjødt, K., Woods, G. M., & Kaufman, J. (2013). Reversible epigenetic down-regulation of MHC molecules by devil facial tumour disease illustrates immune escape by a contagious cancer. *Proceedings of the National Academy of Sciences*, *110*(13), 5103–5108. https://doi.org/10.1073/pnas.1219920110

Stammnitz, M. R., Coorens, T. H. H., Gori, K. C., Hayes, D., Fu, B., Wang, J., Martin-Herranz, D. E., Alexandrov, L. B., Baez-Ortega, A., Barthorpe, S., Beck, A., Giordano, F., Knowles, G. W., Kwon, Y. M., Hall, G., Price, S., Pye, R. J., Tubio, J. M. C., Siddle, H. V. T., … Murchison, E. P. (2018). The Origins and Vulnerabilities of Two Transmissible Cancers in Tasmanian Devils. *Cancer Cell*, *33*(4), 607-619.e15. https://doi.org/10.1016/j.ccell.2018.03.013

Su, J.-L., Yang, P.-C., Shih, J.-Y., Yang, C.-Y., Wei, L.-H., Hsieh, C.-Y., Chou, C.-H., Jeng, Y.-M., Wang, M.-Y., Chang, K.-J., Hung, M.-C., & Kuo, M.-L. (2006). The VEGF-C/Flt-4 axis promotes invasion and metastasis of cancer cells. *Cancer Cell*, *9*(3), 209–223. https://doi.org/10.1016/j.ccr.2006.02.018

Sumiyoshi, H., Matsushita, A., Nakamura, Y., Matsuda, Y., Ishiwata, T., Naito, Z., & Uchida, E. (2016). Suppression of STAT5b in pancreatic cancer cells leads to attenuated gemcitabine chemoresistance, adhesion and invasion. *Oncology Reports*, *35*(6), 3216–3226. https://doi.org/10.3892/or.2016.4727

Tallarida, R. J. (2011). Quantitative Methods for Assessing Drug Synergism. *Genes & Cancer*, *2*(11), 1003–1008. https://doi.org/10.1177/1947601912440575

Tokheim, C. J., Papadopoulos, N., Kinzler, K. W., Vogelstein, B., & Karchin, R. (2016). Evaluating the evaluation of cancer driver genes. *Proceedings of the National Academy of Sciences*, *113*(50), 14330–14335. https://doi.org/10.1073/pnas.1616440113

Verhoeven, Y., Tilborghs, S., Jacobs, J., De Waele, J., Quatannens, D., Deben, C., Prenen, H., Pauwels, P., Trinh, X. B., Wouters, A., Smits, E. L. J., Lardon, F., & Van Dam, P. A. (2020). The potential and controversy of targeting STAT family members in cancer. *Seminars in Cancer Biology*, *60*, 41–56. https://doi.org/10.1016/j.semcancer.2019.10.002

Vogelstein, B., Papadopoulos, N., Velculescu, V. E., Zhou, S., Diaz, L. A., & Kinzler, K. W. (2013). Cancer Genome Landscapes. *Science*, *339*(6127), 1546–1558. https://doi.org/10.1126/science.1235122

Wingelhofer, B., Neubauer, H. A., Valent, P., Han, X., Constantinescu, S. N., Gunning, P. T., Müller, M., & Moriggl, R. (2018). Implications of STAT3 and STAT5 signaling on gene regulation and chromatin remodeling in hematopoietic cancer. *Leukemia*, *32*(8), 1713–1726. https://doi.org/10.1038/s41375-018-0117-x

Woods, G. M., Fox, S., Flies, A. S., Tovar, C. D., Jones, M., Hamede, R., Pemberton, D., Lyons, A. B., & Bettiol, S. S. (2018). Two Decades of the Impact of Tasmanian Devil Facial Tumor Disease. *Integrative and Comparative Biology*, *58*(6), 1043–1054. https://doi.org/10.1093/icb/icy118

Wu, X., Li, T., Jiang, R., Yang, X., Guo, H., & Yang, R. (2023). Targeting MHC-I molecules for cancer: Function, mechanism, and therapeutic prospects. *Molecular Cancer*, *22*(1), 194. https://doi.org/10.1186/s12943-023-01899-4

Zammarchi, F., De Stanchina, E., Bournazou, E., Supakorndej, T., Martires, K., Riedel, E., Corben, A. D., Bromberg, J. F., & Cartegni, L. (2011). Antitumorigenic potential of STAT3 alternative splicing modulation. *Proceedings of the National Academy of Sciences*, *108*(43), 17779–17784. https://doi.org/10.1073/pnas.1108482108

6. Zusammenfassung

Devil facial tumor 1 and 2 (DFT1/2) sind übertragbare Tumore, die den Tasmanischen Teufel vom Aussterben bedrohen. Derzeit gibt es noch keine erfolgreiche Therapie für diese sich schnell ausbreitenden Malignome. Bisherige Impfversuche waren erfolglos, was die Notwendigkeit eines besseren Verständnisses der Krankheitsmechanismen unterstreicht, um wirkungsvolle Behandlungen zu entwickeln. Das Ziel dieses Projekts war daher, die Hauptsignalwege von DFT1/2 zu charakterisieren, indem die Expression und Funktion ausgewählter Proteine, inklusiv Rezeptor Tyrosinkinasen und STAT-Transkriptionsfaktoren, analysiert wurden. Zytotoxizitäts-Assays zeigen, dass Sapitinib, ein ERBB-Inhibitor, selektiv gegenüber DFT1-Zellen wirksam ist, während Imatinib, ein PDGFR-Inhibitor, selektiv DFT2-Zellen beeinflusst. Basierend auf den unterschiedlichen Eigenschaften von DFT1/2 wurde eine Analyse der Gen- und Proteinexpression durchgeführt. Die Ergebnisse bestätigen erhöhte Levels von totalem und phosphoryliertem STAT3 in DFT1-Zellen im Vergleich zu DFT2-Zellen und Fibroblasten. In DFT2 hingegen wurden höhere Mengen von STAT5 und PDGFRα festgestellt, was auf eine Interaktion zwischen diesen Proteinen als bislang unerforschte Signalachse hinweist, die nur in DFT2 aktiv ist.

Aufgrund einer überraschend hohen Expression von ERBB3 in DFT2, obwohl keine Reaktion auf die ERBB-Inhibition festgestellt wurde, wurden Kombinationsbehandlungen mit Sapitinib und Imatinib durchgeführt. Jedoch konnten nur schwache synergistische Interaktionen zwischen diesen beiden Medikamenten festgestellt werden. Die Analyse der resistenten DFT2 Zelllinien, die gegen PDGFR-Inhibition resistent waren, zeigten jedoch Veränderungen im RTK-Signalweg und eine Aktivierung von STAT3, ähnlich wie zuvor bei DFT1 beschrieben. Neben der Aktivierung von STAT3, kam es auch zu Veränderungen im Mechanismus der Immunabwehr, da MHC-I runterreguliert wurde. Diese Erkenntnisse zeigen nicht nur, dass DFT2 eine Signalplastizität bei der Behandlung aufweist, sondern verbindet auch RTK-getriebene Signalwege mit der Immunabwehr.

Zusammenfassend zeigen die vorliegenden Ergebnisse, dass beide Tumorzelllinien unterschiedliche Signalmechanismen aufweisen, aber aufgrund der Signalplastizität alternative Signalwege aktivieren können, die zur Immunabwehr der Tumoren beitragen. Dieses Wissen kann dazu beitragen, wirksamere Behandlungen zu entwickeln und den Tasmanischen Teufel zu schützen. Gleichzeitig können die Erkenntnisse über diese übertragbaren Tumore in die menschliche Krebsforschung übertragen werden und unser Verständnis der Krebs-Signalwege und Immunabwehr vorantreiben.

7. Supplements

7.1. Drug Screen

HITS	Inhibitor	Target
DFT1	Belinostat	HDAC
	Sapitinib	ERBB family inhibitor
	Erlotinib	ERBB family inhibitor
	Lapatinib	ERBB family inhibitor
	Ibrutinib	Brutons tyrosine kinase
	Saracatinib	Abl, Scr
DFT2	Axitinib	VEGFR-1, VEGFR-2, VEGFR-3, PDGFRβ, c-Kit
	Sorafenib	Raf-1, B-Raf, VEGFR2, VEGFR-3, PDGFRβ, c-Kit, Flt-3
	Dasatinib	Abl, Src, c-Kit
	Ponatinib	Abl, PDGFRα, VEGFR-2, FGFR1, Src
	Sunitinib malate	VEGFR-2, PDGFRβ
	AZD2932	VEGFR-2, PDGFRβ, Flt-3, c-Kit
	Cabozantinib	VEGFR-2
	Vandetanib	VEGFR-2, VEGFR-3, EGFR
	Imatinib	v-Abl, c-Kit, PDGFR
DFT2	Pazopanib	VEGFR-1, VEGFR-2, VEGFR-3, PDGFR, FGFR, c-Kit, c-Fms
	Linifanib	KDR, CSF-1R, Flt-1/3, PDGFRβ
	Crenolanib	PDGFRα/β
	Masitinib	c-Kit, PDGFRα/β
	Tivozanib	VEGFR-1, VEGFR-2, VEGFR-3, PDGFR, c-Kit
	Doxorubicin	Chemotherapy
DFT1 and DFT2	Afatininb	EGFR, HER2, HER4
	Chidamide	HDAC
	Vorinostat	HDAC
	Regorafenib	VEGFR-1, VEGFR-2, VEGFR-3, PDGFRβ, c-Kit, RET, Raf-1
	Motesanib Diphosphate	VEGFR-1, VEGFR-2, VEGFR-3
	Dasatinib	Abl, Src, c-Kit
	Entinostat	HDAC
	Romidepsin	HDAC

Supplemental Table 1: Drug Screen Hits

7.2. Analysis of core cancer pathways in DFT1 and DFT2 cells

7.2.1. RTK Expression

7.2.1.1. ERBB Family

	Gene Expression	
Cell Lines	***ERBB3* (n=3)**	***EGFR* (n=3)**
DFT1 strain 1 vs. DFT1 1426	ns	ns
DFT1 strain 1 vs. DFT1 C5056	ns	*
DFT1 strain 1 vs. DFT2 Snug	****	*
DFT1 strain 1 vs. DFT2 RV	**	*
DFT1 strain 1 vs. DFT2 JV	****	*
DFT1 strain 1 vs. FIBS	ns	****
DFT1 1426 vs. DFT1 C5056	ns	ns
DFT1 1426 vs. DFT2 Snug	****	ns
DFT1 1426 vs. DFT2 RV	**	ns
DFT1 1426 vs. DFT2 JV	****	ns
DFT1 1426 vs. DFT2 FIBS	ns	****
DFT1 C5056 vs. DFT2 Snug	****	ns
DFT1 C5056 vs. DFT2 RV	****	ns
DFT1 C5056 vs. DFT2 JV	****	ns
DFT1 C5056 vs. FIBS	ns	****
DFT2 Snug vs. DFT2 RV	ns	ns
DFT2 Snug vs. DFT2 JV	ns	ns
DFT2 Snug vs. FIBS	****	****
DFT2 RV vs. DFT2 JV	ns	ns
DFT2 RV vs. FIBS	****	****
DFT2 JV vs. FIBS	****	****

Supplemental Table 2: Statistical Analysis of *ERBB3* and *EGFR* Gene Expression in DFT1 strain 1, DFT1 1426, DFT1 C5056, DFT2 Snug, DFT2 RV, DFT2 JV and fibroblasts. To determine statistical significance a two-way ANOVA with Bonferroni comparison was performed. ns = non-significant, * = p-value < 0.05, *** = p- value < 0.001, **** = p-value < 0.0001.

7.2.1.2. PDGFR family

	Gene Expression		Protein Expression	
Cell Lines	***PDGFRA*** **(n=2)**	***PDGFRB*** **(n=2)**	**PDGFRα (n=3)**	**PDGFRβ (n=2)**
DFT1 strain 1 vs. DFT1 1426	ns	****	ns	ns
DFT1 strain 1 vs. DFT1 C5056	ns	****	ns	*
DFT1 strain 1 vs. DFT2 Snug	****	****	****	ns
DFT1 strain 1 vs. DFT2 RV	****	****	**	ns
DFT1 strain 1 vs. DFT2 JV	****	****	***	ns
DFT1 strain 1 vs. FIBS	ns	****	ns	ns
DFT1 1426 vs. DFT1 C5056	ns	****	ns	ns
DFT1 1426 vs. DFT2 Snug	****	*	****	ns
DFT1 1426 vs. DFT2 RV	****	*	***	ns
DFT1 1426 vs. DFT2 JV	****	**	***	ns
DFT1 1426 vs. DFT2 FIBS	ns	**	ns	ns
DFT1 C5056 vs. DFT2 Snug	****	****	****	*
DFT1 C5056 vs. DFT2 RV	****	****	***	*
DFT1 C5056 vs. DFT2 JV	****	****	***	*
DFT1 C5056 vs. FIBS	ns	**	ns	*
DFT2 Snug vs. DFT2 RV	****	ns	***	ns
DFT2 Snug vs. DFT2 JV	****	ns	***	ns
DFT2 Snug vs. FIBS	****	****	****	ns
DFT2 RV vs. DFT2 JV	****	ns	ns	ns
DFT2 RV vs. FIBS	****	****	**	ns
DFT2 JV vs. FIBS	****	****	***	ns

Supplemental Table 3: Statistical Analysis of *PDGFRA*/*B* Gene Expression and PDGFRα/β Protein Expression in DFT1 strain 1, DFT1 1426, DFT1 C5056, DFT2 Snug, DFT2 RV, DFT2 JV and fibroblasts. To determine statistical significance a two-way ANOVA with Bonferroni comparison was performed. ns = non-significant, * = p-value < 0.05, *** = p- value < 0.001, **** = p-value < 0.0001

7.2.2. STAT Signaling

	Gene Expression		Protein Expression	
Cell Lines	***STAT1*** **(n=2)**	***STAT5B*** **(n=3)**	**t-STAT1 (n=3)**	**t-STAT5 (n=5)**
DFT1 strain 1 vs. DFT1 1426	***	ns	ns	ns
DFT1 strain 1 vs. DFT1 C5056	ns	**	ns	ns
DFT1 strain 1 vs. DFT2 Snug	ns	****	ns	***
DFT1 strain 1 vs. DFT2 RV	ns	**	ns	***
DFT1 strain 1 vs. DFT2 JV	**	**	ns	**
DFT1 strain 1 vs. FIBS	**	ns	*	ns
DFT1 1426 vs. DFT1 C5056	***	****	ns	ns
DFT1 1426 vs. DFT2 Snug	*	*	ns	***
DFT1 1426 vs. DFT2 RV	ns	ns	ns	**
DFT1 1426 vs. DFT2 JV	ns	ns	ns	**
DFT1 1426 vs. DFT2 FIBS	ns	***	ns	ns
DFT1 C5056 vs. DFT2 Snug	ns	****	ns	ns
DFT1 C5056 vs. DFT2 RV	ns	****	ns	ns
DFT1 C5056 vs. DFT2 JV	**	****	ns	ns
DFT1 C5056 vs. FIBS	**	ns	*	ns
DFT2 Snug vs. DFT2 RV	ns	ns	ns	ns
DFT2 Snug vs. DFT2 JV	*	ns	ns	ns
DFT2 Snug vs. FIBS	*	****	ns	ns
DFT2 RV vs. DFT2 JV	ns	ns	ns	ns
DFT2 RV vs. FIBS	ns	****	ns	ns
DFT2 JV vs. FIBS	ns	****	ns	ns

Supplemental Table 4: Statistical Analysis of *STAT1* and *STAT5B* Gene Expression and t-STAT1 and t-STAT5 Protein Expression in DFT1 strain 1, DFT1 1426, DFT1 C5056, DFT2 Snug, DFT2 RV, DFT2 JV and fibroblasts. To determine statistical significance a two-way ANOVA with Bonferroni comparison was performed. ns = non-significant, * = p-value < 0.05, *** = p- value < 0.001, **** = p-value < 0.0001

	Gene Expression	Protein Expression		
Cell Lines	***STAT3* (n=3)**	**t-STAT3 (n=3)**	**pY-STAT3 (n=3)**	**pS-STAT3 (n=4)**
DFT1 strain 1 vs. DFT1 1426	ns	ns	ns	ns
DFT1 strain 1 vs. DFT1 C5056	ns	ns	ns	ns
DFT1 strain 1 vs. DFT2 Snug	****	ns	*	**
DFT1 strain 1 vs. DFT2 RV	****	*	**	**
DFT1 strain 1 vs. DFT2 JV	****	ns	*	**
DFT1 strain 1 vs. FIBS	****	*	**	*
DFT1 1426 vs. DFT1 C5056	ns	ns	ns	ns
DFT1 1426 vs. DFT2 Snug	****	ns	ns	*
DFT1 1426 vs. DFT2 RV	****	ns	ns	*
DFT1 1426 vs. DFT2 JV	****	ns	ns	*
DFT1 1426 vs. DFT2 FIBS	****	ns	ns	ns
DFT1 C5056 vs. DFT2 Snug	****	ns	ns	**
DFT1 C5056 vs. DFT2 RV	****	ns	ns	**
DFT1 C5056 vs. DFT2 JV	****	ns	ns	**
DFT1 C5056 vs. FIBS	****	ns	ns	*
DFT2 Snug vs. DFT2 RV	ns	ns	ns	ns
DFT2 Snug vs. DFT2 JV	ns	ns	ns	ns
DFT2 Snug vs. FIBS	ns	ns	ns	ns
DFT2 RV vs. DFT2 JV	ns	ns	ns	ns
DFT2 RV vs. FIBS	ns	ns	ns	ns
DFT2 JV vs. FIBS	ns	ns	ns	ns

Supplemental Table 5: Statistical Analysis of *STAT3* Gene Expression and t-STAT3, pY-STAT3 and pS-STAT3 Protein Expression in DFT1 strain 1, DFT1 1426, DFT1 C5056, DFT2 Snug, DFT2 RV, DFT2 JV and fibroblasts. To determine statistical significance a two-way ANOVA with Bonferroni comparison was performed. ns = non-significant, * = p-value < 0.05, *** = p- value < 0.001, **** = p-value < 0.0001

List of Figures

Figure 29: Simplified EGFR and PDGFR signaling. EGFR and PDGFR are both members of the RTK family and therefore share some similarities in their signaling pathways. They both activate several common downstream signaling pathways including JAK/STAT, PI3K/AKT, RAS/RAF/ERK, PLCγ//PKC and the activation of Src kinases. This image was created using PowerPoint (Perrone et al., 2009).

List of Tables

Supplemental Table